



• Paranal
• La Silla
• La Serena
• Santiago

Munich

No. 73 – September 1993

A Message from the New Editor

It is an honour and a pleasure to take on the responsibility of the Editorship of THE MESSENGER. The former editors, and in particular Richard West who was editor for two terms (1976–1979 and 1986–1993), made the Messenger an informative and friendly publication. It is therefore clear that no large changes should be brought to the Messenger.

However, because of the forthcoming deployment of the VLT-VLTI, the ESO observers' community has an increasing need for technical information in all domains: site infrastructure, telescopes, instrumentation and detectors, calibration, data analysis and archiving. More emphasis will be given to these topics concerning both Paranal and La Silla. The Messenger will also carry articles on the use of the VLT-VLTI for specific astronomical topics. These articles are written by astronomers invited by the Editor to present their views. As before, observational results obtained at La Silla will also be presented. In this area, there will be no attempt at presenting a complete panorama of the observations carried out at ESO, and the number of articles in the observations section is likely to fluctuate from issue to issue. The most apparent change in the look of the journal is a division into sections: first the telescopes and instrumentation including detectors. This will be followed by articles on science with the VLT. Then there will be a section on scientific results obtained at La Silla and a section on other astronomical news. The last section groups all the announcements of ESO conferences and workshops, some announcements for positions (mostly in the Science Division), the titles of the accepted programmes and similar matters.

The technical editor of the Messenger remains Kurt Kj ar and I look forward to our collaboration in producing the Messenger.

*Marie-H el ene Ulrich
email Internet: mulrich@eso.org*

TELESCOPES AND INSTRUMENTATION

The 8.2-m Primary Mirrors of the VLT

R. MUELLER, H. HOENESS, Schott Glaswerke, Mainz, Germany

J. ESPIARD, J. PASERI, REOSC, Longjumeau, France

P. DIERICKX, ESO

1. Introduction

The 8.2-m Zerodur primary mirrors of the VLT telescopes are on their way to the observatory. On June 25, the first of the four mirror blanks (code name Joe Dalton) was delivered by SCHOTT,

the mirror blank manufacturer, to REOSC, who will polish it and mount its interfaces. Inspections performed before delivery have not only demonstrated the compliance of the blank with its specifications, but also the performance of the blank manufacturer in

achieving superb quality.

On July 19 at 14:20, Joe was transported to Mainz harbour, a few kilometres away from the SCHOTT plant (Figure 1). At 9 p.m. it was loaded onto the barge ELDOR. The ELDOR went down the Rhine to Rotterdam, travelled south

to Calais, then up the Seine to Evry after crossing Paris on Friday 23 overnight. On Monday 26 at 10 a.m. it was unloaded and placed onto a trailer. The road transport to the REOSC plant started at 0:00 on Tuesday 27 and Joe arrived at REOSC at 02:30 a.m. The container was opened the same day at 14:00¹.

One of the greatest difficulties in the design of telescopes larger than about 4 or 5 metres is the manufacturing of the primary mirror blank. The classical design of a thick and solid mirror would imply enormous masses. First of a long series of problems, the homogeneity of a 200-ton casting is very unlikely to satisfy the stringent requirements applied to high accuracy optical components. Even under the unrealistic assumption that all manufacturing and assembling issues could be solved, an 8-m mirror more than 1 m thick would still deform too much under its own weight. Remember the basic idea: get a surface the size of a small apartment down to sub-micron accuracy, and maintain it.

There are three possible diets to get the mass down: reduce its weight, make it out of segments, or get it slim and use its support to control its shape. The three names behind these solutions are: Palomar, Keck, NTT, respectively. However, in the 8-m range, a Palomar-type primary mirror still needs some active control as gravity and thermal loads may affect the surface accuracy. The effectiveness (with regard to performance and safety) of very large honeycomb structures is still to be proven, while the second 10-m Keck telescope is on its way, and the NTT has already provided superb images. Each of the three solutions has its pros and cons, and the trade-off is extremely difficult. There are no miracles, just tremendous efforts to bring the concepts into operation.

2. The Actively Controlled Meniscus Concept

The concept selected by ESO for the VLT is an extrapolation of the concept demonstrated first with an experimental mirror 1 m in diameter and subsequently with the NTT. It consists of a f/1.8, 8.2-m diameter actively supported Zerodur meniscus, 175 mm thick. The mirrors will be supported axially by 150 hydraulic actuators. These actuators can be seen as computer-controlled springs: they do not constrain the spa-



Figure 1: Joe on its way to Mainz harbour.

tial position of the mirror at 150 locations but aim at providing a force distribution which results in a fully predictable elastic deformation of the mirror. With an active mirror, flexibility is used to compensate for manufacturing error and for on-line, real-time optimization of the optical properties of the telescope.

The hydraulic support system is divided into three sectors, each of them providing a virtual fixed point. Therefore, the axial position and tilt of the mirror is fixed. The actuators interface to the mirror through axial pads, the geometry of which is a three-leg spider. Each leg is connected to an invar pad about 50 mm in diameter, which is glued onto the convex surface. The distribution of the supports has been optimized to provide the lowest possible print-through on the mirror's surface. Additionally, the tripods introduce shear forces which reduce local deformations. The residual error is in the $\lambda/40$ rms range, and will be almost totally polished off as the mirrors are figured on their tripods. (See section 4.3, Effectiveness of the FLIP method.)

During operation the exact shape of the mirror will be monitored by Shack-Hartmann sensors. These sensors collect the light of an off-axis star to form an image of the pupil of the telescope onto a grid of lenses. A CCD camera records the distribution of the point images provided by the individual microlenses. A phase error of the incoming wavefront would imply a variable inclination of the rays with respect to the axis of each microlens thus resulting in a deviation from the nominal distribution

of spot images on the CCD. This deviation is measured and the wavefront reconstructed. The necessary correction is translated into a force distribution which is applied to the mirror through its active support. With active optics the frequency of correction is below about 1Hz. With its six rings of support the VLT should be able to compensate errors with spatial frequencies up to about 1 m^{-1} , within an accuracy in the range of 50 to 100 nm rms, i.e. well beyond the effect of atmospheric turbulence.

On the user's side active optics should be fully automatic, i.e. the only noticeable effect should be the high quality of the data collected under permanent computerized optimization. Of course this situation is quite demanding in terms of tuning and reliability, and the concept inevitably requires permanent maintenance, as any large and complex telescope. On the other side the positive aspects of the active optics concept extend far beyond the potential excellence of the optical properties. Indeed it provides far more design and manufacturing perspectives than a passive concept, with positive consequences both on performance and cost.

The fragility of the thin meniscus requires particular attention. All supports and auxiliary equipment which will interface to the mirror at one stage or the other are designed to keep the probability of damage under about 10^{-5} under maximum loads. Nevertheless, given the high flexibility of the mirrors and the highly non-linear relation between damage probability and load parameters

¹ On ESO side the whole process has been extensively recorded by Messrs. Heyer, Madsen and Zodet. They shall be acknowledged for their exceptional dedication and efficiency.

(e.g. area of stress fields, magnitude of stress, duration, surface finish), transport, handling and operation of any large mirror have to follow strict and rigorous rules.

The mirror itself is made out of a highly homogeneous Zerodur substrate, with near-zero residual stresses. Table 1 summarizes the main specifications for the mirror blanks, together with the achievement by SCHOTT for the first mirror blank. In many respects the mirror blank is of exceptional quality.

In addition to the geometrical and material properties, the internal quality was specified in terms of maximum number of bubbles and inclusions. Again, the result is well within the specification. The convex surface has two holes (to be compared to 10 allowed), maximum diameter 34.8 mm and maximum depth 40 mm, which result from the removal of inclusions before ceramization. Local acid etching has been applied and the effect of the holes on stress fields is such that the probability of breakage is still beyond 10^{-5} .

The optical specifications given to the optical manufacturer are in line with the active optics concept and follow the formalism developed at ESO to quantify optical performance of ground-based telescopes.

The mirrors will be polished on an active support system which interfaces to the tripods. The manufacturer is permitted to physically remove low spatial frequency errors, provided that he stays within the specified budget of ± 120 Newton maximum active force. The operational performance of the mirrors is given by the residual errors after active correction. The latter have been

Table 1.

Parameter	Specifications	Achievement	
Outer diameter	8200 ± 2	8201.52	mm
Inner diameter	1000 ± 0.5	999.81	mm
Concentricity	≤ 1	0.01	mm
Thickness ¹	$176 + 2 - 0$	177.9	mm
Radius of curvature (concave surface)	28975	28968 ²	mm
(convex surface)	28977	28979 ³	mm
Profile tolerance (concave surface)	2	0.12 ⁴	mm
(convex surface)	2	0.05 ⁵	mm
Residual stresses (tensile)	≤ 0.10	max. 0.07	MPa
(compressive)	≤ 0.60	max. 0.08	MPa
Coefficient of thermal expansion (mean value)	0 ± 0.15	-0.043	$10^{-6} \text{ }^\circ\text{K}^{-1}$
(homogeneity)	≤ 0.05	0.009	$10^{-6} \text{ }^\circ\text{K}^{-1}$

¹ Normal to convex surface, on a diameter of 8160 mm. – ² Best fitting sphere. – ³ Best fitting sphere. – ⁴ Including the effect of the 7 mm error on the radius of curvature of the concave surface. – ⁵ Including the effect of the 2 mm error on the radius of curvature of the convex surface.

specified in such a way that after convolution with the atmospheric seeing their effect on the long-exposure image will be limited to a maximum decrease of 5% of the peak intensity in stellar images, in the visible and with a seeing angle of 0.4 arcseconds full width at half maximum. It can be easily shown that the specification ensures simultaneously seeing-limited angular resolution and high signal throughput and signal-to-noise ratio.

A positive consequence of the active optics concept is that it allows the manufacturer to concentrate on high spatial frequency errors, which have usually lower amplitude but much higher slopes and are therefore more detrimental to performance than the low spatial frequency ones. In other words, an active mirror is likely to be smoother than a passive one, and therefore to provide better contrast and signal-to-noise ratio.

The issue of matching is less critical as well, as the active support can handle a fairly large error of the conic constant. Although the option of a pentaprism test on the primary and secondary mirrors combination can still be ordered, the current strategy for the VLT is to have separate cross-checks performed on the primary and secondary mirrors. These are direct tests, i.e. they do not involve relay lenses which could introduce systematic errors, and they aim at ensuring that no significant matching error is left.

As for any optical component, optical testing is essential as it should ensure that the manufacturing tolerances are fulfilled, and as a proper measurement of the surface data (radius of curvature and conic constant) is requested for the calibration of the field aberrations. Indeed, the latter have to be deducted from the off-axis measurement by the wavefront sensors, in order that the active system applies the appropriate corrections.

3. Mirror Blanks

Large-diameter and medium-thickness menisci are economically manufactured by using the spin casting technique. This technique was specifically developed by SCHOTT in 1986–1987 for the production of mirror blanks of the 8-m class. Contrary to the conventional casting technique, spin casting is able to produce a meniscus which approaches the final shape of the mirror with only small oversizing, thus reduced mass. The meniscus shape is obtained by rotating the mold (which has a spherical bottom) while the glass is not yet solidified.

The spin casting technique has proven successful in the production of several raw blanks of the 8-m class.

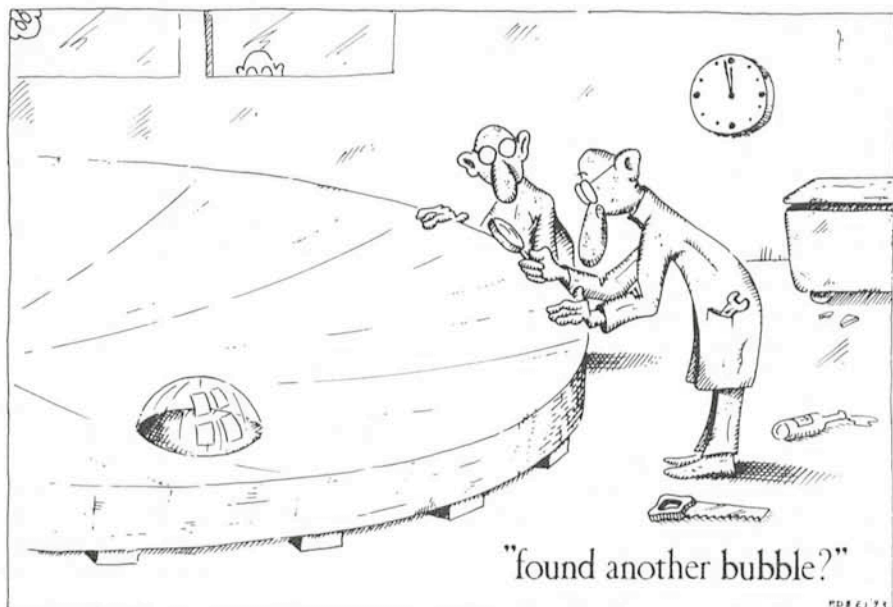




Figure 2: Lifting the overhead heating system.

After the resolution of start-up problems, several castings could be successfully cooled down to room temperature. The subsequent quality inspections showed that the high requirements set to the inner quality of ZERODUR are completely fulfilled.

All subsequent operations like handling, ceramization and machining were carried out without any problems. The first blank is already delivered, and the second blank is currently in the process of being transformed into glass ceramics in the ceramization furnace.

For the spin casting production of mirror blanks of the 8-m class, all facilities and the respective buildings were built between June 1989 and March 1991. The facilities are entirely dedicated to the manufacture of ZERODUR blanks (mirror substrates of the 8-m class and smaller blanks of 0.6 m up to 4.4 m in diameter). Production structures include new buildings with about 50,000 m³ of enclosed space, and modified and enlarged buildings.

The main steps of the manufacturing process are:

- Melting of glass in 70-t melting tank (discontinuous)

- Pouring of molten glass into the casting mold (which has a curved bottom), and generation of meniscus by spinning
- Coarse annealing of vitreous blank to ambient temperature
- Machining (rough grinding of front side, rear and edge)
- Transformation into glass ceramic (ceramization) by thermal retreatment
- Drilling of centre hole
- Final grinding

The handling and quality controls which are necessary between the individual production steps are not mentioned. In the following paragraphs the production process is described in some more detail.

● Melting

For this purpose, the batch is fed into the tank and melted, refined, and subsequently homogenized by stirring. A melting cycle lasts 24 days.

● Pouring

The casting mold is preheated for about 2 days, with the overhead heating system being lowered. Following this, the casting mold is lifted to allow the feeder (platinum tube for feeding the

molten glass from the tank into the casting mold) to protrude downward from the bottom of the mold.

After heating the feeder nose with the help of proper devices, the molten glass flows from the melting tank onto a conveyor.

Then the mold is progressively lowered to keep the feeder nose at a specified distance of the bottom of the casting mold. The discharged glass flow is cut by an appropriate device which allows the casting mold to be filled while it is slowly being lowered. This filling operation lasts approximately 4 hours.

After completing the filling operation, the mold is moved from the casting area onto the spinning area with the help of the transfer vehicle.

● Spinning

Once the transfer vehicle has been fixed to the spinning unit along with the casting mold, the overhead heating system is fastened to and slightly lifted by some hoisting equipment from the casting mold (Figure 2). This is followed by spinning the casting mold containing the molten glass at a specified rotation rate. A cooling cap is placed above the mold after the concave upper surface of the glass has been produced. The released radiation energy (20 MW immediately after lifting the heating system) is dissipated through the evaporation of water. During the spinning phase, the molten glass cools down in such a way that the glass surface retains its contour. The spinning process lasts approximately 1 hour.

● Annealing

After the spinning process, the casting mold with the raw blank is entered into the annealing furnace. Subsequently, the transfer vehicle is moved out and the furnace is closed. This is followed by annealing the vitreous-state raw blank to ambient temperature. During this process, the blank is supported by an adaptable support system which follows the deformation and shrinking of the convex surface through the annealing process. The annealing period lasts approximately 3 months.

● Lifting and turn-over

When annealing has been completed, the annealing furnace is opened, after which the raw blank is lifted from the casting mold with a vacuum lifter and moved to the turning position by the crane equipment. There it is turned over (convex surface up) with the help of the turn-over installation (Figure 3).



Figure 3: Turning the mirror blank.

During all handling operations, deformations of the handling equipment should not be transferred to the blank. Therefore the handling equipment must have a flexible and adaptable coupling to the mirror blank. For this reason hydraulic cylinders are used. All support systems are designed in such a way that tensile stresses induced in the blank are kept well below 1 MPa.

● *Rough machining*

After turning over the raw blank, it is placed on the support system of the CNC grinding machine. This support system has a design similar to the design of the handling equipment. The blank convex surface and edge are roughly machined with diamond grinding wheels. This is followed by turning

over the blank again and machining the front side.

● *Transformation to a semi-crystalline state (ceramization)*

After completing the rough machining the blank is submitted to a thermal after-treatment in the annealing furnace, which causes the vitreous state to be transformed into a semi-crystalline state. This procedure causes the material to acquire its outstanding properties of thermal *zero expansion*.

This crystallization process is exothermic. During crystallization, the volume shrinks by approximately 3%. Hence, all efforts should be made to cause crystallization to proceed very slowly, in order to prevent stresses from coming up and leading to the fracture of the disk due to non-controlled crystallization and resultant non-uniform shrinkage. This is why transformation from the vitreous to the semi-crystalline state takes approximately 8 months.

During the transformation process, the blank is supported by an adaptable support system within the annealing furnace.

● *Drilling of the centre hole and final grinding*

After transformation into a glass



Figure 4: The blank during quality inspection.

ceramic, the centre hole is drilled with the CNC grinding machine.

The final grinding is also performed on the machine, the accuracy of which is as follows:

Rotating table at 7000 mm diameter:	
radial (x) runout	< 10 μm
axial (z) runout	< 15 μm
angular positioning	< 120 μm
Positioning in x and z:	< 20 μm
Reproducibility in X and Z	< 2 μm
To preserve this accuracy the machine room has a temperature control giving	
spatial temperature homogeneity	< $\pm 1.5^\circ\text{C}$
temporal temperature inertia	< $\pm 1.5^\circ\text{C/h}$.

● Quality controls

Quality controls and acceptance by customers are provided during and between the individual production steps (Figure 4).

Material characteristics are determined by the corporate Service RESEARCH & DEVELOPMENT. The project-tied inspection means consist of: overall geometric testing system (theodolite with process control computer), local geometric testing system, ultrasonic thickness gauge system, stress measuring system, video system for testing and documenting the inner quality. For stress measurements the blank is put onto a special quality control support system that generates extremely low stresses in the blank.

● Transfer to transportation system

After final acceptance, the blank is placed onto the transportation system with the vacuum lifter and the crane. The transportation system (REOSC) is assembled beforehand in the production wing.

4. Mirror Figuring and Polishing

On July 25, 1989, REOSC obtained from ESO the contract for the polishing of the four VLT mirrors and the following tasks:

- design and manufacture of the mirror handling tool and container,
- transportation of each VLT mirror blank from SCHOTT's plant in Mainz (Germany) to REOSC's plant,
- design, manufacture and assembly on the mirror of special devices for the mirror fixation in the cell,
- grinding, polishing and testing of the four VLT mirrors.

One of the governing design drivers in this project was the very important flexibility of the VLT mirrors as they feature a huge diameter of 8.2 m associated to a very low thickness of only 17.5 cm.



Figure 5: The REOSC optical shop.

4.1 THE OPTICAL SHOP

The new 8-m REOSC shop (Figure 5) was dedicated by the French Minister of Research and Space on April 24, 1992.

This plant is located close to the Seine, in order to optimize the mirror transport. Its total surface is 1100 m² and its dimensions are: length 70 m, width at the tower base 22 m, width of the shop 12.6 m, testing tower height 32 m.

4.2 OVERVIEW ON THE TECHNICAL PROCESS FOR FIGURING THE VLT MIRRORS

Due to their huge size and high flexibility, the conventional technique of the full sized flexible tool previously used for polishing and figuring has been modified in order to obtain a mirror surface free of high frequency defects and compliant with the requested aspherical shape.

Thus, the VLT mirrors will be ground and polished by using tools of adequate sizes associated with the REOSC Computer Controlled Surfacing (CCS) Process, and axially sustained by a support which is accurate enough not to blur the mirror high frequency defects with a large amount of non-axisymmetric low frequency defects.

Grinding machine

The grinding machine is composed of a rotating table, a removable milling bridge, a couple of two-arm machines designed and manufactured according to the REOSC requirements and a simplified axial support composed of 150 pneumatic actuators.

All this assembly is computer controlled through a unique console.

Polishing machine

The polishing machine (Figure 6) is identical to the grinding one but it is not permanently equipped with the milling bridge. Furthermore, this machine, located just under the testing tower, is equipped with an axial support of 150 pneumatic actuators, each of them is computer controlled through a Shack Hartmann CCD camera. The force accuracy delivered by each actuator is better than 2N and this support will be able to remove physically a large amount of low frequency defects.

The support software enables the user to adjust automatically the mirror position and its trim thanks to three length sensors. This software features also the mirror weighting, forces exerted by each actuator, mirror position, etc....

4.3 OVERVIEW OF THE TESTING METHODS

The testing facilities: the tower

As the efficiency of the optical tests depends on the vibration level, thermal stability and on the easiness to pass from a polishing run to a testing one, REOSC has given particular care in designing the testing tower which features an external sun shield, a main wall made of boarding with a thick lagging, an internal tower totally independent from the external one, made of a welded metallic structure which bears a double walled plastic tent. Thermally controlled air is deflected between the two walls of this tent.

Furthermore, in the testing tower, REOSC has foreseen the possibility to test the matching of a convex mirror associated with a concave mirror by using the Pentaprism method as already performed for the ESO 3.6-m telescope.

The testing plan

During the whole surfacing process of the VLT mirrors, the progress of the work is checked by the testing methods summarized in Table 2.

The mirror aspherical shape will be generated on the mirror at the rough grinding stage and checked by spherometry. Then the mirror will be moved to the polishing machine located under the tower. During the fine grinding, the mirror surface is tested by IR interferometry. When the mirror surface is smooth enough and about a few microns from the requested mirror shape, the polishing and the visible interferometric testing will start.

The spherometer

The spherometer body is made of an aluminium honeycomb structure. There are 8 points of measure and about 200 points of the mirror surface can be known. The estimated time for performing this measure and processing the data is about half an hour. The spherometer is carried by the milling bridge and its position and the position of the rotating table are controlled on-line by a computer to which are input the mirror sag measurements.

Visible interferometry and the Flow Interferogram Processing (FLIP)

The residual vibrations of the tower do not allow the use of the conventional phase shift method. The phase method based on Fourier transforms and the works of Claude and François Roddier lead to a too long processing time for averaging a large number of interferograms.

In order to overcome this difficulty, REOSC has developed a new algorithm which allows quick computing of the phase from only ONE interferogram which must present about 80 fringes inclined at 45° if a CCD camera of 250×250 pixels is used for an 8-m mirror. Furthermore, as an image can be

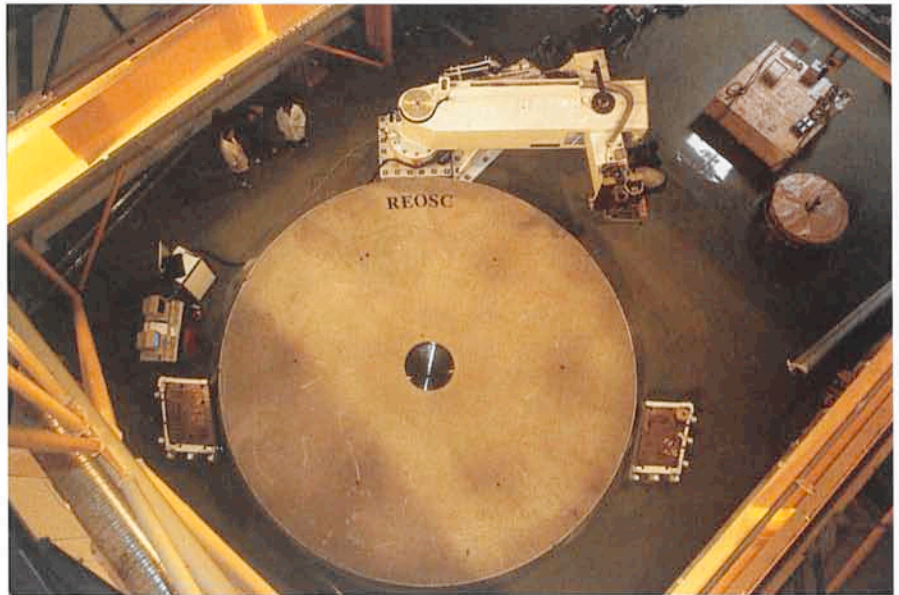


Figure 6: The 8.2-m dummy mirror on the polishing machine, as seen from the test tower.

caught in a thousandth of a second thanks to the use of an electronic shutter, the disturbing effect of the vibrations are eliminated.

FLIP is a special software which can be used with any interferometer provided it is equipped with a CCD camera and an electronic shutter. REOSC thinks that the FLIP method has the best money value.

The interferograms are taken by batches of 50 units and processed in 1 minute for 250×250 points with our present PC 386 equipped with a frame grabber card, an accelerator card and a coprocessor. By adding two accelerator cards, the processing time can be divided by two. The residual vibrations of the tower combined with the averaging of the results allow the elimination of irregularities of illumination.

This software delivers the X and Y slope error map and the values of the RMS and P/V errors, the wavefront error map and the values of the RMS and P/V, as well as the mirror surface profile when the non-axisymmetric defects have been removed.

The programme is user friendly and it is now currently used in REOSC's optical shop.

Effectiveness of the FLIP method

In order to test the effectiveness of the VLT axial support when it is provided

with special tripods as interface between the actuator shaft head and the mirror, REOSC has figured a Zerodur spherical mirror of 1.7 m in diameter, 17.5 cm thick and with a radius of curvature of 28.8 m, the same as the VLT one. This mirror is in fact a part of a whole VLT mirror. For the experiment, this test mirror was resting on seven VLT actuators, each of them was provided with a tripod. Furthermore, some of them were equipped with a large dish in order to compare the residual high frequency defects between two kinds of support for polishing: on the tripod and on the dishes.

Since the testing tower of the new plant was not available at the date of this experiment, the 1.7-m mirror and its support were installed under the REOSC old testing tower of the 4-m mirror shop. The light beam was folded twice. The results obtained with this setup and the FLIP method are the following:

When the mirror is resting on 7 single points, the measured and computed mirror deformations are as shown in Table 3.

There is a perfect correlation between the experiment and the FE computation.

In order to evaluate the FLIP ability to detect minute defects among larger ones, we have compared the results obtained by finite elements computation and FLIP measurements when the mirror is resting on the tripods.

The mirror figure obtained by interferometry is the averaging of a batch of 50 interferograms taken by the FLIP method to which we have subtracted the 1.7-m mirror figure (see Table 4).

The conclusion is that the finite elements results are very close to the experimental ones. The difference in the

Table 2.

Manufacturing stage	Test	Number of points	Absolute accuracy	Sensitive-ness P/V	Tower requested
Rough grinding	Spherometry	198	5000 nm	1000 nm	No
Fine grinding	IR Interferometry	2000	500 nm	300 nm	Yes
Polishing, final figuring	FLIP method	250×250	5 nm	5 nm	Yes

Table 3.

	Interferometry		Computation	
	P/V	RMS	P/V	RMS
Mirror surface	148 nm	24 nm	107 nm	25 nm

P/V values comes from the presence in the laser beam of some artefacts which generate a few local sharp defects.

It is worth noting that the RMS value of the high frequency defects generated by the axial support is three times lower when the mirror is resting on the tripods. This factor of three is in very good agreement with the computation.

In order to evaluate the noise of the measurements, we have computed the difference between the average of three

batches of fifty interferograms of the mirror resting on the tripods. The RMS error on the mirror surface error is 5.6 nm.

Table 4.

	Interferometry		Computation	
	P/V	RMS	P/V	RMS
Mirror surface	59 nm	7.3 nm	37 nm	8 nm

Ground-Based Astronomy in the 10 and 20 μm Atmospheric Windows at ESO – Scientific Potential at Present and in the Future

H. U. KÄUFL, ESO

1. Introduction

This article is especially written for those who have little or no experience with astronomical observations in the infrared, especially longwards of 2.2 μm . In recent issues of the *Messenger* (Käufel et al. 1992, Käufel 1993) there were several reports on instrumentation at ESO for observations in the 10 and 20 μm atmospheric windows (N and Q band in Johnson's photometric system). In this article a description of the perspectives of ground-based astronomy in these windows will be given. A special focus is set on the astronomical applications with respect to what is possible (and what not) with the present equipment; which improvements are anticipated at the VLT and how these observations compare to air-borne and space-based infrared astronomy.

2. Targets for Ground-based Infrared Observations at Wavelengths longer than 5 μm ¹

2.1 Atmospheric constraints

The terrestrial atmosphere has a substantial opacity in the infrared due to

rotational-vibrational transitions of trace molecules (e.g. CO_2 , H_2O , CH_4 , O_3). In some spectral regions these molecular transitions blend creating a practically opaque sky. The region between 8 and 13 μm , however, is reasonably free of interfering molecular transitions. Remaining absorption lines in the window itself and at the "red" edge are rather stable and observations can be easily corrected for these perturbations. On the "blue" edge H_2O is a source of variable opacity following the rapid variations of local humidity. Close to this edge more careful observing procedures are required. Beyond $\approx 13.3 \mu\text{m}$ the atmosphere becomes opaque due to the ν_2 -band of CO_2 and opens again around 16.5 μm . A forest of lines of H_2O , however, prevents the sky from getting clear so that even in the best part of the 20 μm window the average opacity more or less corresponds to 50% and is variable. Beyond 20 μm the water vapour lines become a real problem. The term "Q-window" is misleading and should be replaced by "Q-venetian-blind". Depending on site and local weather, limited astronomical observations are possible up to 30-35 μm . Beyond $\approx 35 \mu\text{m}$ the atmosphere remains opaque until the sub-millimetre region ($\geq 300 \mu\text{m}$) is reached.

In conclusion, long wavelength in-

5. Conclusion

Joe Dalton was delivered in time and well within specifications. It is now lying on the grinding machine at REOSC, where everything is ready for the next steps: glueing of the axial interfaces (in August 1993), followed by the exciting tasks of grinding it aspherical to a few microns accuracy, and then polishing to optical accuracy. Looking forward to meeting Bill, William and Averell!

frared astronomical observations are constrained to:

- $\lambda \approx 8\text{--}13 \mu\text{m}$ with very good conditions
- $\lambda \approx 16.5\text{--}30 \mu\text{m}$ with reasonable to poor conditions

2.2 Wien's Law, Kirchhoff's Law and their consequences

Wien's law relates the maximum of the Planck curve for black body radiation with its temperature

$$\lambda_{max} = \frac{2898 \mu\text{m}}{T[\text{K}]}$$

For a telescope at ambient temperature λ_{max} lies exactly in the centre of the 10 μm atmospheric window. Translated into the words of optical astronomy this is equivalent to observing stars from within a furnace (like the one in which the VLT blanks have been casted) rather than from a dark astronomical site.

To those readers not familiar with infrared astronomy it is also useful to recall Kirchhoff's law

$$\alpha(\lambda, T) = \varepsilon(\lambda, T)$$

which states that for all wavelengths and temperatures the emissivity equals exactly the absorptivity. For ground-based infrared astronomy this means that e.g. a

¹ Some of the argumentation holds also for the range of 3–5 μm . This transition region between the near infrared and the thermal infrared, however, is outside the scope of this article.

change in opacity from 5% to 20% has the minor effect of reducing the signal by $\approx 16\%$ but increases the background radiation level by a factor of 4.

Typical background generated signals at $10\mu\text{m}$ are of the order of 10^{10} electrons/pixel, equivalent to a magnitude $m_N \approx -2.50$ (for details of background noise limited operation see e.g. H.U. Käuffl et al. 1991). In spite of the high background it can be expected (based on experience with today's instrumentation) that a limiting magnitude at N of the order of 12 will be achievable with ESO's VLT, i.e. 14.5 magnitudes fainter than the background.

At this point the reader may ask the question: why bother to try to observe under such conditions at all? Part of the answer is again Wien's law: if one wants to study radiation from the cold universe one cannot do it at short wavelengths. For objects colder than 500K the radiation is best (i.e. with the highest signal to noise ratio) detected at wavelengths around $10\mu\text{m}$. Also many objects (most stars, galaxies and QSOs) tend to have $m_V - m_N > 0$. Usually, however, this is not quite sufficient to outweigh the background induced loss in sensitivity compared to visible wavelengths. There is, however, a substantial number of infrared bright but obscured sources with $m_V - m_N \approx 15$ to 25. In some of these cases it is not even sure if the light at V is radiation from the object itself or just scattering of interstellar light on the dust-shell.

2.3 On the scientific interest in dust²

By now it is well known that there is a lot of dust in the universe which comes in all grain sizes, basically from macroscopic grains to aggregates of several 100 atoms (e.g. the PolyAromatic Hydrocarbonates, PAH). Working at $\lambda \geq 2.2\mu\text{m}$ allows one to actually penetrate dust aggregations. For a nice example see e.g. the article by Peletier and Knapen (1992) who compare V and K images of the edge-on galaxy NGC 7814. The strong dust-lane apparent in the V image is fairly transparent at $2.2\mu\text{m}$. Observation of the dust itself (e.g. to study its chemical composition) is governed by Wien's law and much of the dust is simply too cold to be observable in the infrared, even at the longest wavelengths accessible from the ground. But there exist interesting exceptions: compact objects and PAHs.

Many objects are sufficiently compact so that the dust is hot enough to be observable with ground-based IR as-

tronomy. Usually these dust shells provide for a "calorimeter" which allows to determine bolometric fluxes from the integrated infrared radiation with very little uncertainties. It is also in many of these objects (especially stars on the Asymptotic Giant Branch, AGB) where the dust is actually being produced. While the physics of the mass-loss of these objects is poorly understood (see e.g. the review paper by Lafon and Berruyer, 1991) it is now clear that they are of some importance for galactic evolution, since all stars having main-sequence masses $\leq 8M_{\odot}$ will follow the track from a red giant via the AGB to a Planetary Nebula, leaving a white dwarf as compact remnant and returning the rest of the mass to the interstellar medium. The 2nd ESO/CTIO workshop held in La Serena in 1992 was also entirely devoted to this topic (proceedings edited by H.E. Schwarz, now available from ESO). Dust is of course also of extreme interest in the context of young stars and star formation, especially of low mass stars. This ranges from Herbig-Haro type objects to circumstellar disks in young stars. A recent highlight in this context: sub-arcsec spatial resolution $10\mu\text{m}$ images of the disk of β -Pictoris obtained with TIMMI at ESO's 3.6-m telescope (P.O. Lagage, private communication).

The PAHs – normally too cold to be detectable – are small enough that the energy of single UV photons hitting them raises their temperature to typically 1000K. The PAHs then cool via their well-known molecular vibrations giving rise to several strong features in the $10\mu\text{m}$ atmospheric window.

The spectroscopic observation of dust in the $10\mu\text{m}$ atmospheric window is best done with a resolution $\frac{\Delta\lambda}{\lambda} \approx 300$ because only this resolution allows for an unambiguous discrimination of broad solid-state dust features, narrow PAH-transitions and very narrow emission lines.

2.4 Molecules

Many molecules of astrophysical importance (e.g. SiO , CO_2 , C_2H_2 , C_2H_4 , C_2H_6 , SiH_4 or NH_3) have rotational-vibrational transitions between 8 and $13\mu\text{m}$ creating absorption lines in spectra of cool stars. These spectra contain practically all information on chemistry and physical conditions of photospheres and circumstellar envelopes. Depending on quality (noise, resolution) such spectra allow to retrieve much of this information. Molecular spectra usually form bands which allow to select "strategic" portions containing transitions sensitive to temperature and/or gradients and with optical depths close to unity. Isotopic shifts of transitions are easily

resolved. In AGB objects the molecular spectra tend to originate from the region where the dust formation and the acceleration of the outflowing material to its terminal velocity takes place. Dust and parent molecules can be observed simultaneously. Radio observations, on the contrary, are usually restricted to rotational transitions in the vibrational ground state and thus to cold material in regions where the dust formation is completed and the material has been accelerated to its terminal velocity. Typical linewidths are of the order of the sound-speed. The spectral resolution should match this, i.e. approach the km/s realm.

Two of the three lowest energy quadrupole transitions of molecular hydrogen in the vibrational ground state (H_2 (0,0) S (2) at $12.38\mu\text{m}$ and H_2 (0,0) S (1) at $17.03\mu\text{m}$) are observable from ground-based telescopes. Since they are partially overlapping with telluric lines such observations require a spectral resolution high enough to discriminate against the atmosphere, regardless of their intrinsic line width.

2.5 Ions and atoms

A variety of atomic lines are accessible for ground-based observations in the 10 and $20\mu\text{m}$ atmospheric windows. Those include normal hydrogen recombination lines ($\text{H I}(7-6)$ at $12.36\mu\text{m}$ or $\text{H I}(9-7)$ at $11.30\mu\text{m}$) and forbidden lines (e.g. $[\text{FV}]$ at $13.4\mu\text{m}$, $[\text{NII}]$ at $12.79\mu\text{m}$, $[\text{NaIV}]$ at 9.04 and $21.3\mu\text{m}$, $[\text{PIII}]$ at $17.87\mu\text{m}$, $[\text{SIII}]$ at $18.68\mu\text{m}$, $[\text{SIV}]$ at $10.52\mu\text{m}$, $[\text{ClIV}]$ at 11.76 and $20.37\mu\text{m}$, $[\text{ArIII}]$ at 8.99 and $21.84\mu\text{m}$, $[\text{ArV}]$ at $13.07\mu\text{m}$, $[\text{KVI}]$ at $8.84\mu\text{m}$ and $[\text{CaV}]$ at $11.47\mu\text{m}$, for more details as well as a discussion on the formation of these lines in HII regions see e.g. the original article by Simpson 1975). Many of these lines have already been utilized to assess physical conditions of ionized materials while others still await their discovery in the interstellar medium. Of extreme interest for quantitative modelling in this context is that extinction corrections are much simpler or even not required at all, since most objects are practically optically thin at $\lambda \approx 10 - 20\mu\text{m}$. For a very recent example see e.g. Jennings et al. (1993) who report fully resolved spectra of $[\text{CoII}]$ at $10.52\mu\text{m}$, $[\text{NiI}]$ at $11.31\mu\text{m}$ and $[\text{FeII}]$ at $17.94\mu\text{m}$ in SN 1987A, 612 days after outburst.

Since typical intrinsic linewidths are of the order of 10–30 km/s they can be observed with maximum sensitivity if one uses a spectrograph which just not resolves these lines. At a spectral resolution exceeding ≈ 20 km/s kinematic studies inside of objects opaque for visi-

² This is not at all complete, just a couple of examples.

ble light become possible. Observing such lines in external galaxies requires highest sensitivity and therefore is best done with a resolution matching the typical velocity dispersion inside the field of view of one pixel (i.e. resolutions between 10 and 500 km/s are required).

2.6 Magnetic fields

The ratio of Zeeman-splitting to Doppler-width for atomic lines increases linearly with the wavelength of observations, i.e. Zeeman-splitting of lines at $10\mu\text{m}$ is 20 times larger than at $0.5\mu\text{m}$. Braut and Noyes (1983) observed and identified for the first time such Zeeman splitting of transitions of MgI at $12\mu\text{m}$ in solar spectra. Deming et al. (1988) used these lines to map with arcsec spatial resolution magnetic fields around sunspots. Applying such techniques on other stars so far is quite difficult because of a lack of suitable instrumentation on large enough telescopes.

3. State of the Art, Now and in the Near Future

3.1 The IRAS database

With the publication of the IRAS catalogues a great wealth of precise high quality data readily accessible to non-specialists became available to the astronomical community. Thus the scientific value of infrared astronomy became recognized in a much broader community than was reached in the pioneering days. Still the IRAS mission had its limitations:

- being largely a survey-type mission the sensitivity is not extremely high: 250–1000 mJy at $10\text{--}20\mu\text{m}$ (for point sources; equiv. $m_N = 3.9\text{--}5.3$, $m_D = 2.5\text{--}4.0$)
- spatial resolution is limited (≈ 25 arcsec)
- spectroscopic data are only available for the brightest sources while the spectral resolution of $\frac{\lambda}{\Delta\lambda} \approx 25$ allows only for rather restricted investigations/conclusions.

Just for comparison it should be noted that in the $10\mu\text{m}$ window a bolometer at the ESO 1-m telescope would allow for deeper photometry.

3.2 Do not wait for ISO

"This star is not in the IRAS catalogue, so we have to wait for ISO to settle this question" (quote from a colloquium speaker at ESO). This is just one example of the widely spread belief that follow-up observations in the infrared at long wavelengths need to wait for ISO (the ESA Infrared Space Observatory). Clearly ultimate sensitivity on point

sources and especially on extended sources at $10\mu\text{m}$ can only be achieved with cryogenic telescopes from space; but space-based infrared observing platforms are like apparitions of bright comets: they are rare and short transient things (e.g. 18 months for the case of ISO). Any form of synoptic observations (e.g. bolometric light curve of a Mira) are virtually excluded. Also observations requiring sub-arcsec spatial resolution (and consequently telescopes larger than 4 m) can only be done from ground. In addition, as a rule of the thumb, the higher the spectral resolution the less it is advantageous to observe from space. In that sense the working group on infrared aspects for the VLT also recommended to equip the VLT with instrumentation which complements the performance of space observations (c.f. Moorwood, 1986). At this point I would also like to add the advice: do not wait for the VLT. In the following chapters I will describe what is available at ESO now or in the near future and what is planned to be available at the VLT.

3.3 TIMMI, ESO's $10\mu\text{m}$ Camera/Spectrometer

Recently ESO has complemented its suite of infrared instrumentation (the photometers/bolometers at the 1-m, 2.2-m and 3.6-m telescopes, IRSPEC, the $1\text{--}5\mu\text{m}$ medium resolution spectrograph at the NTT, and IRAC2, the $1\text{--}2.5\mu\text{m}$ near-infrared camera at the 2.2-m telescope) by adding TIMMI (see e.g. Käufel et al. 1992 for a detailed description of the instrument). While this camera has been first offered on a shared risk basis in period 52, ESO has already received 24 observing proposals asking for a total of 85 nights. TIMMI will now be mounted for 2 (out of 6 available) full moon periods in the coming semester. The proposals cover a great variety of topics: solar system, stars (young, old, circumstellar disks, outflow), interstellar medium and galaxies. They involve broad- and narrow-band imaging and mostly rely on sub-arcsecond resolution which is only possible from a good 3–4-m-class ground-based telescope. A further increase of the demand is expected once the spectroscopic mode ($\frac{\lambda}{\Delta\lambda} \approx 300$, 1-pixel sampling in long slit mode) of the camera is implemented. It should be noted that there are more than 10 similar camera projects under way or already in use worldwide. Still TIMMI is to the best of our knowledge the only system available without restrictions to visiting astronomers.

3.4 Potential upgrades of TIMMI

The implementation of the spectros-

copic mode in TIMMI will be done using gratings. These gratings need the grating structure to be machined directly into the base prism material (e.g. Germanium). Such devices are not easily available commercially. ESO has a contract with the Institut für Festkörpertechnologie, München, of the Fraunhofer Gesellschaft to produce such prisms. Once they are available they can immediately be built into TIMMI to provide for the spectroscopic mode. TIMMI works today with a 64×64 -element detector (gallium doped silicon) produced by LETI/LIR of Grenoble/France. At this laboratory there is, also with ESO participation, a new device under development which will have both a substantially higher quantum-efficiency and format³. Since this new detector will be basically pin-compatible with the one presently in use in TIMMI, an upgrade with this device is feasible. While all modes will benefit substantially from the increase in quantum-efficiency and better sampling, the device would also allow to increase the spectral resolution for grism spectroscopy to $\frac{\lambda}{\Delta\lambda} \approx 500\text{--}600$ with 2-pixel sampling per spectral element.

4. Present Plans at ESO for the 10 and $20\mu\text{m}$ Atmospheric Window at the VLT

4.1 VLT specific aspects

Great care is being taken in the VLT design to preserve the intrinsic quality of the site (Paranal). The design ensures good performance in the infrared (pupil on M2 for a field of up to 3 arcmin, no baffles, in-situ mirror cleaning and washing, emissivity at Cassegrain $\approx 6\%$ and provision of a chopping secondary).

Extrapolating the Paranal seeing measurements at 500 nm to $\lambda \approx 10\mu\text{m}$ using Kolmogorov-Taylor theory yields a monthly averaged seeing between 0.3 and 0.5 arcsec, i.e. close to the diffraction limit of the VLT ($1.22 \frac{\lambda}{D} = 0.3$ arcsec at $10\mu\text{m}$ at the VLT). According to measurements done with a $10\mu\text{m}$ interferometer (Bester et al. 1992), this is a conservative extrapolation. Thus the spatial resolution will always be close to diffraction limited. This image quality also ensures that unresolved sources can be observed ≈ 25 times faster with the VLT than with the 3.6-m telescope. With its fairly dry atmosphere (precipitable H_2O less than 2 mm for half of the time in southern winter) Paranal is a substantial improvement for working at $20\mu\text{m}$ when compared to La Silla.

³ In a forthcoming issue of the *Messenger* there will be a status report of this project.

4.2 Anticipated operating modes of the 10/20 μ m instrument at the VLT

According to ESO's instrumentation plan for the VLT (see e.g. S. D'Odorico, 1992) the Cassegrain focus of unit telescope 2 will carry a dedicated 10/20 μ m multi-purpose instrument. Installation and commissioning of the instrument is presently scheduled for the second half of 1999. The following operating modes have been identified as the minimum to be implemented to match most scientific objectives addressed above, both for galactic and extragalactic astronomy:

- diffraction limited imaging in the N-band with variable magnification for fields as large as 80 \times 80 arcsec with a suite of filters (incl. potentially fixed-spacer Fabry-Perot etalons)
- diffraction limited imaging for the part of the Q-band accessible with Ga:Si detectors (16.5 to 17.8 μ m)
- long slit⁴ spectroscopy at 7.9–14 μ m with
 - $\frac{\lambda}{\Delta\lambda} \approx 300 - 500$ (i.e. covering the entire band in 'one shot')
 - $\frac{\lambda}{\Delta\lambda} \approx 7000$
 - limited access in spectroscopy to the 16.5–17.8 μ m region at $\frac{\lambda}{\Delta\lambda} \approx 3000$

additional (optional) observing modes which would be highly desirable:

- high resolution (i.e. $\frac{\lambda}{\Delta\lambda} \approx 30,000 - 50,000$, potentially as high as 100,000) long-slit spectroscopy mode for 10 μ m
- long slit spectroscopy mode for most of the Q-band ($\frac{\lambda}{\Delta\lambda} \approx 3000$ at $\approx 17-24\mu$ m)

This instrument shall be manufactured by a consortium of institutes in the ESO member states. A study contract has been awarded to a team led by P.O. Lagage at the Service d'Astrophysique of CEN-Saclay (France)⁵. After completion of the study the operating modes may be revised.

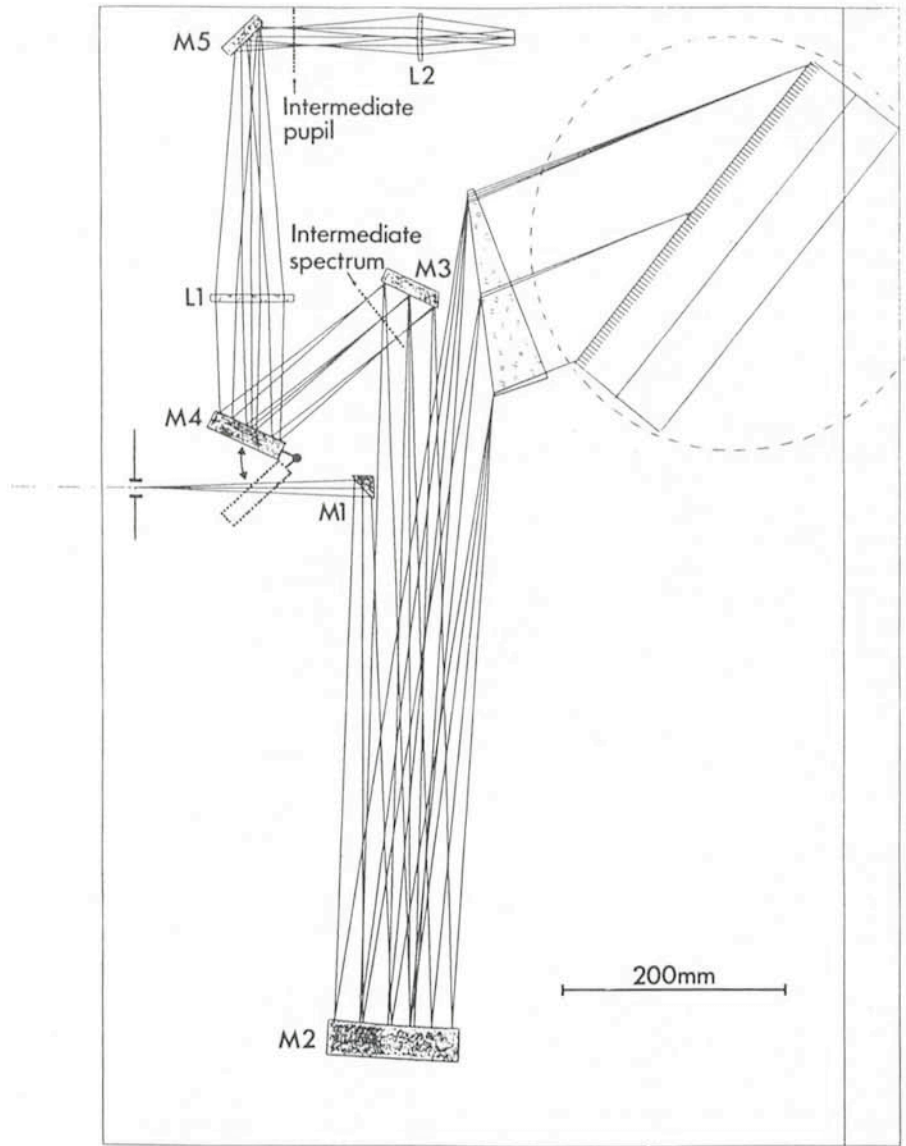
4.4 Possible embodiments

In order to define the scope of the above-mentioned study contract, pre-designs were made internally at ESO resulting in two proposals:

- A dedicated concept for a 10/20 μ m instrument taking full advantage of the relaxed optical requirements in the infrared (Käufel and Delabre, 1992). All observing modes sketched above are feasible with generally close to optimum performance while retaining

⁴ A slit length of the order of 30–40 arcsec is considered sufficient.

⁵ See also *The Messenger*, 72, p. 44 for some background.



Optical Design of the 10/20 μ m Camera/Spectrometer: The instrument is shown in its spectroscopy mode utilizing the anamorphic beam-expansion for highest resolution ($\frac{\lambda}{\Delta\lambda} = 30 - 45000$, diff. limited). The flat entrance window is omitted. M 1 is a cylindrical and M 2 a toroidal mirror. Whereas the 2-mirror collimator produces a circular beam (diameter ≈ 50 mm) this is changed to an elliptical beam of 50×166 mm² by the Germanium prism operating close to the Brewster angle. Even if no suitable coating for the grazing incidence into Germanium can be found still an overall efficiency of collimator plus grating exceeding 40% can be achieved. In the normal spectroscopy mode the expansion prism will be replaced by a folding mirror which sends the beam to a standard grating unit. M 3 is a folding mirror. Behind M 3 the intermediate spectrum is formed which could be diverted by another kinematic folding mirror (not shown) to feed a dedicated spectroscopic camera for the 20 μ m atmospheric window.

M 4 (kinematic mirror) allows to select between the camera mode (dotted position) and the long slit spectroscopy mode. L 1 is the camera collimator lens (Germanium, $f = 268$ mm, $f \# = 13.4$) which forms an intermediate pupil of 20 mm diameter behind the folding mirror M 5. This is also the location of the filter wheel. L 2 (mounted to a lens wheel) is one of the camera lenses. Shown here is the most critical lens (scale of $6 \frac{\text{arcsec}}{\text{mm}}$). To achieve background noise limited performance all components before the pupil stop have to be cooled below ≈ 70 K, pupil stop, filter and lens wheel have to be cooled below ≈ 50 K.

a comparatively moderate size and complexity. Figure 1 shows this instrument in its high-resolution spectroscopic mode.

- The opto-mechanical concept of ISAAC, the corresponding instrument for the near-infrared (for a description see e.g. Moorwood, 1992), lends itself to an easy modification to imple-

ment most of the above-defined observing modes. Only the implementation of high-resolution spectroscopy needs further studies.

The final embodiment will depend on the result of the study. The ESO-internal dedicated design will be used for the sensitivity/performance estimates in the following chapter.

4.5 Sensitivity of such an instrument at $\lambda \approx 10\mu\text{m}$ in an astronomical context⁶

Broad Band Imaging: The limiting flux is expected to be 5.4×10^{-4} Jansky (i.e. 12.1 mag). Operating at the diffraction limit of the VLT (i.e. $0.33''$ at $10\mu\text{m}$) this instrument will allow to image any celestial object exceeding a brightness temperature of $\approx 90\text{K}$, irrespective of its distance as long as it is spatially resolved. For point sources this instrument will be ≈ 3 orders of magnitude more sensitive than the IRAS point source catalogue.

Narrow Band Imaging: At a spectral resolution of $\frac{\lambda}{\Delta\lambda} \approx 100$ the limiting line-integrated flux for ionic lines (e.g. [ArIII], [NeII], [SIV]) will be $\approx 1.3 \cdot 10^{-17} \frac{\text{W}}{\text{m}^2}$ per 0.3×0.3 arcsec pixel. This implies that galactic Planetary Nebulae such as NGC 7009 or IC 418 would be detectable up to typically their 150-fold distance, i.e. ≈ 75 kpc. If the size of the intermediate pupil is chosen to be ≈ 20 mm, monochromatic images for a field of $30''$ with a spectral resolution as high as 300 are feasible for selected transitions. Because of the better background rejection the sensitivity limits would then be a factor $\sqrt{3}$ fainter.

Low Resolution Long Slit Spectroscopy: In this mode the entire $10\mu\text{m}$ window could be observed in one integration with $\frac{\lambda}{\Delta\lambda} \approx 300$ – 500 to study dust (temperature, composition) and to survey emission lines. The limiting continuum flux for this mode will be 8.7 mJansky (9.0 mag). Spectroscopy of typical galactic C stars or OH stars will be possible even if they were located at distances of 500 to 1000 kpc. Many extragalactic sources are exceeding that limiting flux (e.g. the QSO 3C48 at $z \approx 0.4$ is 8 times brighter than the limiting flux given above). While $10\mu\text{m}$ spectroscopy of QSOs will certainly be restricted to few bright quasars, these spectra will be of extreme interest because they will allow to study dust (temperature, composition) in these objects and the redshift will move a variety of interesting atomic emission lines into the observable window.

Medium Resolution Long Slit Spectroscopy: This mode allows for the observation of atomic and ionic emission lines combining highest sensitivity and spectrophotometric precision. Limited molecular spectroscopy will be feasible. The limiting flux for sources emitting a

continuum is of the order of 60 mJansky (7.0 mag) or $2 \times 10^{-18} \frac{\text{W}}{\text{m}^2}$ for emission lines. Galactic PNs (e.g. NCG 7009 or IC 418) would be observable at 300 to 400 times their distance which will enhance the research capabilities on PNs in the Magellanic Clouds substantially. For compact sources, the instrument when compared to the IRAS spectroscopic channel, will have a 200 times higher spectral resolution, will be 100 times more sensitive and provide $0.3''$ spatial resolution along the slit. As e.g. the QSO 3C273 exceeds the limiting flux by a factor of 8, extragalactic work at this spectral resolution even up to cosmological distances will become possible.

High Resolution Long Slit Spectroscopy: The limiting flux averaged over one pixel could be of the order of 300 to 500 mJansky. For point sources this implies that most sources in the IRAS point source catalogue are bright enough to be detected with a $\frac{S}{N} \geq 10$ within one hour. This will provide new insight into the kinematic and physical structure of optically thick or obscured compact ionized objects. In stars molecular transitions or Zeeman-sensitive hydrogen-like metal lines can be studied with this mode. Particularly interesting is also that many Asymptotic Giant Branch objects known in our Galaxy could be observed at LMC/SMC distances thus providing for a coherent sample of AGB stars where physics of mass loss and dust formation could be studied in an unprecedented way.

Imaging in the 16.5 to 17.8- μm passband: It can be expected to reach a limiting flux of 13mJy ($m_Q \approx 7$) for this mode on point sources. This would exceed the sensitivity of the IRAS $25\mu\text{m}$ channel for point sources with a flat spectrum by a factor of 10–20. E.g. the above-mentioned QSO 3C48 is 50% brighter than the limiting flux. For many sources this channel can thus provide extremely valuable photometric information to judge the bolometric luminosities.

Performance in other parts of the Q-band is difficult to judge since one lacks a precise knowledge or models of the atmospheric spectrum at the VLT site. Furthermore, little is known about detectors which could be available to ESO to be used for this window.

5. Conclusions and Outlook

It has been demonstrated that a dedicated $10/20\mu\text{m}$ instrument at ESO's VLT, located on Paranal, certainly an excellent site for IR astronomy, will allow to investigate a significant amount of scientific objectives ranging from the solar system to cosmological distances. In the passbands set by the terrestrial atmosphere, it will in many respects out-

perform space-based or air-borne observing platforms. The sensitivity increase of such an instrument at the VLT as compared to a 4-m class telescope will be substantial and give astronomers a wide access to objects in the Magellanic Clouds for programmes which today are restricted to few bright stars (also due to lack of suitable focal plane instrumentation). A big boost is especially expected for stars in their early and late stages of evolution. Infrared spectroscopy at spectral resolutions approaching photospheric sound speeds which today are rarely done and restricted to the few brightest stars will become possible for several 10000 stars, thus allowing the systematic study of samples selected with coherent criteria. It is also expected that this instrument will contribute enormously to research, where a multi-wavelength approach is required or beneficial, e.g. in the study of winds in hot stars, Planetary Nebulae, Herbig-Haro objects or other forms of low-mass star formation.

References

- M. Bester, W.C. Danchi, C.G. Degiacomi, L.J. Greenhill, C.H. Townes: *Astrophysical Journal*, **392**, p. 357, 1992.
- J.W. Brault, Noyes R.W.: *Astrophysical Journal Letters*, **269**, L61, 1983.
- D. Deming, R.J. Boyle, D.E. Jennings, G. Wiedemann: *Astrophysical Journal* **333**, p. 978 (1988).
- S. D'Odorico: 1992, proceedings of the ESO conference on *Progress in Telescope and Instrumentation Technologies*, p. 557, M.-H. Ulrich editor.
- D.E. Jennings, R.J. Boyle, G.R. Wiedemann, S.H. Moseley: *Astrophysical Journal* **408** p. 277, 1993.
- H.U. Käufel, P. Bouchet, A. van Dijsseldonk, U. Weilenmann: *Experimental Astronomy* **2**, 1991, p. 115.
- H. U. Käufel, B. Delabre: 1992, proceedings of the ESO conference on *Progress in Telescope and Instrumentation Technologies*, p. 597, M.-H. Ulrich editor.
- H.U. Käufel, R. Jouan, P.O. Lagage, P. Masse, P. Mestreau, A. Tarrus: *The Messenger*, **70**, 1992, p. 67.
- H.U. Käufel, 1993, *The Messenger* **72**, p. 42.
- H.U. Käufel, R. Jouan, P.O. Lagage, P. Masse, P. Mestreau, A. Tarrus: 1993, *Infrared Physics*, special issue on CIRP V, in press.
- J.-P.J. Lafon, N. Berruyer: *Astron. Astrophys. Rev.* **2**, 1991, p. 249.
- P.O. Lagage, R. Jouan, P. Masse, P. Mestreau, A. Tarrus, H.U. Käufel, 1993, *Proceedings SPIE Conf.: Infrared Detectors and Instrumentation*, Orlando, USA, April 1993, Vol 1946 (in press).
- A. Moorwood: "Working Group Report on Infrared Aspects" in proc. of *2nd Workshop on ESO's Very Large Telescope*, p. 55-82, S. D'Odorico and J.-P. Swings editors, 1986.
- A. Moorwood: 1992, proceedings of the ESO conference on *Progress in Telescope and Instrumentation Technologies*, p. 567, M.-H. Ulrich editor.
- R.F. Peletier, J.H. Knapen: 1992, *The Messenger* **70**, p. 57.
- J.P. Simpson: *Astron. Astrophys.* **39**, 1975, p. 43.

⁶ Assumptions for sensitivity calculations: Background Limited Performance, quantum efficiency 30%, emissivity of sky and telescope 20% at 273K, transmission of filters 80%, grating eff. 80% for medium resolution and 50% for high resolution mode. The limiting fluxes are always for a $\frac{S}{N}$ of 10 σ in 1 hour in the brightest pixel.

On the Linearity of ESO CCD #9 at CAT + CES

E. GOSSET and P. MAGAIN, Institut d'Astrophysique, Université de Liège, Belgium

1. Introduction

The Coudé Echelle Spectrograph (CES) is the main facility at ESO for doing high resolution, high signal-to-noise spectroscopy. The amount and quality of the work done with it clearly show its great interest. Reaching such high resolution ($\lambda/\Delta\lambda \sim 50,000-100,000$) with a conveniently high signal-to-noise ratio would have been nearly unfeasible without the availability of efficient silicon detectors such as the CCDs. An RCA SID 006 EX High Resolution CCD (ESO number 9) is equipping the short camera (SC) since 1987, and has equipped the long one (in alternance with the Reticon) from 1987 to 1992. The CCDs have, compared to older detectors (e.g. the photographic plates), several advantages such as their high quantum efficiency and their linearity. The linearity is normally better than 1 per cent, sometimes reaching 0.1 per cent, in particular for an RCA CCD (McLean, 1989). This latter property greatly facilitates the reduction of the data while making it more precise. The idea that CCDs are linear is so common and the manuals are so much dwelling on that, that it became an every day unquestionable evidence.

In the course of the reduction of their data, both authors of the present article had sometimes the feeling that something went wrong. A few facts, noticed by several users, hinted towards a problem with that instrument:

- the equivalent widths measured at CAT + CES + SC + CCD #9 are dependent on the exposure level in the continuum;
- the equivalent widths measured with the Reticon are smaller than those measured with the CCD (5 to 15% discrepancy);
- the result of the division of two consecutive columns of the CCD has a complicated, spectrum dependent shape;
- flat fields at levels differing too much from the science exposure are not adequate for flat fielding;
- flat fields corresponding to different exposure times are not always strictly proportional.

The above-mentioned statements are not necessarily independent and could furthermore represent different aspects of the same effect. Most of the time, they were attributed, without further

analysis, to complicated, pernicious effects related to vignetting or, alternatively, to diffuse light in the spectrograph.

Recently, Magain et al. (1992) reported problems in the reduction of their data, including a clear non linearity of CCD#5. Shortly after, J. Surdej, J.P. Swings and A. Smette took the opportunity of an observing run to perform extensive tests on the CCD#8 mounted at the 2.2-m telescope, which led to the discovery of strong problems. At the same time, one of us (E.G.) was observing with the CAT. Following a telephone conversation with J. Surdej and A. Smette, E.G. decided to conduct similar tests on CCD#9 in order to further investigate the question. After all, although the idea of the existence of non-linearities in ESO CCDs could appear as heresy, a mere lack of linearity would naturally explain, at least qualitatively, all the above-mentioned problems. Indeed, quite recently (however not independently), Schwarz and Abbott (1993) reported the actual existence of such problems.

2. Test of the Linearity of CCD #9

At the end of the night 01-02/03/92, we acquired a sequence of triplets and pairs of internal flat fields with the CES in the configuration SC + CCD#9. This corresponds to sequence number 5 in Table 1. The sequence was designed to study the linearity of the CCD. In par-

ticular, we waited for the lamp to stabilize and the shortest exposure time was chosen to be 5 s in order to avoid possible problems linked to the precision of the shutter at too short exposures. In addition, the sequence of exposure times is first decreasing and then increasing in order to check the stability of the flat-field lamp. We adopted the following sequence: 3×140 s, 3×120 s, 3×100 s, 3×80 s, 3×60 s, 3×40 s, 3×20 s, 3×5 s, 3×10 s, 2×30 s, 2×50 s, 2×70 s, 2×90 s, 2×110 s, 1×130 s (the sequence had been abruptly interrupted by a switch-off of the remote control line from La Silla). These exposures allow to explore the response curve up to 10,000 ADU.

The first method (M1) we used to analyse the data is based on the hypothesis that the flux rate is constant. If F is the received flux integrated over the exposure time Δt , then the flux rate $F/\Delta t$ is independent of the exposure time. If, in addition, the CCD is linear, the observed flux f should share the same property $f/\Delta t = \text{constant}$.

First, a mean bias was subtracted from each flat field exposure. Then, 3 areas were defined on the CCD (they are given in Table 1) so that the spatial variation of the flux inside them was minimal. The observed flux rate $f/\Delta t$ is plotted in Figure 1 as a function of f . For the sake of clarity, the points coming from the three zones have been normalized to the same incident flux. Fig-

Table 1: Additional information on the different sequences selected for our study (LS: La Silla; RC: Remote Control from Garching).

Sequence	Date	Central wavelength	Number of flat fields	Place	Selected zone
1	02-03/05/1987	7790 Å	30	LS	X346-X355 Y939-Y995
2	12-13/06/1990	4057 Å	18	RC	X300-X306 Y200-Y350
3	12-13/06/1990	3835 Å	21	RC	X300-X306 Y650-Y800
4	25-26/05/1991	4057 Å	33	RC	X418-X423 Y170-Y350
5	01-02/03/1992	4542 Å	38	RC	X365-X380 Y270-Y330 X365-X380 Y470-Y530 X365-X380 Y670-Y730
6	09-10/03/1992	4057 Å	33	RC	X367-X377 Y040-Y140 X367-X377 Y300-Y400 X367-X377 Y850-Y950
7	21/07/1992	4130 Å	28	RC	X417-X429 Y409-Y754

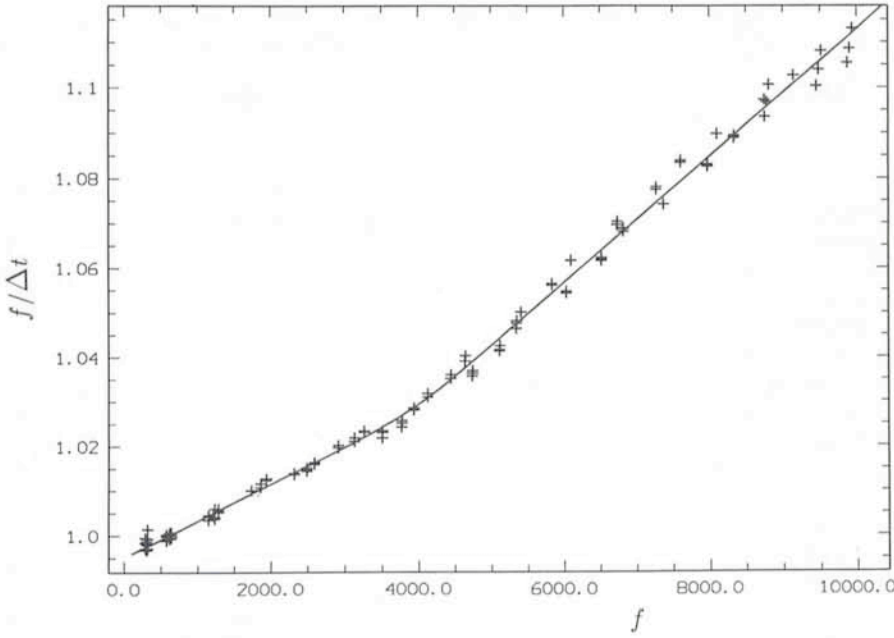


Figure 1: Plot of the normalized observed flux rate $f/\Delta t$ versus the observed flux f . The units are ADU. The continuous line is the fitted function $P(f)$.

Figure 1 shows that $f/\Delta t$ is not constant. A linear increase (i.e. a second order response curve) is visible up to 3000 ADU; then, an elbow is present and a second linear increase, with a different slope, stands up to $\sim 10,000$ ADU. This is highly suggestive of non-linearities with a rather complex behaviour.

A function $P(f)$ (fourth order polynomial up to 4500 ADU and a straight line beyond, the continuity being imposed up to the first derivative) has been fitted and is also shown in Figure 1. Unfortunately, this method (M1) suffers from several weaknesses in the form of implicit hypotheses not necessarily satisfied. For example, it assumes the constancy of the flat field lamp emission. A slow drift is effectively present (one can see small oscillations in Figure 1 due to exposures of the increasing branch alternating with exposures of the decreasing branch) but the sequence has been designed to minimize the corresponding consequences. Faster variations could also be present and would be more cumbersome. In particular, uncertainties (particularly systematic ones) in the functioning of the shutter could annihilate any confidence in the results.

To further ascertain our approach, we used a second method based on the properties of the variance of a Poisson process.

The variance σ_f^2 of the flux is given by

$$\sigma_f^2 = (RON)^2 + \frac{f}{g} \quad (1)$$

where RON is the read-out noise (possibly corrected for the effect of the bias subtraction) and g is the gain. If the CCD is linear, the law is also valid for the

observed flux f . Usually, CCD#9 is operated at $\sim 7 e^-/ADU$.

We estimated σ_f^2 by dividing two flat fields of the same exposure time ($f_1 \sim f_2$) and by computing σ_{f_1/f_2}^2 . We approximate σ_f^2 by $0.5 f^2 \sigma_{f_1/f_2}^2$. In Figure 2, we plotted $\sigma_f^2 - (RON)^2$ as a function of f . Although the first part of the curve is compatible with linearity, an elbow is again present at about 3000 ADU and, beyond, the slope is markedly different. The data have been fitted with a function $Q(f)$ of the same form as $P(f)$ but constrained to go through the origin.

The lack of linearity of the variance could be due either to a lack of linearity

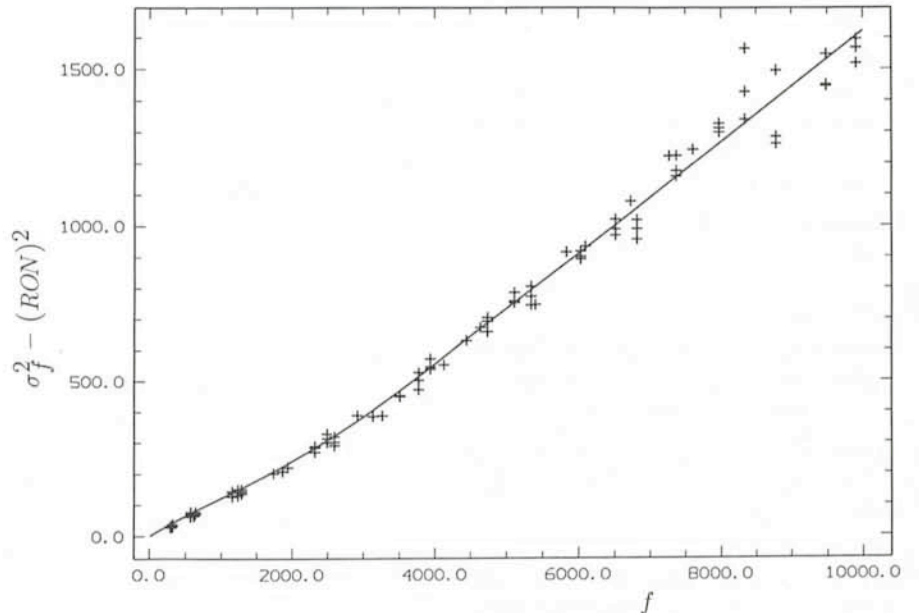


Figure 2: Plot of the variance $\sigma_f^2 - (RON)^2$ as a function of the observed flux f . The units are ADU. The continuous line is the fitted function $Q(f)$.

of the response curve or to the presence of an additional, non poissonian, flux dependent noise. The discrimination between the two causes is possible by comparing the functions $P(f)$ and $Q(f)$.

If R is the response curve, we have

$$f = R(F). \quad (2)$$

We are interested in the reciprocal response function which is also the linearizing function

$$F = R^{-1}(f). \quad (3)$$

We fitted the function

$$P(f) \propto \frac{f}{\Delta t}. \quad (4)$$

F is proportional to Δt , so we obtain the following proportionality

$$R^{-1}(f) \propto \frac{f}{P(f)}. \quad (5)$$

On the other hand, the variance of the observed flux as a function of the latter is given, in the case of no additional noise, by

$$\sigma_f^2 = (RON)^2 + \frac{R^{-1}(f)}{g} \left\{ \dot{R} \left[R^{-1}(f) \right] \right\}^2. \quad (6)$$

To check the equivalence of the two approaches, we derived the expected σ_f^2 from the fitted function $P(f)$ through Eqs. 5 and 6. We found that the expected $\sigma_f^2 - (RON)^2$ function found in this way corresponds quite well to the function $Q(f)$. Therefore, we conclude that we have to deal with a clear non-linearity present in the response curve and not with the apparition of an additional strange noise.

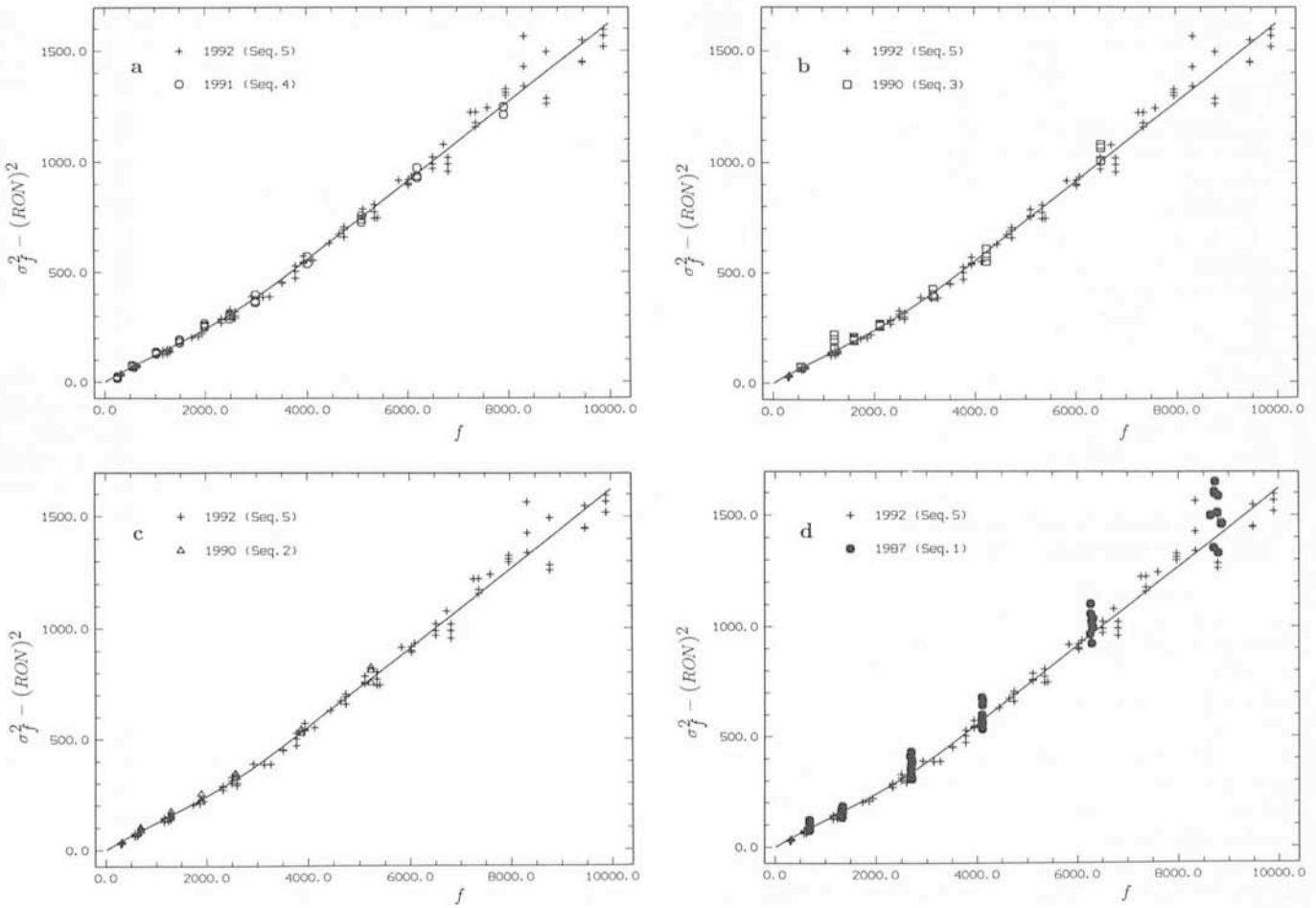


Figure 3: Comparison of the variance plots corresponding to different epochs. The crosses correspond to the 1992 reference data. Panel (a) corresponds to the 1991 data (sequence 4); panel (b) to the 1990 data (sequence 3) and panel (c) to the same year (sequence 2); finally panel (d) corresponds to the 1987 data (sequence 1).

It is rather surprising that we have to deal with the inverse phenomenon of a saturation: the higher the received flux is, the more strongly is the observed flux overestimated.

3. Persistence of the Phenomenon

After the existence of a non-linearity had been ascertained, we studied its evolution with time. Within our own archive, we found a few sequences of flat fields useful for such an investigation; they were however not designed for that purpose. We found an interesting sequence on the night 25–26/05/91, and two on the night 12–13/06/90. We can also add an older sequence on 02–03/05/87. Additional information is given in Table 1. The variance diagram ($\sigma_f^2 - (RON)^2$) as a function of f is plotted in Figure 3 for all the selected sequences along with the 1992 one as a reference. It is seen that sequences 2 and 3 (1990) are in excellent agreement with the reference. Concerning the 1991 sequence (4), we had to increase $1/g$ by 15 % to get the agreement. Most probably, the gain was different at that time although

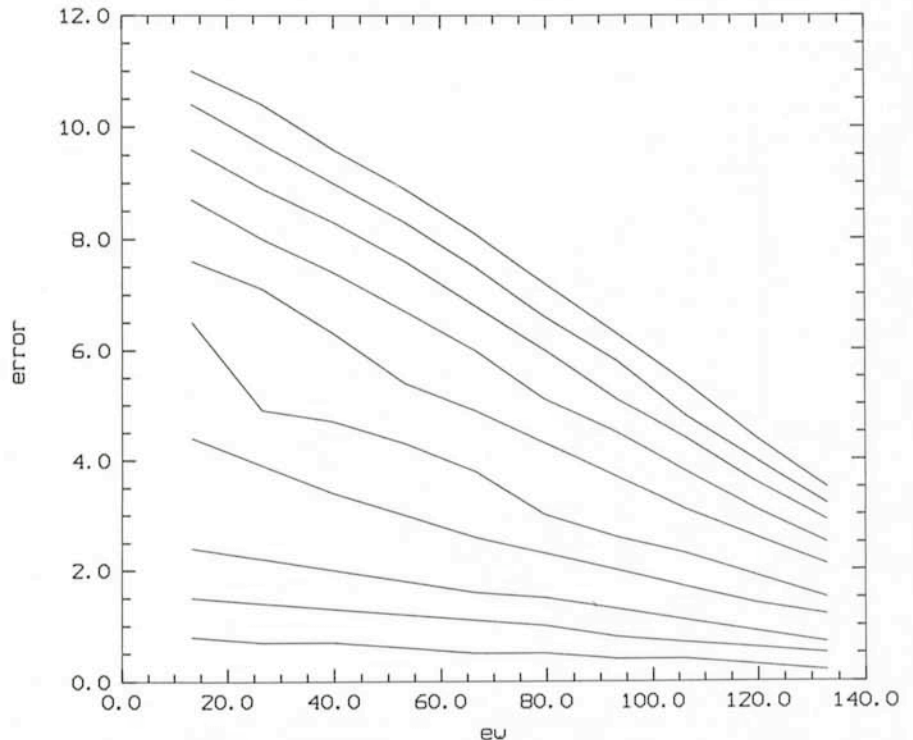


Figure 4: Relative error on the measured equivalent width, as a function of the equivalent width (expressed in mÅ), for different levels of the continuum. The continuum varies from 1000 ADU (lower curve) to 10,000 ADU (upper curve) by steps of 1000 ADU. The line width remains fixed; the line depth varies from 10 % (left) to 100 % (right) of the continuum level.

this was not mentioned in the descriptors (15 % is approximately one e^- at 7 e^- /ADU). The only slight discrepancy concerns the 1987 data. Clearly, the non-linearity is already present but the elbow could be at somewhat lower counts. In any case, the similarity between the curves is so strong that it indicates that the non-linearity was probably there from the beginning.

After our run (March 2, 1992), we complained about the problem described here and the electronic settings have been modified on several occasions, therefore changing the response curve. The situation after March 2, 1992 is described in section 6.

4. Correction of the Non-Linearity as Before March 2, 1992

Strong evidence of the stability of the inadequate response curve, at least since 1990, has been given in section 3. Therefore, we used the reference, sequence 5, as analysed in section 2, to derive a response curve and thus a linearizing function, adequate for correcting data obtained during that period.

From the function $P(f)$ fitted on the flux rate (Eq. 4), which is perfectly compatible (through Eqs. 5 and 6) with the fit $Q(f)$ made on the $\sigma_f^2 - (RON)^2$ corresponding either to sequence 5 alone or to sequences 2, 3, 4, 5 altogether, we can deduce the reciprocal response curve function $R^{-1}(f)$ (Eq. 5) within a multiplicative factor. Therefore, the linearized flux f_{LIN} which is directly proportional to F

Table 2: Power expansion of the reciprocal response function $R^{-1}(f)$ (see equation 9).

Parameter	Value $f \leq 4500$	Value $f \geq 4500$
α_1	1.00475	1.02824
α_2	- 0.7456.10 ⁻⁵	- 1.4840.10 ⁻⁵
α_3	- 1.0272.10 ⁻⁹	+ 2.142.10 ⁻¹⁰
α_4	+ 5.0929.10 ⁻¹³	- 3.09.10 ⁻¹⁵
α_5	- 8.0300.10 ⁻¹⁷	+ 4.5.10 ⁻²⁰
α_7	+ 1.9823.10 ⁻²⁵	—

$$f_{LIN} \propto F \quad (7)$$

can be expressed by

$$f_{LIN} \propto R^{-1}(f) \quad (8)$$

$$= a_1 f + a_2 f^2 + a_3 f^3 + a_4 f^4 + a_5 f^5 + a_7 f^7. \quad (9)$$

The coefficients are given in Table 2. The high order of the polynomial is basically due to the elbow. The correction should be applied to the debiased exposures (science and flat field ones) prior to flat fielding.

5. The Scientific Impact of the Problem

On Figures 1 and 2, deviations from linearity of 5 to 10 % are clearly visible. The observed spectrum changes with exposure level and is different from the correct one. The line profiles are modified, the equivalent widths overestimated.

The effect on equivalent widths depends on the continuum level, on the shape of the spectrum perpendicular to the dispersion and on the line profiles.

Simulations have been carried out for a typical case, and show the equivalent widths to be overestimated typically by 5%, but by more than 10% for weak lines on a well-exposed continuum (the best case for abundance analyses ...). Figure 4 exhibits the results of such a simulation.

6. The Response Curve After March 2, 1992

We had another run from 06/03/92 to 10/03/92. We took this opportunity to acquire another sequence of flat fields in order to further study the above-mentioned problems, particularly, as we knew that the electronic settings were changed. The variance diagram corresponding to this sequence (numbered 6 in Table 1) is given in Figure 5 along with the curve $Q(f)$ (introduced in section 2) for comparison. The response curve clearly changed: the non-linearity is anyway still present but to a lesser extent and the elbow is less obvious than in Figure 2. The variance however behaves more like a second-degree polynomial which underlines the persistence of the non-linearity.

Finally, we could make a last check in July 1992. Sequence 7 was acquired on 21/07/92; the corresponding variance diagram is also given in the same Figure 5. The curve is again different from all the others shown above. A non-linearity is still present but its nature seems more complex.

The conclusion is that, during the course of 1992, the non-linearity problem was not solved at all and that, in addition, variability of the response curve prevents to apply a general correction to the data similar to the one proposed in section 4.

As a last illustration, we decided to use a third method (M3) to investigate the linearity of CCD #9. The principle is that the shape of a spectral feature should remain the same, independently of the exposure level. So, the profile of a strong line observed with different exposure times could be used to derive the non-linearity curve.

Here, we simulated such a broad emission line by narrowing the exit slit of

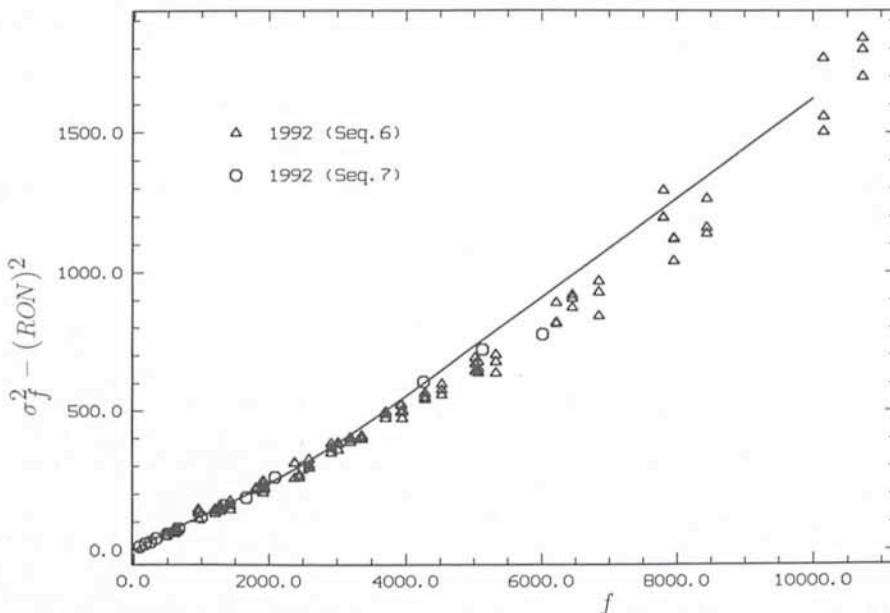


Figure 5: Plot of the variance $\sigma_f^2 - (RON)^2$ as a function of the observed flux f for sequence 6 (triangles) and sequence 7 (circles). The units are ADU. The continuous line is the function $Q(f)$ as introduced in section 2; it is given for comparison.

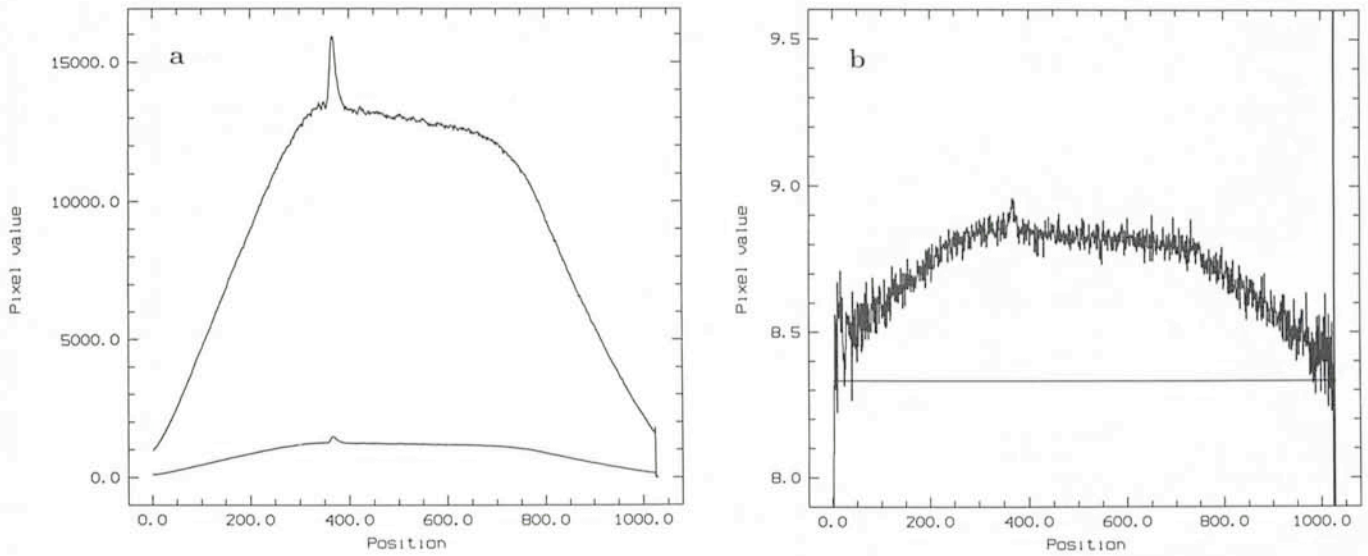


Figure 6: Ratio of two vignetted flat fields of different exposures. Panel (a) shows the two flat fields (1000 and 120 seconds of exposure) averaged over the slit height. Panel (b) gives the ratio of the two flat fields compared to the ratio of the exposure times (the straight horizontal line).

the pre-disperser in order to get strong vignetting of the flat fields. As an illustration, two flat fields of different exposure levels are shown in Figure 6. The ratio of the two is clearly flux dependent, showing that the response curve of CCD #9 was still clearly non linear in July 1992.

7. Conclusion

We gave evidence that ESO CCD #9 used at CAT + CES has never been linear from 1987, shortly after its installation at the CES, to 1992. The response curve seems to have been rather stable from the beginning up to March 2, 1992; this is certainly true during the years 1990 and 1991.

We briefly analysed the impact of the problem on abundance analysis works as those customarily done at CAT. We

proposed a first order correction to be applied on the debiased frames. This correction is to be considered a first order one because we do not know the exact origin of the problem; the dependency of the response curve on the bias level, for example, is completely unknown.

RCA CCDs are usually thought to be pretty linear (McLean, 1989). This suggests that the problem of CCD #9 originates in fact in the electronics behind the CCD itself. This is supported by the strong dependency of the response curve on the electronic settings as evidenced after March 2, 1992.

Acknowledgements

Calculations on polynomials have been performed thanks to Mathematica: we would like to acknowledge the ex-

pertise of Philippe Tombal. We are also indebted to Dr. Gang Zhao for a preliminary look at the 1987 data. This research was supported in part by contract ARC 90/94-140 "Action de recherche concertée de la Communauté Française" (Belgium) and by the Belgian Programme Service Centres and Research Networks initiated by the Belgian State, Prime Minister's Office, Science Policy Programming.

References

- Magain, P., Surdej, J., Vanderriest, C., Pirenne, B., Hutsemékers, D.: 1992, *The Messenger*, **67**, 30.
- McLean, I.S.: 1989, *Electronic and computer-aided astronomy: from eyes to electronic sensors*, Chichester: Ellis Horwood Ltd.
- Schwarz, H.E., Abbott, T.M.C.: 1993, *The Messenger*, **71**, 53.

CCD Linearity at La Silla – a Status Report

T.M.C. ABBOTT and P. SINCLAIRE, ESO, La Silla

We believe that the non-linearities reported above by Gosset and Magain arise from a combination of two effects. First are the non-linearities reported in Schwarz and Abbott (1993), resulting from a failure in some new A/D converter chains in the Generation III CCD controllers. Secondly, in the process of replacing these converters, we discovered that many of our RCA CCDs exhibited some intrinsic non-linearities which may

be related to the age of these devices. Unfortunately, we do not have adequate test data to demonstrate that our RCA CCDs were ever linear to better than 1 %, but they were certainly non-linear to as much as 8 % over their full dynamic range before March of 1993. At this time, we determined that we could reduce these non-linearities to acceptable levels by careful adjustment of the bias level of the output FET's drain vol-

tage. It was found that a fraction of a volt may have a significant effect on the linearity. All RCA CCDs required adjustment, except RCA#13.

Below is a list of our CCDs and the most recently measured or most representative degree of non-linearity. For the RCA CCDs, data prior to adjustment of the output drain bias voltage is included. Non-linearities are expressed as the fractional amplitude of any trends in

CCD Name	Telescope & Instrument	Date	Nonlinearity (%)	Range (e^-) of Measurement	Comments
RCA#5	0.9-m Adapter	22/2/93	3	180,000	Effect unrepeatable CCD retired 3/93
GEC#7	0.9-m Adapter	3/3/93	1.3	55,000	CCD retired 12/92
RCA#8	2.2-m Adapter	19/3/93	6 < 0.6	75,000 62,000	$V_{od} = 17.0V$ $V_{od} = 18.5V$
RCA#9	CAT CES Short	19/3/93	8 < 0.7	100,000 73,000	$V_{od} = 16.0V$ $V_{od} = 18.0V$
RCA#13	1.52-m ECHELEC	6/4/93	< 0.5	120,000	$V_{od} = 21.0V$ No adjustment necessary
TH#19	2.2-m EFOSC II	18/4/93	< 0.1	60,000	
FA#24	1.52-m B & C	13/4/93	< 0.5	90,000	
TK#25	NTT SUSI	19/6/93	~ 1	200,000	
TK#26	3.6-m EFOSC I	11/8/93	~ 0.5	115,000	
TK#28	1.54-m Adapter	11/6/93	< 0.5	110,000	
TK#29	0.9-m Adapter	4/8/93	~ 1	260,000	Temporary location
FA#30	CAT CES Long	11/8/93	< 0.5	47,000	Non-linear transfer curve*
TK#31	NTT EMMI Blue	24/7/93	< 0.2	150,000	
TK#32	3.6-m CASPEC	20/12/92	< 0.25	140,000	
TK#33	0.9-m Adapter	15/5/93	< 0.5	465,000	Temporarily out of service
LO#34	NTT EMMI Red	6/3/93	< 0.2	42,000	

* Although FA#30 has a linear response to incident light, we have discovered a noise source in this system which is proportional to the signal level; work continues to identify its cause.

count rate over the measured range. Most of the linearity tests were performed using a beta light placed in front of the CCD, a few utilized an LED pre-flash light, powered with a stable, low-noise power supply.

Please note that these results are expressed in terms of the maximum ob-

served non-linearity. In most cases, the linearity was measured over the full, useful dynamic range of the CCD. The extent to which an observer's data will be affected is dependent on the fraction of the CCD's dynamic range which was used for the observations; normally, the effect will be insignificant. In those few

cases where the non-linearity may affect observations, work continues to correct the situation.

Reference

Schwarz, H.E. and Abbott, T.M.C., 1993 *The Messenger* 71, 53.

The Magellanic Clouds and the VLT

J. LEQUEUX, *Observatoire de Paris-Meudon and Ecole Normale Supérieure, France*

The Magellanic Clouds do not need to be presented to the readers of the *Messenger*! I wish however to remind them of their interest in general:

(1) they are the closest galaxies of a type different from our own Galaxy;

(2) they are sufficiently close for detailed studies, similar to many of those which can be done in our Galaxy;

(3) they are relatively small systems compared to their distance, thus all the objects they contain are more or less at the same (known) distance; moreover, interstellar extinction is generally small; these properties make the Magellanic Clouds especially interesting for studying objects whose distance is difficult or impossible to obtain in our Galaxy (giant stars, AGB and post-AGB objects including planetary nebulae, symbiotic and other strange stars, X-ray binaries, novae, etc.);

(4) the abundances of heavy elements are different from those in our Galaxy; this allows to study the formation and evolution of stars as a function of abundance;

(5) linked to these differences in abundance, the properties of interstellar matter (ISM) in the Clouds are strongly different from those of the Galactic ISM.

It is obvious that the largest telescopes of the future like the VLT will be of much interest for Magellanic Cloud studies, since they will already be of interest for many Galactic studies. My goal in this article is to review some areas where the VLT will make possible considerable progress in our understanding of the Magellanic Clouds. The present study bears heavily upon a number of recent reviews by myself and by others, and upon the following books entirely devoted to the Magellanic Clouds: IAU Symposium No. 108; IAU Symposium No. 148; *Recent Developments of Magellanic Cloud Research* (1980, K.S. de Boer, F. Spite & G. Stasinska, eds., Observatoire de Paris); *New Aspects of Magellanic Cloud Research* (1993, B. Baschek, G. Klare & J. Lequeux, eds. Springer-Verlag, Berlin). I will make reference to some of the VLT instrumentation: for a general presentation see D'Odorico et al. 1991, *The Messenger* 65, 10. For the presentation of the 4 instruments under construction see Lenzen & von der Lühne 1992, *The*

Messenger 67, 17 (CONICA, the high-resolution near-IR camera); Appenzeller & Ruprecht 1992, *The Messenger* 67, 18 (FORS, the focal reducer/low dispersion spectrograph); Moorwood 1992, *The Messenger* 70, 10 (ISAAC, the infrared spectrometer and array camera); Dekker & D'Odorico 1992, *The Messenger* 70, 13 (UVES, the UV-visual echelle spectrograph). The multi-fiber spectrograph FUEGOS is in Phase A only and no description is generally available yet.

Structure and Kinematics of the Magellanic Clouds

In spite of much effort, the structure of the Magellanic Clouds is not yet completely understood especially for the SMC which has a very irregular shape. The SMC contains up to 4 different gaseous components with different radial velocities and associated young stellar populations, but their relative location in depth and their distances are not well known. Interstellar absorption lines can show which component is in front of the studied star, but there are not yet enough such measurements due to the faintness of the suitable stars; the VLT will allow fast observation of interstellar lines (especially the sodium lines) in front of many stars; the most suited instrument will be UVES and also FUEGOS in its high-resolution mode ($R = 30,000$, enough for a kinematic study). However this does not give distances. They have to be obtained from cepheids using their period-luminosity relation preferably in the infrared. Measurement of the mean radial velocity of each cepheid will allow to know to which component it belongs. Present attempts at using this method have not been fully convincing for lack of photometric and radial velocity measurements covering evenly the period of the cepheid. While the photometry part of this programme does not necessarily require a very large telescope, the radial velocity one does, using correlation methods, if one wishes to observe a large number of cepheids. FUEGOS appears most adapted to this programme which would require an enormous amount of telescope time with single-object spectrographs. As a very important by-product, this pro-

gramme will supply a data base for our understanding of the cepheid phenomenon. Similar interstellar absorption line and cepheid studies will also be interesting for the LMC: absorption lines in the LMC often show multiple velocity components, the origin of which is not well understood, and the cepheids will allow a direct measurement of the inclination and of the shape of the disk of the LMC.

Another topic of great interest is the kinematics of the old populations in the Magellanic Clouds. While the kinematics of the young population is well understood, that of the older one is much more difficult to study. Objects like planetary nebulae and carbon stars will yield the kinematics of intermediate-age populations: from what we know, they do not seem to differ much from that of the young populations. However the old clusters of the LMC seem to have a different kinematics from the younger clusters, but this observation is at the limit of the present telescopes and deserves confirmation with the VLT. We know almost nothing of the kinematics of the halo stars of both Clouds and this will be a new field to open with the VLT. Presumably FORS and FUEGOS are most suited for such studies.

Finally the VLT is needed for studying in detail the stellar population and (via observation of interstellar absorption lines on background objects) the interstellar matter in the bridge which connects the two Clouds and in the Magellanic stream. While young stars are known to exist in the Bridge, no bona fide member star has been found in the Stream. This may point to different origins, the Bridge being a tidal feature or at least having experienced a tidal perturbation responsible for star formation, and the Stream being perhaps due to tidal stripping. Observations with the VLT should allow to settle this long-debated question.

Interstellar Matter

Interstellar matter in the Clouds is very different from that in our Galaxy: the abundance of heavy elements is 4 and 10 times smaller in the LMC and the SMC respectively, the dust-to-gas ratio

is smaller in the same proportions and the properties of dust are qualitatively different (smaller absorption bump at 200 nm, higher far-UV absorption, smaller far-infrared emission by very small dust particles). The higher far-UV radiation field together with the lower abundance of dust produce an increased photodissociation of molecular hydrogen, of CO and of other molecules which affect considerably the properties of the molecular clouds. I do not clearly see observations of the ISM which could be unique to the VLT, but it is clear that the very large sensitivity of this instrument will allow improvements with respect to what is done at present, for example by densifying the observations by FUEGOS of interstellar absorption lines allowing studies of the fine structure of the ISM, or by making easier visible and infrared observations of star-forming regions, interfaces between ionized and neutral gas, supernova remnants, etc. The latter studies will make use of FORS, ISAAC and perhaps CONICA. An interesting possibility which requires both high sensitivity and excellent image quality is to investigate through extinction (star counts and photometry) the internal structure of the molecular clouds (not accessible to the SEST). This will check if the properties of the molecular clouds in the Magellanic Clouds differ from those in our Galaxy only due to the differences in photodissociation as explained before, or due to differences in structure.

Stellar Populations and Star Formation

Due to various causes (not always well understood) the properties of stellar populations in the Magellanic Clouds differ from those in our Galaxy. For example, the Clouds like M 33 and a few irregular galaxies are known to contain young globular clusters which are lacking in our Galaxy. The youngest of all could be the dense clusters of O stars that ionize the biggest HII regions (30 Dor in the LMC and to a lesser degree N 66 in the SMC). Of course the dynamical study of those young clusters and also of those of intermediate age is of high interest since in our Galaxy only old globular clusters are seen. Such studies have started in particular with the ESO telescopes, but they will be made considerably easier by the VLT and will reach stars of earlier spectral type for which accurate radial velocities are more difficult to measure. Due to crowding one will have to use a medium-to-high resolution field spectrograph. Once again one will use FUEGOS in the compact fiber mode for the centre of the cluster, or in the normal mode for the rest of the cluster.

One very important goal of Magellanic Cloud stellar observations is to help understanding stellar evolution. While sophisticated models exist for this evolution, the physics introduced in these models is to a large extent arbitrary and as a result this evolution is still very poorly known: for example the evolutionary status of the progenitor of SN 1987A is still controversial. For low- and intermediate-mass stars, high-quality photometric and spectroscopic observations of individual stars in clusters of different ages and metallicities will help tremendously understanding their evolution; although much is presently being done with 4-m class telescopes, the VLT will allow doing more and better. For massive stars, the observational problem is more difficult. The only way to progress seems to locate the observed massive stars in a "theoretical" (L vs. T_{eff}) HR diagram, to measure their densities in the different parts of the diagram, to study surface abundance anomalies due to internal mixing, then to confront these observations with the predictions of models. It is also necessary to measure the strength of the stellar wind which plays an enormous role in the evolution. All this should be done for stars with different metallicities in order to understand the role of metallicity in the internal evolution and in the acceleration of the wind. The Magellanic Clouds are ideal places for such investigations. They contain a sufficient number of massive stars for statistical studies, they have very different metallicities and a comparison will be possible between a complete sample of stars belonging to Galactic open clusters and associations. One problem is to build the sample, requiring fine spectral classification of stars first selected by colours, and another one is to secure the high-resolution spectroscopy necessary for determining the abundance of carbon and nitrogen from their rather faint lines. It is also desirable to study the HR diagram down to 6–8 solar masses where the transition between the two main regimes of stellar evolution occurs. A 6-solar-mass star on the main sequence has $V = 18$ in the SMC, and it is clear that the VLT is necessary for high-resolution, high-quality spectroscopy of such a star. As one wants to perform this kind of analysis for several hundreds of stars in each cloud, a multi-object spectrograph is required, once again FUEGOS.

Apart from this, the VLT will be ideal for detailed observations of all sorts of more or less exotic objects whose study in the Galaxy is hampered by the lack of distance information. This fauna is too

varied to be discussed here in any detail. It seems to me that the AGB and post-AGB stars are the most interesting class of such objects. Their evolution is still very poorly known in spite of much effort – in part due to the lack of distance information in our Galaxy – and may depend on metallicity. Once again, a multi-object spectrograph is appropriate as the surface density of most classes of such objects (e.g. carbon stars) is relatively large.

Finally, observing star formation in a different context than the galactic one is a very exciting perspective. Already it has been demonstrated that massive stars occur in small compact groups in the Clouds, but we would like to know why and how, and also to know more about the formation of lower-mass stars. For this, one will use the VLT mainly in the near- and mid-infrared using ISAAC and the foreseen mid-IR imager/spectrometer. Such studies are still in their infancy in the Magellanic Clouds (only a few images in the K band have been published, for instance). While it is hard to predict what the outcome of future VLT studies will be in this field, it would be very surprising if the results would not be of great interest.

Chemical Abundances and Evolution of the Magellanic Clouds

In spite of being a relatively ancient topic, this is a very controversial one. Determinations of the abundances of heavy elements in different classes of young objects in the Magellanic Clouds often give discrepant results: while HII regions exhibit a remarkable degree of homogeneity in either Cloud, indicating efficient mixing of the interstellar matter during the evolution of the Clouds, young stars like hot or cold supergiants have been claimed to have rather different abundances between them and with the HII regions. If real, this result is very difficult to understand. However there are some doubts about determinations of abundances in supergiants, which are made difficult by the strong non-LTE effects and by problems in measuring effective temperature, gravity and interstellar extinction. One would very much like to have such determinations made in stars with higher gravities. Unfortunately these stars are faint in the Magellanic Clouds and generally out of reach of the present telescopes. This will be a very important programme for the VLT, presumably using UVES or FUEGOS. I will not specifically discuss the evolution of the Clouds, but it is underlying most of the previous discussion.

Conclusion

I hope to have convinced the reader that the VLT will allow very significant advances in our knowledge of the Magellanic Clouds, and perhaps more

importantly of stellar evolution in general: I would like to stress once again how unique the Clouds are for studying the various stages of the evolution of massive stars and the late stages of evolution of stars of all masses. The most

useful of all the foreseen focal-plane instruments for that purpose appears to be FUEGOS, and I very much hope that its construction will not be unduly delayed by budgetary restrictions.

Nuclei of Non-Active Galaxies with the VLT

M. STIAVELLI, *Scuola Normale Superiore, Pisa, Italy*

1. The Physical Properties of Galactic Cores and Nuclei

Since the very beginning of extragalactic studies it was realized that galaxies have very compact central parts. However, only in the last decades it has been fully appreciated that atmospheric seeing was the major limiting factor for the angular resolution that could be achieved from the ground and that, in turn, the observed core properties were often just artifacts of the limited resolution available (Hoyle 1965; Schweizer 1979, 1981). Of the two galaxies known in the late 1970s with truly resolved cores, one, M31, had a nuclear, very dense, spike roughly in the centre of its broader core, while the other, the radio galaxy M87, presented a central spike in the light profile, which was interpreted as due to an unresolved non-stellar point source. Despite this, the notion of *isothermal cores* was introduced, i.e. of cores with a light profile that flattens to a plateau at small radii. This was partly inspired by theoretical arguments, in practice it reflected precisely the kind of profile that seeing effects were producing. On the other hand, spectacular phenomena like the M87 optical jet opened up the issue of the nature of the nuclear energy sources in galaxies and of the possible existence of nuclear supermassive black holes. It is very intuitive that a supermassive black hole would affect the stellar orbits in the core, producing spikes in velocity dispersion and nuclear rotation curves with steep gradients. Theoretical arguments showed that a black hole would influence also the core light profile, by capturing stars in a very concentrated cusp detectable in the light profile. Indeed, both indicators were used by Young and collaborators (1978, 1979) to claim the existence of a central black hole in M87. Unfortunately, even models without a central black hole can be constructed able to give adequate fit to the data (Binney and Mamon 1982).

Developments in the following years were in a way frustrating. On the one

hand the red herring of isothermal cores was brought up and followed by several investigators, who found less and less truly isothermal cores as the resolution increased. Even in the late 80s it was possible to find statements concerning a broad subdivision of galaxies into those with isothermal cores and those without. On the other hand, dynamicists were able to produce (often contrived) models able to fit the observed kinematic and photometric profiles of galaxies without the need of a supermassive black hole. Unfortunately, the intrinsic freedom allowed by stellar dynamics

equilibrium configurations and the availability of powerful and flexible modelling techniques, makes it difficult to obtain an irrefutable proof of the existence of a black hole in any given galaxy (see, e.g., Kormendy 1993). Although the central black hole hypothesis is probably the simplest to explain objects like M87, it is important to obtain such a proof by improving resolution and accuracy of observations.

Galaxy cores are also important as benchmarks for theories of galaxy formation. Great progress has been made in this field, often guided by our interpre-

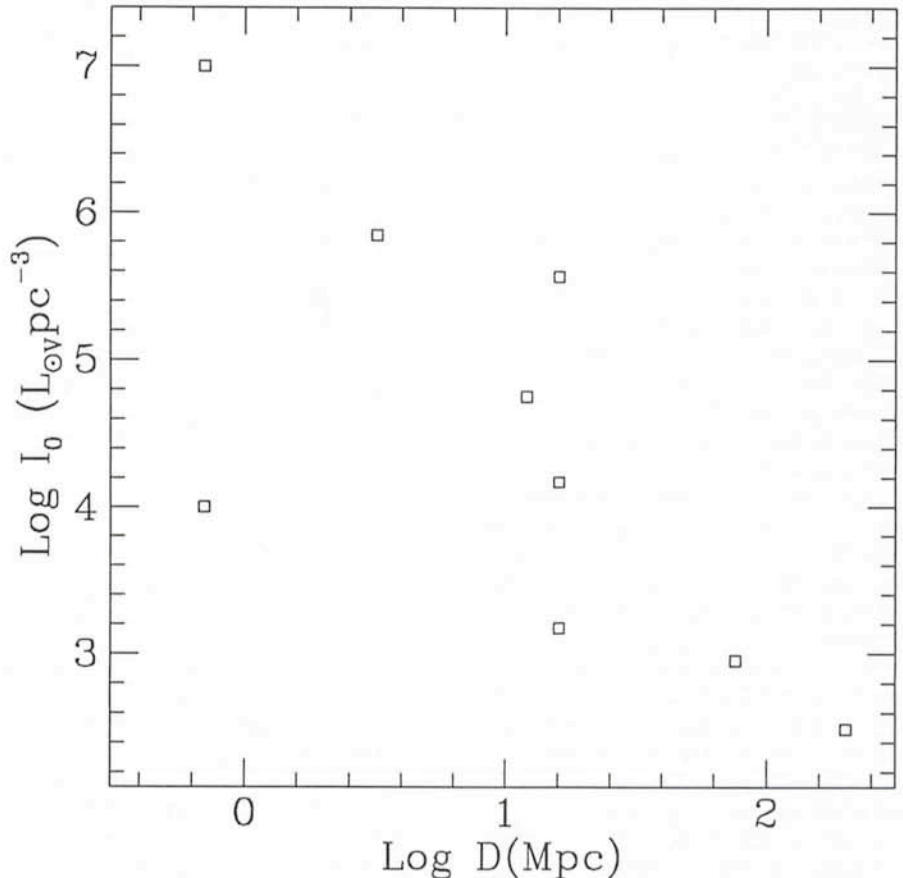


Figure 1: The apparent central light density of galaxies appears to anticorrelate with galactic distance. This is a resolution effect also present in Hubble Space Telescope data (Crane et al. 1993).

tation of what the core properties were and how they originated. For instance, the discovery of counter-rotating and decoupled cores was seen as a proof that merging and accretion is occurring, with the remnants of tidally destroyed companions settling into the cores of larger galaxies with their residual angular momentum. Better data and new indicators have shown that this is probably not the case, since (at least some of) these decoupled nuclei turn out to be much more metal rich than the main galactic body (Bender and Surma 1992, Davies et al. 1993), in opposition to the dissipationless merging prediction. Should all decoupled cores have the same property, what was seen as a successful prediction of late-time merging would turn into a fatal blow to this idea. Most likely, further strong constraints on the formation of galaxies will come from deeper studies of their cores.

2. Progress with the Current Generation of Telescopes

Cores are the brightest parts of galaxies. In addition, the desire of having a spatial resolution as high as possible forces us to consider relatively nearby objects. Why then should one use a large telescope? Shouldn't telescopes of the 3.6-m class or even smaller be adequate? This question has two opposite aspects.

Experience shows that typical integration times with e.g. the SUSI camera at the 3.5-m NTT or the stand-by camera at the 2.5-m NOT are, respectively, 2 and 5 minutes. Therefore, the use of these cameras often leads to low-efficiency observations, since the integration time is shorter or comparable to the read-out time. From this point of view, and considering that so far the angular resolution which could be obtained was dictated by atmospheric seeing rather than telescope diffraction limit, a large telescope does not seem to be necessary. In fact, at the CFHT it is a well established procedure to diaphragm the main mirror reducing its size to 1.8 m to improve optical quality and angular resolution.

From what we have seen, one could therefore argue that a small telescope in space would be better than a large telescope on the ground. This is not true. Indeed, it is now becoming apparent that many galaxy cores remain unresolved even at the HST resolution. Crane et al. (1993) have observed a sample of 10 objects with the FOC camera. They find an anticorrelation between the central density and the distance of the galaxy (see Figure 1), well described by a power law with power 1.8. Since a power of 2 would indicate that the core properties

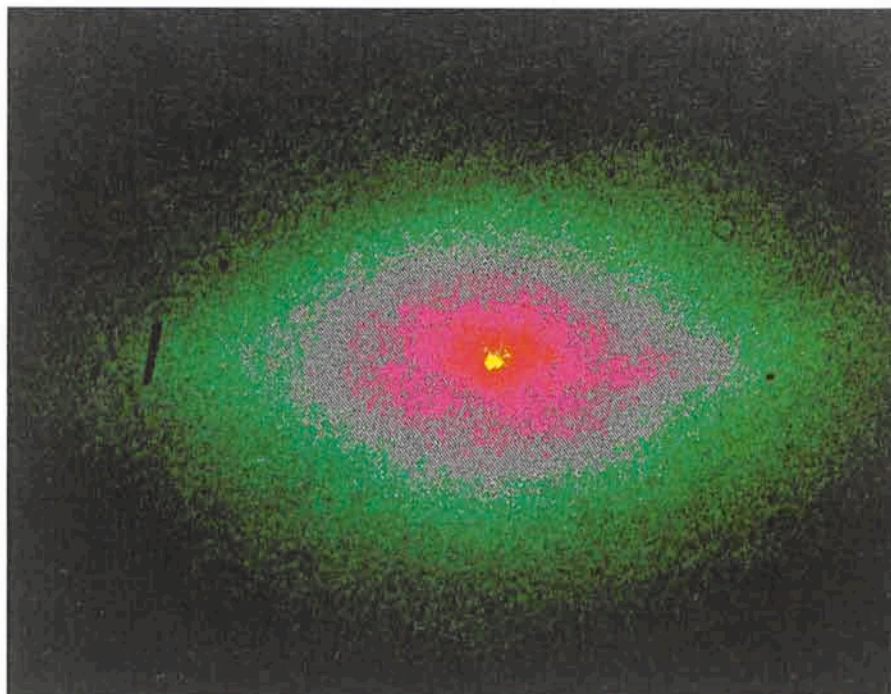


Figure 2: *Hubble Space Telescope FOC image at 3420 Å of the core of the Sombrero Galaxy (NGC 4594). Visible are the point-like nucleus as well as the dust lanes and patches (from Crane et al. 1993).*

are just the result of a finite resolution effect, we have to conclude that even at their resolution of about 0.05 arcsec FWHM the derived core properties are strongly affected by resolution. It is unlikely that this will be changed significantly by COSTAR, since the gain in resolution will only be moderate. In addition, some cores, and perhaps the most interesting ones, like those of NGG 4261 (Ford et al. 1993), of Sombrero (NGC 4594, Crane et al. 1993, see also Figure 2), and of NGC 3557 (Zeilinger et al. 1993), contain dust. This is a reason to shift the preferred observational wavelengths to the Near Infrared. Note that after COSTAR only the UV (and dust!) sensitive FOC will sample the Hubble Space Telescope PSF properly.

Not only direct images but also long slit spectra are desired. Indeed, spectra allow one to derive stellar kinematical information, stellar line-strengths, and ionized gas kinematics and metal content. These data are essential in understanding dynamics and formation of cores.

The need of both high spatial and wavelength resolution forces one to use very narrow slits and high dispersions, at the price of reducing the signal to noise. As an example, a one-hour spectrum of the core of NGC 1399 with EMMI Red Arm at the NTT, with 0.5 Å resolution, only yields a signal to noise of about 30 in the core, adequate to derive kinematical information but not enough to carry out more sophisticated

analyses involving the study of line profiles. The latter will probably be fundamental in proving the existence of a black hole in a given galaxy since they probe directly the stellar distribution function. Another example is the rotating gas disk in the nucleus of NGC 3557 identified by Zeilinger et al. (1993). The disk was detected in a spectrum taken at the ESO 3.6-m telescope with a resolution of 1 Å per pixel, by resolving the [NII] (λ 6583.4 Å) into two wings both appearing in the core of the galaxy. East and west of the nucleus only the approaching and receding wings, respectively, are observed, thus producing a typical-looking rotation curve. This spectrum already gives strong hints for the existence of a central black hole in this galaxy (Zeilinger et al. 1993). A further attempt to derive more accurate line shapes by using the echelle spectrograph CASPEC at the 3.6-metre telescope failed because even with 4 hours of integration not enough photons were collected. For very high resolution work, a 3.6-metre-class telescope is simply too small to observe galaxy cores with typical B surface brightness of 17 magnitudes/arcsec² or more.

3. Developments with the VLT

A number of factors concur to make the VLT (see Figure 3) a superb telescope for a variety of applications: the site, the size of the unit telescope, the instrumental developments. Here we

will consider separately the contribution that CONICA, FORS, ISAAC, and UVES will make to the study of galaxy cores.

3.1 CONICA

CONICA is the Coudé Near-Infrared Camera (Lenzen and von der Lühse 1992). It is the prime instrument for exploiting the high resolution potentially available at the single VLT unit. In fact, the diffraction limit of a single VLT mirror is for a given wavelength almost 4 times as small as for the Hubble Space Telescope. With adaptive optics it is expected that the diffraction limit will be reached in the Near Infrared for $\lambda > 2.2$ micron and that partial correction will be attempted at 1.25 micron. The PSF for the case of partial correction is characterized by a diffraction limited core with most of the power in the PSF wings, i.e., a situation similar to that of the pre-COSTAR HST, so that one will be able to exploit all techniques developed for HST data. The CONICA Camera will be able to sample with 0.012 arcsec pixels the PSF at 1.25 micron, yielding a resolution of 0.032 arcsec FWHM, and with 0.024 arcsec pixels the PSF at 2.2 micron, yielding a (fully corrected) resolution of 0.057 arcsec FWHM. Thus effectively exceeding, with well sampled images, the spatial resolution provided by HST at optical wavelengths. The gain of a factor 2 in resolution over HST is certainly welcome, but very important is also the ability to take such high resolution images in the Near Infrared, where the effects of obscuration by dust are much less important.

The major problem of adaptive optics at the VLT, at least until the technique of artificial reference stars will be introduced, is that only a small fraction of galaxies will be suitable for such a study, since adaptive optics requires the presence of a reference star (brighter than about 15) within the isoplanatic patch, i.e. at, say, less than 10 arcsec from the target. Luckily, many galaxies turn out to have central point sources (Lauer et al. 1991, Crane et al. 1993). For a number of objects including, e.g. M87, the central (non-thermal) point source is bright enough to serve as a reference star. When this is possible, this is an optimal observing mode since reference star and target coincide in position. CONICA offers other possibilities for galaxies without a suitable reference star near the core. These techniques include speckle imaging and various forms of coaddition. A basic requirement is that an object in the field of view is bright enough to get enough photons in a very short integration time to, e.g., allow for the measurement of the frame reference coordinates and carry out a

Layout of the VLT Observatory

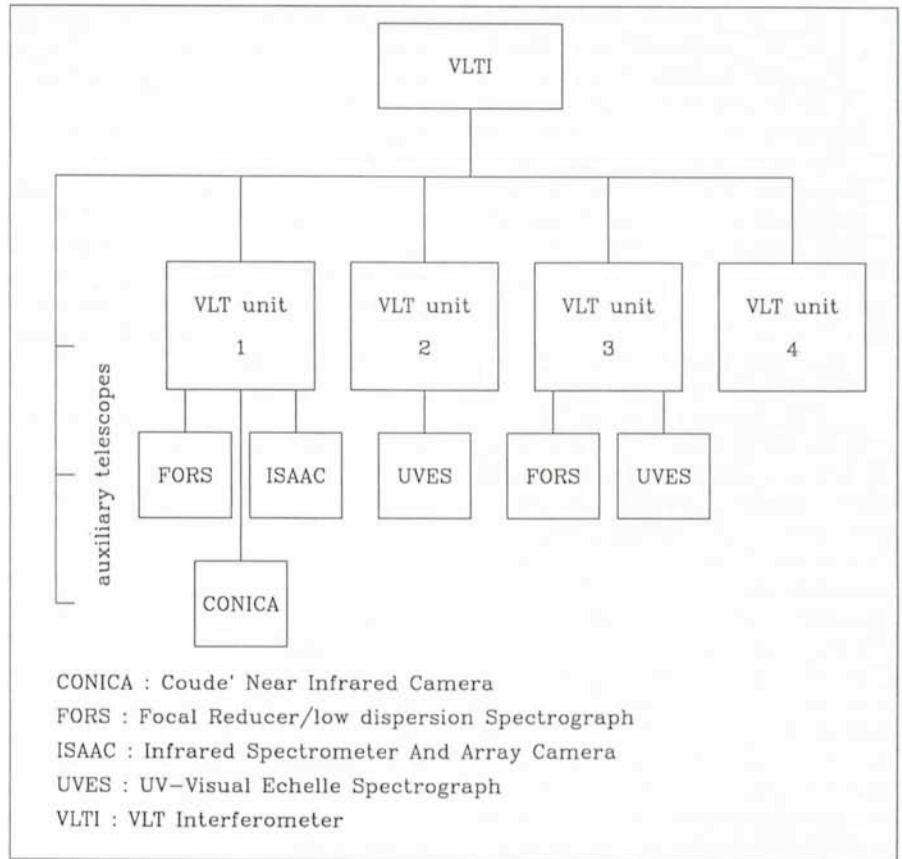


Figure 3: Schematic drawing of the VLT with the instruments considered in the text.

“shift and add” operation. A typical elliptical galaxy core with surface brightness $\mu_J = 13.8$ and $\mu_K = 12.7$ will be detected as 20 photons/sec/pixel (0.012 arcsec/pixel) in the J band and as 110 photons/sec/pixel (0.024 arcsec/pixel) in the K band. These fluxes are too small to use sampling rates larger than 10 Hz. However, many galaxies turn out to be brighter by about a factor 10 at milliarcsec scales compared to the arcsec scales; in addition, many contain point sources brighter than 20 in V. The latter are usually too faint to serve as reference stars for adaptive optics but can be used to align the images. Globular clusters may also be suitable for similar purposes, provided some are present in the restricted FOV of 3 arcsec in J and 6 arcsec in K.

At lower resolution, the capability of extending the observing wavelength to 5 micron is also very important, especially since no high-resolution data are available for galaxies at these wavelengths. In the L and M bands respectively, a diffraction-limited resolution 0.093 and 0.12 arcsec FWHM will be obtained for a significant fraction of the sky, thanks to the less demanding requirements of adaptive optics at these wavelengths. In addition to the high res-

olution achieved, these wavelengths will allow unique opportunities for those objects with cores obscured by dust lanes, like, e.g., NGC 5128.

3.2 FORS

FORS is a focal reducer with parallel beams (Appenzeller and Rupprecht 1992). For imaging application the setup of choice will be the High Resolution mode with 0.1 arcsec/pixel. Such a pixel size should allow a suitable sample of the typical seeing conditions at the VLT Observatory. The large collecting area of the VLT unit however would imply very short exposure times and therefore inefficient observations. Apart from the resolution benefits in using very short exposures, we therefore expect that the use of FORS in the study of cores will primarily be spectroscopic. With a grism and narrow slits, it will be possible to obtain spectra with a resolution of about 100 Å/mm of the core regions of galaxies. In good seeing, with a 0.4 arcsec slit, spectra with 2.5 Å per pixel and S/N 200 in the centre will be obtained in one hour for typical galaxy cores. Such a resolution is adequate for deriving accurate kinematical properties (errors smaller than 20 km/s in radial velocity and

velocity dispersion), line profiles, and absorption line strengths. Therefore, with a moderate amount of telescope time, it will be possible to make a complete two-dimensional mapping with high spatial resolution of the cores of nearby galaxies. Such a mapping will allow us to construct an accurate dynamical model for the core and also to infer its stellar population properties and possibly its star formation history.

3.3 ISAAC

The Infrared Spectrometer and Array Camera (Moorwood 1992) is another Near-IR instrument for the VLT. The instrument has a relatively large field (up to 2 arcmin) and medium spectral resolution capabilities. In imaging applications, particularly interesting would be the inclusion of the tip-tilt option of the secondary mirror. Such control should allow diffraction limited imaging in the L and M bands, where the images would however be undersampled by the 0.125 arcsec pixels. Despite the problems of undersampling (possibly cured by a reduction in pixel size with the use of detectors of a new generation) imaging at these wavelengths, and also in J and K, with ISAAC can be an important complement to CONICA given the larger field and the higher sensitivity resulting from being at the Nasmyth focus rather than at the coudé. The use of a shift-and-add technique should in any case guarantee very good spatial resolution at the longer wavelengths. The expected count rates from a typical galaxy core are 4000 and 5600 counts/pixel/second, respectively in the J and K bands. They should allow integration times shorter than 0.1 second.

Especially interesting is the possibility of obtaining long-slit spectra at a resolution of 5000 (for a 1 arcsec wide slit). Indeed, Near-IR spectroscopy of galaxies is a relatively new field which will benefit considerably from the availability of ISAAC at the VLT. The observation of CO lines is perhaps the only way to derive central velocity dispersions for heavily obscured cores like NGC 5128. In addition, important applications will be possible also in stellar population studies.

3.4 UVES

The prime instrument for the study with high wavelength resolution of both line profiles from stellar absorption lines and ionized gas emission lines will be represented by the UV-Visual Echelle Spectrograph (Dekker and D'Odorico 1992). This instrument will profit from the size of the VLT and allow for observations which have not been possible so far.

In good seeing, with a 0.4 arcsec slit exploiting the 0.19 arcsec/pixel of the blue arm, one will be able to obtain high spatial and spectral resolution. Stellar kinematics in the blue arm will be carried out preferably on the CaII H + K band and on the G band. The slit length will have to be limited at 8 arcsec to avoid order overlapping. The overall efficiency should be around 8 per cent. For a galaxy of typical surface brightness $\mu_B = 17.6$, a signal-to-noise of 20 will be reached with two hours of integration. Such a signal to noise would be adequate to derive kinematical information. It appears that several galaxy cores may have low velocity dispersions in the range of the few tens km/s (see, e.g., M33), such cores would require the use of UVES to be detected outside the local group.

The red arm would allow for a higher sensitivity. With a 0.7 arcsec slit and 0.31 arcsec/pixel one could obtain high resolution spectra of the MgI blend and of the Ca + Fe E band, which are the standard regions used for stellar kinematical measurements. A signal to noise exceeding 30 should be obtained with two hours of integration.

Longer integrations will probably be of interest to improve the accuracy of the measurement but also to allow for a more reliable determination of the line profiles, which will give a direct observational constraint on the stellar distribution function in the parent galaxy. Such a measurement will have an impact both on the problem of galaxy formation and on that of the presence of central black holes, since the various models make very clear and specific predictions on the distribution function properties.

One possible additional application for such an instrument is in the direct measurement of the gravitational potential in galaxy cores. Such a measurement is made possible by gravitational redshift, which for a big galaxy is expected to be of the order of 10 km/s. The effect has already been detected in accurate radial velocity profiles (Stiavelli and Setti 1993) but it would require a very high resolution and signal to noise to actually measure the potential variation in the core, i.e. reach a velocity resolution below 1 km/s.

In addition to stellar kinematics, gas emission lines will also be measured and used to derive information on the physical properties of gas in the dust and gas disks often seen in the centres of ellipticals. This is especially important since these dust rings appear to be involved in the fuelling of nuclear activity in normal galaxies and could also be the progenitors of the kinematically decoupled stellar disks observed in some galaxies.

4. Further Desirable Instruments

The VLT interferometer (Beckers and Merkle 1991) would represent another step further in terms of angular resolution, since it should allow a resolution of about 0.004 arcsec, corresponding to about a factor 10 improvement over HST. It is very hard at this stage to predict the kind of impact that such an instrument would allow. It is perhaps significant to note that it would allow for galaxies in the Virgo Cluster a resolution in physical distance scales comparable to what can be obtained now with the Hubble Space Telescope on M32. If M32 remains unresolved with HST, it is extremely important to understand if it is an extreme, not too significant, object or, rather, a typical core for low mass galaxies. Do NGC 7457 (Lauer et al. 1991) and NGC 4621 (Crane et al. 1993), both unresolved with HST, have similarly compact nuclei? The major limitation for such a study will again be the availability of a suitable reference star. It should be noted that the quasi point-like source in M87, for instance, is partially resolved by HST and therefore cannot be used for this application.

As we have seen, the instruments already foreseen for the VLT guarantee enormous improvements with respect to what can be done now from the ground or from space. Is there any other improvement possible? The need of being able to take high spatial and frequency resolution spectra could be satisfied with a Fabry-Perot spectrograph. Such an instrument could allow for the measurement of the velocity dispersion and rotation velocity fields of galaxy cores. This kind of instruments has been so far limited by technical reasons and by their relatively low sensitivity, requiring the use of a very large telescope.

References

- Appenzeller, I., Rupprecht, G., 1992, *The Messenger*, **67**, 18.
- Bender, R., Surma, P., 1992, *AA* **258**, 250.
- Beckers, J.M., Merkle, F., 1991, *The Messenger*, **66**, 5.
- Binney, J., Mamon, G., 1982, *MNRAS* **200**, 361.
- Crane, P., Stiavelli, M., King, I.R., et al., 1993, *A.J.* in press.
- Davies, R., Sadler, E.M., Peletier, R., 1993, *MNRAS* **262**, 650.
- Dekker, H., D'Odorico, S., 1992, *The Messenger*, **70**, 13.
- Ford, H., Jaffe, W., Ferrarese, L., van den Bosch, F., O'Connell, R.W., 1993, *STSC Newsletter*, **10**, 1.
- Hoyle, F., 1965, *Nature* **208**, 111.
- Kormendy, J., 1993, in *The Nearest Active Galaxies*, J.E. Beckman et al. Eds.

Lauer, T.R., Faber, S.M., Lynds, C.R., et al., 1991, *ApJ Lett* **369**, L 41.
Lenzen, R., von der Lühne, O., 1992, *The Messenger*, **67**, 17.
Moorwood, A., 1992, *The Messenger*, **70**, 10.
Schweizer, F., 1979, *ApJ* **233**, 23.

Schweizer, F., 1981, *AJ* **86**, 662.
Stiavelli, M., Moller, P., Zeilinger, W.W., 1993, *AA* in press.
Stiavelli, M., Setti, G.C., 1993, *MNRAS* **262**, L 51.
Young, P.J., Westphal, J.A., Kristian, J., Wil-

son, C.P., Landauer, F.P., 1978, *ApJ* **221**, 721.
Young, P.J., Sargent, W.L.W., Kristian, J., Westphal, J.A., 1979, *ApJ* **234**, 76.
Zeilinger, W.W., Stiavelli, M., Moller, 1993, submitted.

From Planets to the Big Bang with High-Resolution Spectroscopy at the VLT

R. FERLET, *Institut d'Astrophysique de Paris, France*

Introduction

Some years ago, M. Harwit showed that most cosmic discoveries were connected with the occurrence of a significant technical step or the opening of a new window on the Universe. Without question, high-resolution spectroscopy associated with very large collecting area will be such a major tool to attack vital astrophysical problems. Beside serendipitous discoveries, there are several areas of research to be investigated with a high-resolution VLT spectrographic capability. The VLT should not miss the opportunity to venture into an almost virgin universe and make discoveries.

Here, we are talking about resolving power R of at least $1-1.5 \times 10^5$, simply because many important pending problems cannot be tackled with lower resolution. Many of these are reviewed in the proceedings of the ESO Workshop on "High Resolution Spectroscopy with the VLT" held in Garching in 1992. We will briefly give here only a few exciting examples of potential achievements in various fields through high-resolution absorption spectroscopy at the VLT.

Technical Advances

Measurements of equivalent widths of interstellar lines (IS) are indeed quite independent of the resolution. However, it is well known that they can yield very large errors on column densities when multiple components are present on the line of sight and when lines are saturated (on the flat part of the curve of growth). The former situation appears very general, even for the short lines of sight of the solar neighbourhood. The latter one is less common, at least for part of the IS lines in the visible spectrum. But both cases will become severe limitations when probing the diffuse IS medium beyond what is currently reachable in the galactic plane with the available telescopes.

Sufficient resolution is required to resolve the velocity structure of the lines of sight. This is the only way to gain information on individual clouds, on average separated by a few km/s, that is now badly needed instead of integrated properties. Amongst physical parameters, temperature is directly accessible only through the intrinsic width of the lines. For purely thermal broadening, the width increases with decreasing mass of the studied ions, and the lightest element having an observable resonance line in the visible is lithium (the lighter elements hydrogen, deuterium and helium show up in the currently unaccessible far UV, except $\text{Ly}\alpha$ observable with the Hubble Space Telescope but which is always heavily saturated and blended). Nevertheless, even through the LiI doublet, IS gas at 1000 K gives a full width at half maximum of 2.57 km/s, requiring already $R > 1.2-10^5$. Higher resolution is mandatory in order to derive true b -values from cooler IS gas, even though careful profile fitting analysis of several lines may help to artificially increase the resolution by a factor of perhaps 2 or so depending on the signal-to-noise ratio. Moreover, using lines of different ions in the same velocity components will allow to also determine any turbulent velocity, another important and poorly known parameter for the dynamics of the interstellar medium.

Astrophysical Considerations: Interstellar Medium

The Li^7 equivalent width for IS diffuse clouds such as those in front of ζ Oph or ϱ Oph in which typical temperature is very likely below 100 K, is of the order of the mÅ, claiming thus for S/N ratios well above 100. Because both stars are bright enough, these two lines of sight are well studied with the ESO CES at La Silla, which has provided $R=10^5$ for more than ten years. The CES is usually fed by a 1.4-m telescope. The jump to

an 8-m-class one will so much increase the number of potential targets that many stars more deeply embedded in cloud cores will become accessible, allowing thus to link the properties of the diffuse clouds currently studied in absorption to those of the denser and colder regions detected in the IR or mm radio range.

A more specific programme would be the measurements of the IS abundances of light elements, in particular beryllium and lithium which are only observable in the visible range around 3130 Å and 6707 Å respectively. The knowledge of their present-day abundances, and even more uniquely of the ratios Be/Li and Li^7/Li^6 , is a key-milestone to severely constrain cosmological scenarios and galactic chemical evolution models. This kind of observations needs extremely high S/N ratios. For instance, IS Li^6 has been recently detected for the first time towards ϱ Oph (Lemoine et al., 1993), thanks to a S/N ratio ≥ 2700 per pixel, implying a limiting detectable equivalent width of 0.043 mÅ (3σ). The resulting Li^7/Li^6 ratio ~ 12.5 is in strikingly good agreement with the meteoritic value which is thought to be representative of the early solar system, and cannot as yet be explained by the most recent and elaborated evolutionary models. This has been achieved after 13 hours of integration time with the CES linked to the ESO 3.6-m telescope via fiber optics, on a $m_v \sim 5.0$ star. The same measurement is going to be published for ζ Oph ($m_v=2.7$) with a S/N ratio above $\sim 7000!$ (see Figures 1 and 2). However, this is restricted to the 4-5 stars on the whole sky which are bright enough but still shining through a dense cloud to enhance the expected column density. It should be done in many individual clouds in order to statistically establish the significance of the first results and to directly test the cosmic ray production of Li; the gain from one VLT unit should even allow to see possible variations in the

supernova rate through IS clouds in other galactic spiral arms.

Measurements in the visible range of molecules like CH, CH⁺, CO⁺ or C² are also of prime importance for interstellar chemistry; they can also yield the carbon isotopic ratio C¹²/C¹³ and the dark clouds temperature (see e.g. Black and Van Dishoek, 1988; Crane et al., 1991; Hobbs, 1973, Vladilo et al., 1993). In fact, requiring very high spectral resolution and S/N ratios, all these abundance studies need to be performed towards more and more distant targets, in very different environments or where galactic gradients become sensitive, or in other spiral arms. In several hours of integration time with the VLT, the most abundant of these species might be detectable in the Magellanic Clouds, which would give access to less processed extragalactic material, to be compared to the more extreme metallicity towards the galactic centre. Equivalent widths of several tens of mÅ in neutral IS sodium at 5890 Å, good tracer of HI, are already gathered at R=10⁵ towards the very brightest Magellanic supergiants with the 3.6-m telescope, but CaII at 3930 Å, providing information on ionization, is just barely feasible at that resolution (Molaro et al. and Vladilo et al., 1993). The use of an 8-m telescope would

allow a much more complete mapping of the Clouds, yielding in particular the still poorly known depth structure of the Clouds.

Astrophysical Considerations: Extragalactic

Another example of the need for resolution in the 10⁵ range at the VLT is the study of the narrow absorption lines in quasar spectra. Just to give two exciting cases, one can first mention the measurement of the cosmic background radiation temperature, T_{CBR}, at high redshifts. Besides black body microwave observations, IS lines from the lowest rotational levels of the CN molecule around 3875 Å have been used for many years to derive the precise CBR temperature at the present epoch (e.g. Palazzi et al., 1992). However, this is the only point determined up to now. According to the Big Bang theory, T_{CBR} depends in a simple way upon the redshift, and its determination at different z would really be a new extremely strong observational argument in favour of the Big Bang. A convenient radiometer for directly measuring the background radiation at earlier epochs would be neutral carbon. The ground state of CI splits into three levels separated by energies of the

same order as kT_{CBR} at z > 0.5, when CI lines show up in the visible range. At such epochs, contrary to the galactic ISM where collisions are much more efficient, CI should be appreciably excited by the CBR. Up to now, because of the lack of resolution available even for the brightest QSOs to resolve the CI line splitting, only an upper limit of 16 K at z=1.776 has been assigned by Meyer et al. (1986). Such measurements in several QSOs' absorption systems at different z are waiting for the VLT.

The second case is the measurement of the deuterium abundance in adequate absorption components of the so-called Lyα forest in quasar spectra. Only directly observable in the far UV, the present-day IS value of the D/H ratio is still controversial since variations might exist in the very local ISM (see e.g. Ferlet, 1992). New determinations are under way with HST, but restricted to very short lines of sight. Furthermore, to go from the IS value to the primordial one – which is of major cosmological significance since it is highly sensitive to the universal baryon density and thus can constrain the density parameter – requires very uncertain evolutionary models. While early models suggested a relatively low astration of deuterium (a factor 2–3), the accumulation of obser-

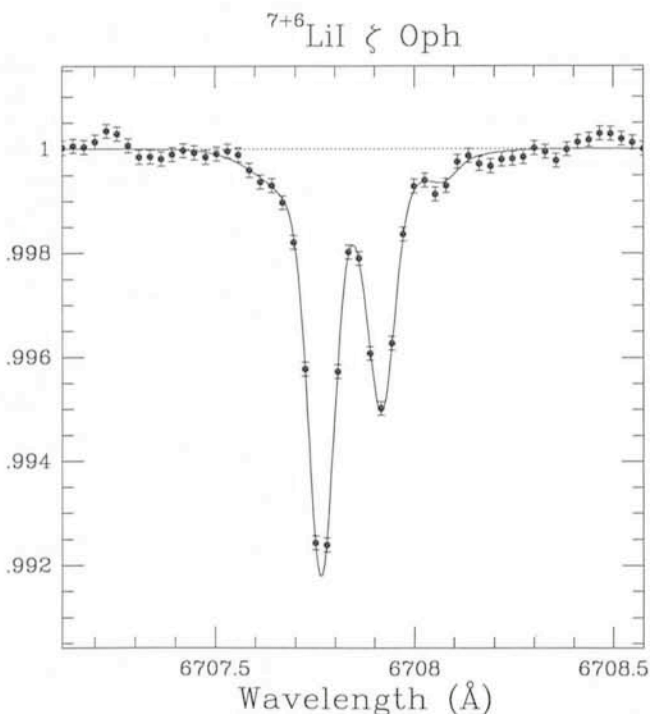


Figure 1: Interstellar ^{6,7}LiI absorption doublets toward ζ Oph. The data were gathered in June 1990 and June 1992 at ESO using the CES linked to the 3.6-m telescope via a fiber link. The total integration time is 15h., the resolution is $\lambda/\Delta\lambda=100,000$, and the signal-to-noise ratio 7500 per pixel, or 11 per resolution element, giving a 3σ limiting detectable equivalent width of 18 μÅ!

The solid line represents the fit to the data with two interstellar absorbing clouds on the line of sight, and taking ⁶Li and ⁷Li absorptions into account. Ordinates are arbitrary units; error bars are 1σ.

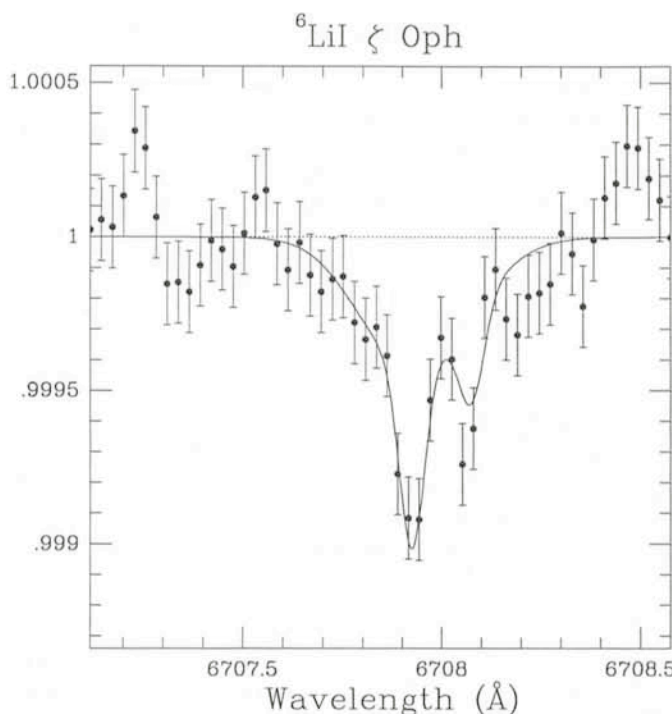


Figure 2: Same as Figure 1, but the calculated ⁷Li absorption was subtracted from the data points. These residuals thus reveal clearly the ⁶Li absorption doublet. The depth of this doublet is less than 0.1% of the continuum (see ordinates). The solid line represents the previously calculated ⁶Li fit to this profile. Error bars are 1σ.

vational data made apparent that factors of 10–50 are needed if the standard Big Bang nucleosynthesis predictions are to remain consistent with the observations (see e.g. Audouze, 1987). The idea is therefore to evaluate D/H in media as primordial as possible, and in absorption systems having a wide range in abundances to be able to discriminate between theoretical models of galactic chemical evolution.

The feasibility of such measurements has been last explored by Webb et al. (1991), assuming existing possibilities: 10 km/s resolution, 10 hours integration time with a 4-m telescope on a $m_v \sim 17.5$ QSO (i.e. S/N=15), and the first 5 Lyman lines are observed, implying $z_{\text{abs}} \geq 2.6$. Deuterium appears detectable only as an extension in some of the Lyman line wings, but the DI line is not resolved and D/H very difficult to measure, although some particular ranges of values for the crucial velocity dispersion b and for the H I column density may increase the chances of making cosmologically significant measurements. Obviously, the VLT will make these D/H analysis not only easier but also, as for the T_{CBR} determination, more numerous: Webb et al. (1991) identify about 35 suitable absorption systems with high enough N_{HI} in the around 30 known QSOs with $z \geq 2.6$ and $m_v \leq 17.5$; about 10 times more potential QSOs as yet undiscovered are expected with these characteristics. It will thus be possible to perform a more extensive statistical investigation in order to place tight constraints on chemical evolution models and the Big Bang itself.

Astrophysical Considerations: Planetary Systems

The study of protoplanetary systems is another field of research we would like to mention here. The β Pictoris disk is the prototype of this new area which will surely become more and more important in the near future with the discovery of other systems. As for the previous fields, this asks for high spectral resolution at high S/N ratios, but also for high temporal resolution. In the case of β Pic, the very large UV and visual circumstellar absorption data base is presently interpreted as the signature of cometary-like bodies evaporating when grazing and falling onto the star, perhaps through perturbations of a huge small bodies reservoir by an already formed planet orbiting β Pic. Such events last few hours and have to be spectroscopically followed in velocity and equivalent width simultaneously in different lines (like the CaII doublet), or as close as possible in time (see e.g. Lagrange-Henri et al., 1992).

The search for extra-solar giant planets through extremely precise radial velocity measurements is also now entering the discovery phase, since a ± 5 m/s sensitivity has been reached for very bright stars by two techniques: Fabry-Perot and gas absorption cell. It has been vigorously put forward as part of the first stage of the recently announced TOPS Program of NASA: Toward Other Planetary Systems. For instance, Jupiter induces an amplitude variation of 13 m/s in the radial velocity of the Sun over a period of 11.9 years. The limits for such long-term follow-up of very many stars are more imposed by the apparent brightness of the observed stars. This is why TOPS is intended to be performed in partnership with the Keck Observatory.

Astrophysical Considerations: Stars

Last, in the field of stellar research, one can briefly mention the study of non radial pulsation in early-type stars. For cooler stars, again the determination of the Li isotopic ratio, the measurements of surface magnetic fields from the Zeeman broadening, the separation of different broadening mechanisms such as rotation and macroturbulence in G and K stars, time-resolved spectroscopy (on time scales as low as ~ 1 sec) of flares, the mapping of stellar surface features (spots) through Doppler imaging techniques, and an approach to astroseismology, etc. This kind of problems, that we have limited to those really needing spectral resolution in the 10^5 range and/or time resolution, are currently tackled at ESO; but the small aperture of the available telescopes simply prevents most interesting targets to be reached, e.g. M dwarfs, T-Tauri stars, stars in clusters, Pop II stars, etc. A new potentially also very interesting case is the study of the remnants of the AGB winds during the post-AGB stellar evolutionary phase towards planetary nebulae. Here again, all the targets are very obscured and optically very faint.

Conclusion

It is obvious that the jump from 4-m to 8-m (and *a fortiori* from 2-m) class telescopes will very much increase the number of observable targets so that entirely new results will undoubtedly come up. The type of scientific questions we have discussed here are only tractable with a spectral resolution VLT mode in the $1-2 \times 10^5$ range. It does not at all mean that an ultra-high resolution mode ($R \geq 3 \times 10^5$) would be useless; an enormous amount of information on physical processes is waiting for that

mode, some examples having been pointed out in e.g. Ferlet (1993) and Dravins (1993). It has to be noted also that for both modes, a small spectral range, say few tens of Å to record simultaneously both lines of the CaII doublet, is often sufficient. It would be advisable to implement these modes at the VLT coude focus, in order to provide enough room and stability, and avoid the field rotation of the Nasmyth focus. This will moreover leave open the future possibility to dedicate a 4-m class "Auxiliary" telescope for high-resolution spectroscopy.

References

- Audouze, J., 1987, in *Observational Cosmology*, IAU Symp. **124**, Dordrecht: Reidel, p. 89.
- Black, J., van Dishoek, E., 1988, *Astrophys. J.*, **331**, 986.
- Crane, P., Hegyi, D., Lambert, D., 1991, *Astrophys. J.*, **378**, 181.
- Dravins, D., 1993, in *High Resolution Spectroscopy with the VLT*, ESO Workshop, Garching, p. 55.
- Ferlet, R., 1992, in *Astrochemistry of Cosmic Phenomena*, IAU Symp. 150, Dordrecht: Reidel, p. 85.
- Ferlet, R., 1993, in *High Resolution Spectroscopy with the VLT*, ESO Workshop, Garching, p. 97.
- Hobbs, L., 1973, *Astrophys. J.*, **181**, 795.
- Lagrange-Henri, A.M., Gosset, E., Beust, H., Ferlet, R., Vidal-Madjar, A., 1992, *Astron. Astrophys.*, **264**, 637.
- Lemoine, M., Ferlet, R., Vidal-Madjar, A., Emerich, C., Bertin, P., 1993, *Astron. Astrophys.*, **269**, 469.
- Meyer, D., Black, J., Chaffee, F., Foltz, C., York, D., 1986, *Astrophys. J. Lett.*, **308**, L37.
- Molaro, P., Vladilo, G., Monai, S., D'Odorico, S., Ferlet, R., Vidal-Madjar, A., Dennefeld, M., 1993, *Astron. Astrophys.*, in press; ESO Preprint 907.
- Palazzi, E., Mandolesi, N., Crane, P., 1992, *Astrophys. J.*, **398**, 53.
- TOPS, A Report by the Solar System Exploration Division, Ed. B. Burke, NASA.
- Vladilo, G., Centurion, M., Cassola, C., 1993, *Astron. Astrophys.*, **273**, 239.
- Vladilo, G., Molaro, P., Monai, S., D'Odorico, S., Ferlet, R., Vidal-Madjar, A., Dennefeld, M., 1993, *Astron. Astrophys.*, in press; ESO Preprint 907.
- Webb, J., Carswell, R., Irwin, M., Penston, M., 1991, *MNRAS*, **250**, 657.

Probing the Properties of Elliptical Galaxy Cores: Analysis of High Angular Resolution Data

W. W. ZEILINGER¹, P. MØLLER² and M. STIAVELLI³

¹ST-ECF, Garching, Germany; ²ESA STScI Baltimore, Md, U.S.A., ³Scuola Normale Superiore, Pisa, Italy

Introduction

The cores of elliptical galaxies provide important clues to the formation and dynamical evolution of the parent galaxies, e.g. recent episodes of star formation, merging and cannibalism and possible presence of black holes. Many "features" are observed in the central region of ellipticals: Cores kinematically

decoupled from the main body of the galaxy are known to exist in many ellipticals and are widely interpreted as evidence for galactic cannibalism. However, different signatures of the decoupling have been found which may not necessarily be related to each other: central light excess (Kormendy 1985), kinematically decoupled cores, i.e. mis-

alignment of the angular momentum vectors of the stellar component in the central region with respect to the main galaxy body, and finally core radio sources and X-ray emission found in ellipticals may indicate the presence of a (super) massive central object. More recently, unresolved nuclei have been discovered in many ellipticals and seem to be a much more common phenomenon than previously thought as also pointed out by the HST observations of the core of the early-type galaxy NGC 7457 (Lauer et al. 1991). Crane et al. (1993) reported central mass densities in excess of $10^3 M_{\odot}/\text{pc}^3$ for several galaxies.

Despite the fact that a wide range of core properties has been found in elliptical galaxies, no homogeneous survey has been carried out so far with the necessary high resolution. Therefore, nature and physical interpretation of galaxy cores are still subjects of discussion. The largest sample published so far is the compilation by Lauer (1985) of surface photometry for the cores of 42 early-type galaxies. Lauer's sample, however, is not complete and based on single waveband observations carried out at a 1-m telescope with a medium seeing of about 1.7 arcsec FWHM and no comparable kinematic survey exists in the literature.

The Survey

On the basis of the morphological classifications in the "Catalogue of Principal Galaxies" (Paturel et al. 1989) and the "Third Reference Catalogue of Bright Galaxies" (de Vaucouleurs et al. 1991) all elliptical galaxies within a redshift of 3000 km/s were selected for the present survey, in total about 230 galaxies. The aim of the survey is to obtain a homogeneous set of high-resolution multi-colour surface photometry data and major-axis long-slit spectra for the whole sample. As a first step VRI images were obtained at the 2.5-m Nordic Telescope (NOT) for the northern hemisphere and at the ESO 3.5-m NTT using the direct imaging facility SUSI for southern hemisphere objects. In addi-

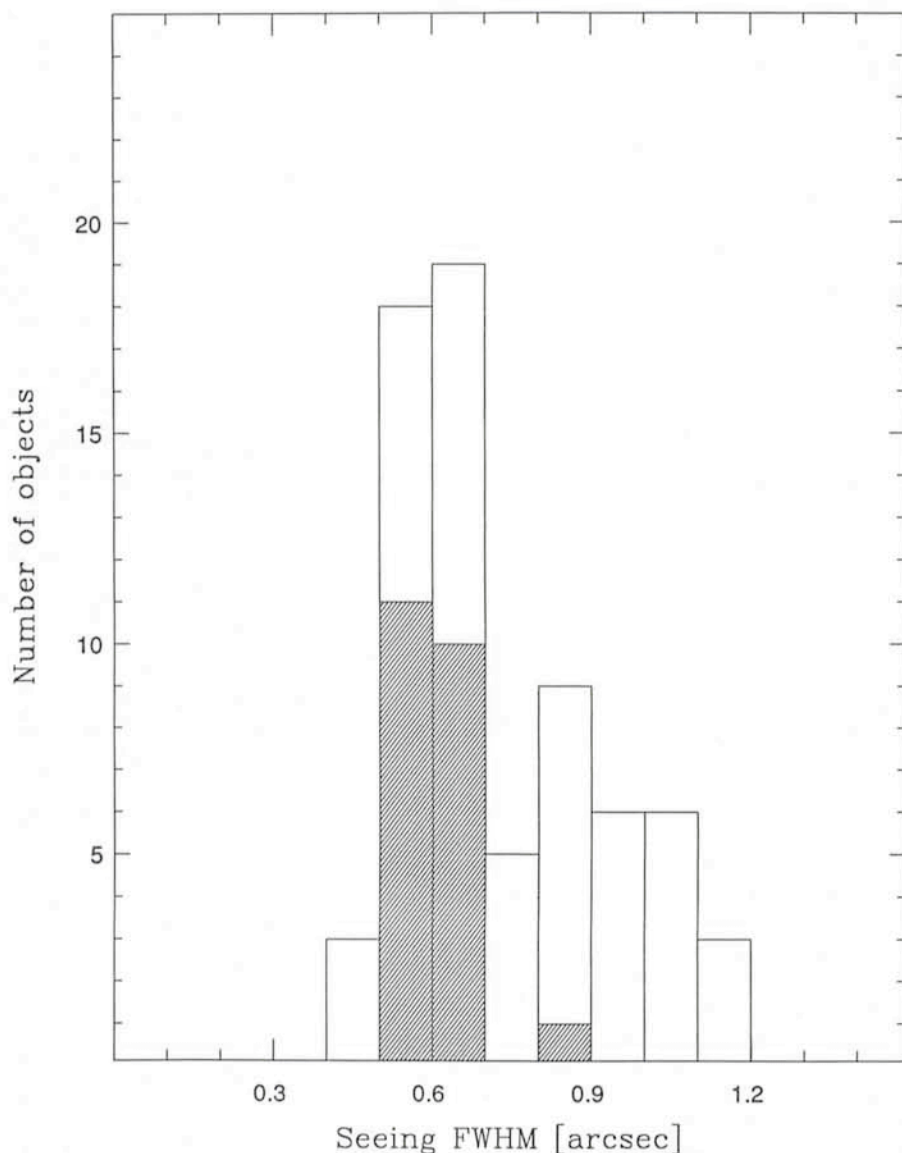


Figure 1: Distribution of best seeing values of a sample of 69 galaxies. The shaded area indicates objects observed at the NOT. The remaining data are from the NTT using SUSI.

tion, using the ESO Archive Database facility within STARCAT, the NTT data archive was systematically searched for adequate galaxy images. Long-slit spectra for southern hemisphere objects were obtained using the ESO 1.5-m telescope during several observing runs. For a sub-sample of objects, images and spectra were obtained at the ESO/MPI 2.2-m equipped with EFOSC2 and IRAC2 and also at the NTT with EMMI. The long-slit spectra should provide information on global kinematic properties on the (ionized) gas and stars and identify candidates for high-resolution studies.

Most of the effort so far has been put in performing surface photometry and further analysis of the images. The resolution of the NOT and NTT-SUSI data are of comparable order. The respective scales on the detector are 0.20 and 0.13 arcsec/pixel. In Figure 1 the best-seeing values for 69 galaxies are presented which have been analysed so far from the VRI data sample. The seeing was measured on stellar-like images in the respective frames. A data base of images obtained at very good (exceptional) seeing conditions is an essential ingredient for this project. However, in order to take full advantage of the high-resolution data one needs also take into account effects of seeing, telescope guiding, etc. which affect the image quality. Some experiences on handling and analysing such images are presented in the following sections.

Parametrization of the (Photometric) Core Properties

The “classical” galaxy core parameters are the central surface brightness and the core radius (i.e. radius of the isophote at which the surface brightness has decreased by a factor of two with respect to the central surface brightness). It is immediately evident that these parameters depend crucially on the seeing conditions during the observations, and several studies have addressed the problem of how to consistently correct the parameters for these seeing effects. The most commonly used methods of seeing correction have been to firstly extract the luminosity profile of the galaxy, and then either (i) deconvolve the profile directly with an appropriate PSF (Lauer 1985, (ii) measure the core parameters of the extracted luminosity profile and apply seeing corrections found by convolution of core models with a PSF (Kormendy 1985), or (iii) use directly the core parameters derived from galaxy models fitted to the luminosity profile (Kormendy & Richstone 1992). It is evident that these methods all have their limitations:

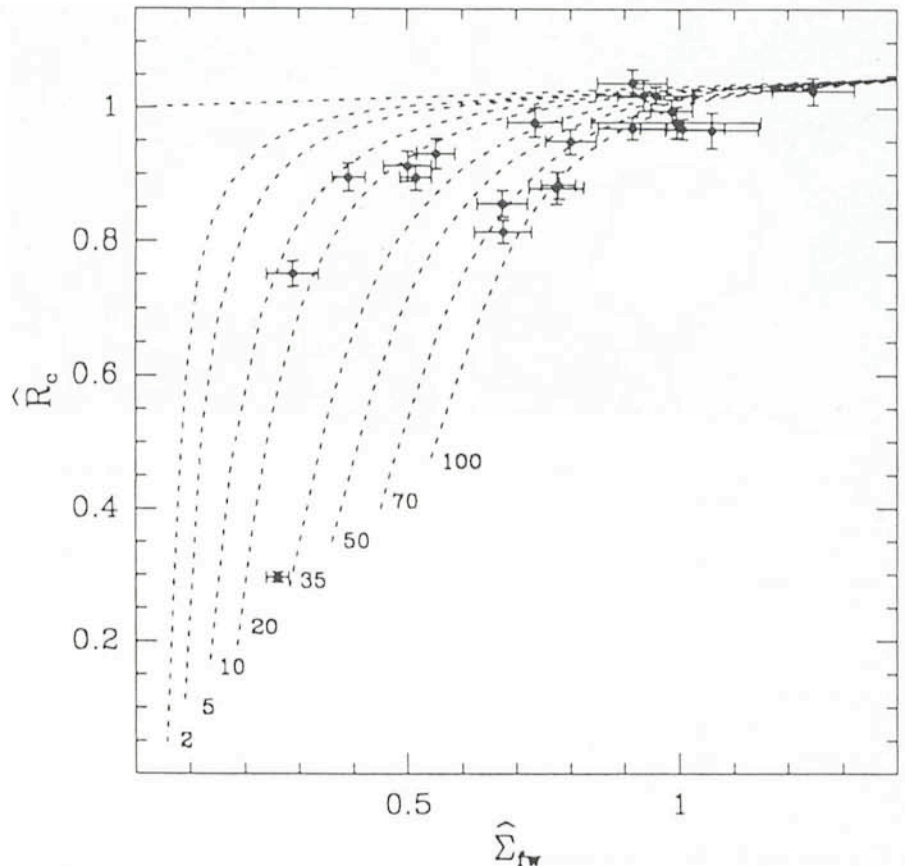


Figure 2: Core resolution diagram for a sample of 21 galaxies observed at the NOT. The galaxy data are plotted with 1σ error bars. The uppermost dotted line indicates the location of isothermal cores. The other dotted curves represent non-isothermal cores with their respective spikyness π_c . The units of π_c are parts per thousand of the underlying core flux. Resolved cores will lie in the left part of the diagram, unresolved ones in the right part.

As shown by Møller, Stiavelli & Zeilinger (1992a, 1992b), deconvolution of luminosity profiles cannot in general compensate for lack of resolution (like bad seeing) and seeing corrections using light profiles derived from galaxy models are necessarily model-dependent (i.e. one has to know in advance the properties and structure of the core and the underlying galaxy, to be able to determine them).

In order to reduce the seeing dependence of the classical core parameters we have introduced a new type of core radius, which for an isothermal (Hubble law) core is identical to the classical core radius but which does not depend strongly on the core structure (e.g. presence of a central point source). The Petrosian core radius (Petrosian 1976), which is defined as the distance from the centre at which the local surface brightness has fallen to some fraction of the mean surface brightness inside that radius, will reduce the influence of the seeing since it depends only on the total flux inside the radius irrespective of its distribution. Two core resolution parameters were introduced in order to quantify the observed core properties,

namely $\hat{\Sigma}_{tw} = \text{seeing FWHM}/R_n$ and $\hat{R}_c = R_c/R_n$ with R_c being the observed core radius and R_n the Petrosian radius as previously defined. \hat{R}_c is an isothermality measure, i.e. for an isothermal core $\hat{R}_c = 1$, while $\hat{\Sigma}_{tw}$ represents an inverse resolution measure, $\hat{\Sigma}_{tw} = 0$ indicates a fully resolved core and becomes larger when the same core is observed with worse seeing. The $\hat{\Sigma}_{tw}$ versus \hat{R}_c plane (core resolution diagram) is therefore a useful tool for the first direct analysis of the observed data and their quality. As a first step of analysing the single galaxy data and their location in the core resolution diagram, one may quantify the non-isothermality of the core in terms of “equivalent point-source flux-fraction” (spikyness parameter π_c). Such an example is shown in Figure 2 using a sub-sample of 21 galaxies observed at the NOT. As a next step one may apply analytical models using parametrized central point sources, power laws or central cusps introduced by a black hole to interpret the data. Such a study has been carried out for the elliptical NGC 1399 (Stiavelli, Møller & Zeilinger 1993).

A more detailed introduction to the core resolution technique together with

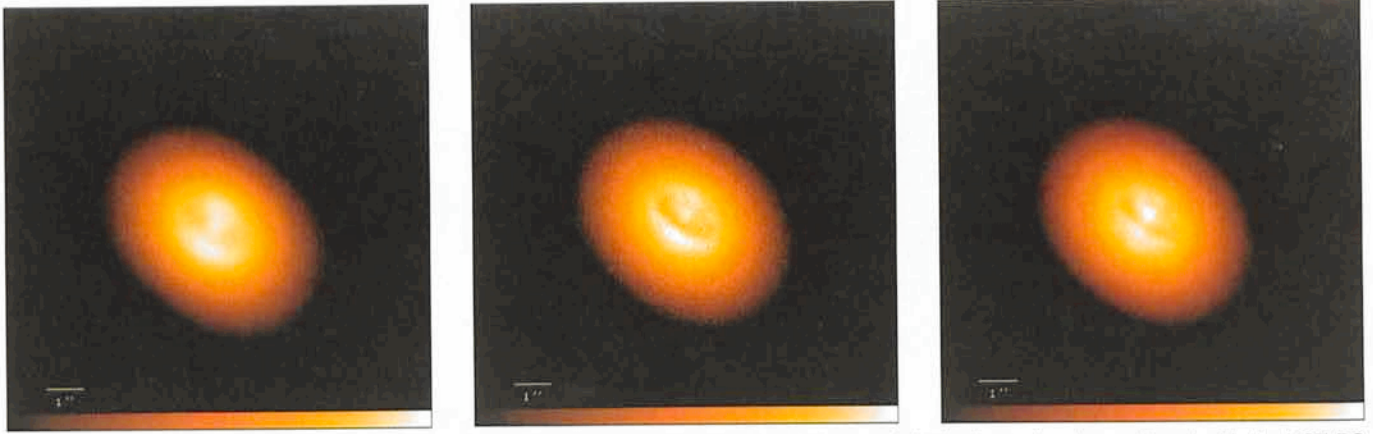


Figure 3: (a) *R* band image of NGC 4261 obtained with NTT-SUSI (exposure time 120 seconds). The frame has been aligned with the HST-PC image and rebinned to the PC detector scale. The seeing FWHM is 0.63 arcsec. (b) F555W band HST-PC image of NGC 4261 (exposure time 1700 seconds). The image is rotated 68° counter-clockwise with respect to the astronomical convention. (c) Combined SUSI and PC image using the co-addition technique after applying 150 iterations of the Richardson-Lucy restoration algorithm. (See also the article on page 37 of this issue.)

a presentation of the first scientific results and implications is given by Møller, Stiavelli & Zeilinger (1992a, 1992b).

The Search for Sub-Components in the Nuclear Region

The use of image restoration techniques becomes more and more popular not only in relation with HST data. One of the most versatile tools is the Richardson-Lucy technique whose algorithm is now part of major image processing packages like IRAF and MIDAS. The straightforward application of this algorithm enables the correction of earlier mentioned impairments of the image quality by means of an appropriate PSF and allows enhancements of faint structures. The study of the nuclear gas and dust disk in NGC 3557 is such an example (Zeilinger, Stiavelli & Møller 1993).

An interesting option of the method is the possibility to combine images having different PSFs (resolutions). The co-adding technique, using the Richardson-Lucy algorithm, consolidates the signal of different images but conserves the resolution of the sharpest one. A more detailed description of the method is given by Lucy (1991) and Hook & Lucy (1992). One is now in the position to take full advantage of the high-resolution images in the HST Data Archive, by co-adding them with (high signal-to-noise) ground-based data. In order to illustrate the capabilities of this method the well-known elliptical NGC 4261 (Ford et al. 1993) has been chosen. The core region of this galaxy is characterized by a dust lane (radial extent less than 2 arcsec) and a point source. Figure 3a shows an NTT image of NGC 4261 obtained with SUSI (detector scale 0.13 arcsec/pixel).

From star-like images a seeing FWHM of 0.63 arcsec was determined. An HST Planetary Camera (PC) image of NGC 4261 (detector scale 0.0439 arcsec/pixel) is shown in Figure 3b as comparison. The frame was extracted from the HST Data Archive. The SUSI image was rebinned to the scale and then aligned with the PC frame. Because of missing field stars, the alignment of the two images was done using the (bright) galaxy nucleus as reference point. Therefore the accuracy of the alignment of the two images is only at the level of 1 (PC) pixel. The selection of the "right" PSF is a crucial part for the image restoration and subsequent co-addition. A well-exposed star within the frame was used for the SUSI image of NGC 4261. In the case of the PC image the situation is much more difficult. Given the fact, that the shape of the PSF varies as a function of the location in the frame, one needs to know the PSF in position of the observed object. Useful stellar images, repeating the exact instrument configuration, are therefore almost never available. A solution to this problem gives the software tool TINYTIM (Kirst 1992) which can calculate an "artificial" PSF for a given observation date and instrument configuration. The usage of the package is straightforward, however, one has to be aware that TINYTIM is only a tool based on current best fits of aberration values for the various mirror positions and current best estimates of the obscuration positions and sizes which may still not describe the HST PSF *exactly*. After applying 150 iterations the deconvolved image was convolved again with the appropriate PSF. The result is shown in Figure 3c. The resolution of the PC image has been retained, shape and structure of the

central dust lane profit however from the better signal-to-noise ratio of the ground-based image.

In the context of studying core regions of elliptical galaxies at high spatial resolution, one of the main open issues is the question of the (non) presence of central black holes. There have been extensive studies in this field (e.g. Kormendy 1993, Nieto 1992) pointing out, however, mostly circumstantial evidence like (radio) jets, compact (unresolved) radio sources or core fluxes in excess of an isothermal galaxy core. The nearby elliptical NGC 4486 (M87) illustrates very well the problem (Zeilinger, Møller & Stiavelli 1993). Despite its obvious signatures of nuclear activity and non-isothermal core, it was up to now not possible to pinpoint the nature of the central source. The kinematics in the nucleus is a key element in this study. It is by now a well-established fact that, in general, giant (high-luminosity) ellipticals are not rotationally flattened systems. Therefore, in order to account for their triaxial shape, they must have an anisotropic velocity distribution. It has been shown that most of the light contribution in excess of an isothermal model can be explained by an even modest anisotropy in the velocity field (Binney & Mamon 1982). The kinematic signature of a central dark mass concentration, however, is very difficult to detect since it requires spectroscopic data with a resolution at the subarcsecond level. NGC 1399 is such a case where the combination of radio, photometric and (stellar) kinematic signatures (each of them alone would not have been conclusive) has led to the confirmation of a central black hole of about $6 \times 10^9 M_{\odot}$ (Stiavelli, Møller & Zeilinger 1993).

References

- Binney, J. & Mamon, G.A., 1982, *Mon. Not. R. Astr. Soc.*, **200**, 361.
- Crane, P., et al. 1993, *Astr. J.*, in press.
- de Vaucouleurs, G., et al., 1991, "Third Reference Catalogue of Bright Galaxies" (Springer).
- Ford, H., Jaffe, W., Ferrarese, L., van den Bosch, F. & O'Connell, R.W., 1993, *STScI Newsletter*, **10**, 1.
- Hook, R. & Lucy, L., 1992, *ST-ECF Newsletter*, **17**, 10.
- Kirst, J., 1992, "The TinyTim User's Manual" (STScI).
- Kormendy, J., 1985, *Astrophys. J. (Lett.)*, **292**, L9.
- Kormendy, J., 1993, in *High Energy Neutrino Astrophysics*, ed. V.J. Stenger et al. (World Scientific).
- Kormendy, J. & Richstone, D., 1992, *Astrophys. J.*, **393**, 559.
- Lauer, T.R., 1985, *Astrophys. J.*, **292**, 104.
- Lauer, T.R., et al, 1991, *Astrophys. J. (Lett.)*, **369**, L41.
- Lucy, L.B., 1991, *ST-ECF Newsletter*, **16**, 6.
- Moller, P., Stiavelli, M. & Zeilinger, W.W., 1992a, in *Structure, Dynamics and Chemical Evolution of Elliptical Galaxies*, ed. I. J. Danziger et al. (ESO).
- Moller, P., Stiavelli, M. & Zeilinger, W.W., 1992b, *Mon. Not. R. Astr. Soc.*, submitted.
- Nieto, J.-L., 1992, in *Morphological and Physical Classification of Galaxies*, ed. G. Longo et al. (Kluwer).
- Patrel, G., Fouqué, P., Bottinelli, L. & Gouguenheim, L., 1989, "Catalogue of Principal Galaxies" (Lyon).
- Petrosian, V., 1976, *Astrophys. J. (Lett.)*, **209**, L1.
- Stiavelli, M., Moller, P. & Zeilinger, W.W., 1993, *Astr. Astrophys.*, in press.
- Zeilinger, W.W., Moller, P. & Stiavelli, M., 1993, *Mon. Not. R. Astr. Soc.*, **261**, 175.
- Zeilinger, W.W., Stiavelli, M. & Moller, P., 1993, *Nature*, submitted.

Light Curves of Miras Towards the Galactic Centre

C. ALARD¹, A. TERZAN², J. GUIBERT¹

¹Centre d'Analyse des Images, Observatoire de Paris, France; ²Observatoire de Lyon, France

Introduction

Long Period Variables represent a late stage in the evolution of stars of intermediate masses. Mass loss, which leads them to planetary nebulae in a few

10^5 years, is a complex process and the object of many investigations. For instance, Vassiliadis and Woods (1993) suggest that mass loss could occur in brief superwind phases separated by long quiescent periods.

A First Step in the Inventory

Here we present the first results of a systematic study of variable objects in a field of about 10×10 degrees towards the Galactic Centre. The first step of our

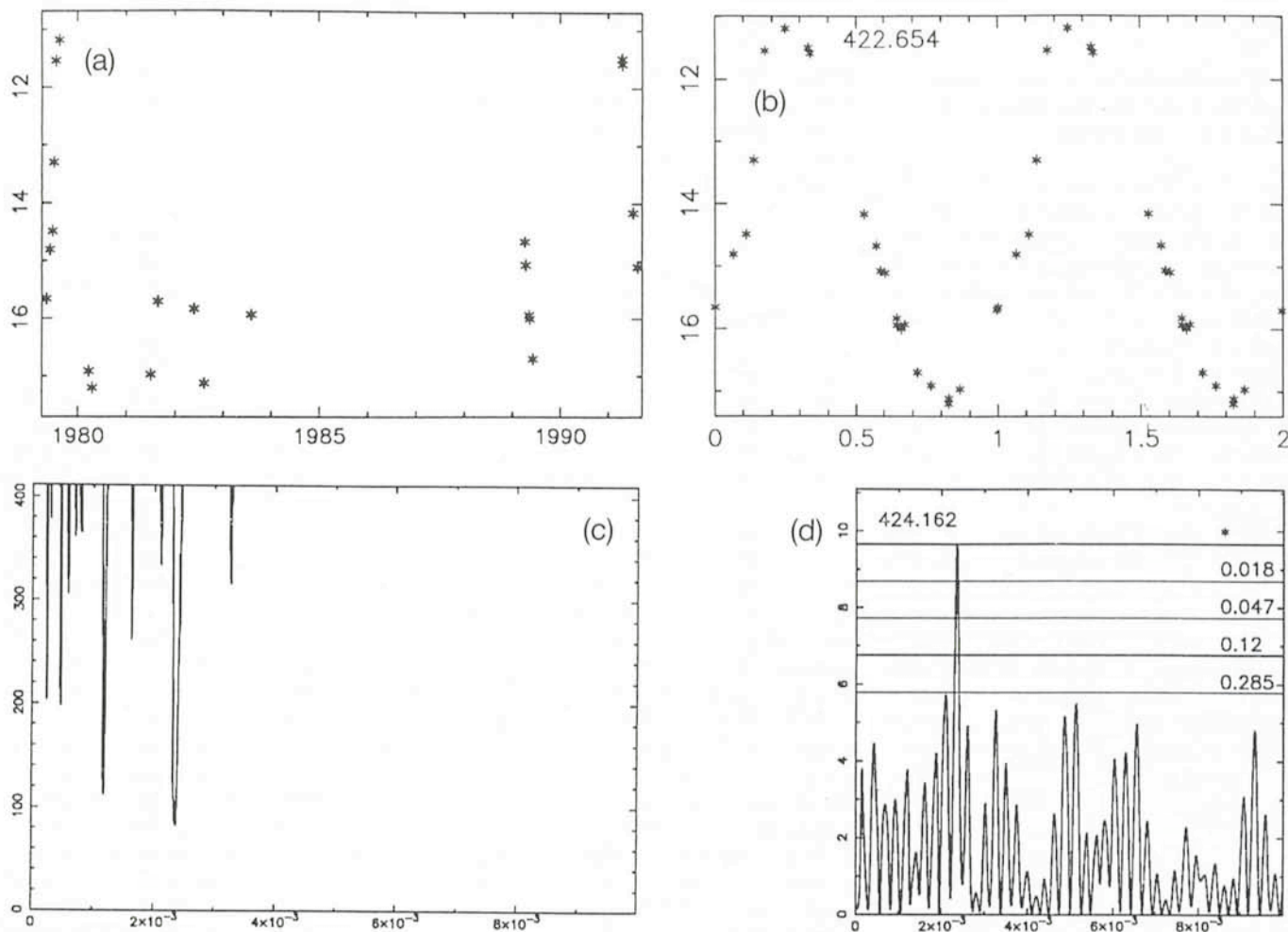


Figure 1: Example of light curve derived from ESO Schmidt plate measurements. (a) time sampling of R magnitudes; (b) derived light curve; (c) Renson's method; (d) periodogram with Scargle's false alarm probability.

investigation deals with the thousands of variable stars discovered by Terzan (Terzan, 1982, Terzan, 1990 and ref. therein) on ESO Schmidt plates. We have scanned 22 ESO Red Schmidt plates centred on the star 45 Oph., with the MAMA measuring machine (e.g. Guibert and Moreau, 1991). In this field, we have selected 150 variables with $\Delta m_R > 2$. The plates were calibrated with 55 photometric standards.

Light Curves

Two methods have been implemented to derive the light curves from the time sampling series. The first one (Renson, 1978), presents the advantage

of not being too sensitive to gaps in the data. The periodogramme yields an estimate of the probability of false periodicity detection. Both methods lead to similar results in most cases, as exemplified by Figure 1. As a result, we have obtained light curves for 118 variables (80% of the stars under investigation).

Developments in Progress

This programme is being continued by a systematic search for variables in the whole 100-square-degree field. It will require additional plates to cover the whole range of periods, as well as near infrared and radio measurements. Interpretation of these data will lead to a

better knowledge of the period-luminosity relations for various kinds of objects, and understanding of the relations between the shape of the light curves, mass loss and other properties of variable objects.

References

- A. Vassiliadis, P.R. Wood, 1993, *Astrophys. J.* in press.
 A. Terzan, 1982, *Astron. Astrophys. Suppl.* **49**, 715.
 A. Terzan, 1990, *The Messenger*, **59**, 41.
 J. Guibert, O. Moreau, 1991, *The Messenger*, **64**, 69.
 P. Renson, 1978, *Astron. Astrophys.* **63**, 125.

NGC 4636 – a Rich Globular Cluster System in a Normal Elliptical Galaxy

M. KISSLER¹, T. RICHTLER¹, E.V. HELD², E.K. GREBEL³, S. WAGNER⁴, M. CAPACCIOLI⁵

¹Sternwarte der Universität Bonn, Germany; ²Osservatorio Astronomico di Bologna, Italy; ³ESO, La Silla, Chile; ⁴Landessternwarte Heidelberg, Germany; ⁵Dipartimento di Astronomia, Università di Padova, Italy

1. What Drives the Investigations of Globular Cluster Systems of Elliptical Galaxies?

In 1918 Shapley started to use the galactic globular clusters to explore the spatial dimensions of our Milky Way. Three quarters of a century later, we still cannot claim to have understood the properties of our globular cluster system (GCS) in the context of the early evolution of the Galaxy. This is mainly due to the fact that there are severe problems in disentangling age and metallicity, which are the most significant parameters in theories of galaxy evolution.

Given these problems with well observable clusters, what can we hope to learn from the study of faint images of globular clusters around distant galaxies, where individual clusters appear star-like and only integrated magnitudes can be determined?

Research on GCSs over the past 20 years showed that there is an amazing variety in the morphologies of GCSs (see Harris 1991 for a review). Most studies refer to elliptical galaxies, because globular clusters in spirals are normally much less numerous and they are difficult to identify due to the inhomogeneous background of bright stars or HII regions. Relating the properties of GCSs (such as total number of

clusters, colour, and spatial distribution) to those of their host galaxies, the study of extragalactic GCSs leads to a new level of problems, which could not be foreseen by the study of the galactic GCS alone. One of the systematic patterns emerging from all previous studies is that the richness of a GCS depends somehow on the environment of the host galaxy. M87 became the first example of a giant elliptical galaxy, located in the dynamical centre of a rich galaxy cluster, found to be surrounded by a huge number of globular clusters (Baum 1955, Sandage 1961). Later on, very rich GCSs have been also discovered in the central giant ellipticals NGC 1399 in the Fornax cluster (e.g. Wagner et al. 1991), NGC 3311 in the Hydra cluster (Harris et al. 1983), and NGC 4874 in the Centaurus cluster (Harris 1987). Harris and van den Bergh (1981) introduced the "specific frequency" S as a quantitative measure: $S = N \cdot 10^{0.4(M_v + 15)}$, where N is the total number of globular clusters and M_v the absolute visual brightness of the host galaxy. The above mentioned galaxies have S values between 12 and 18.

All galaxies that do not occupy central positions in galaxy clusters possess poorer GCSs, but a relation with the environment persists: e.g., the normal elliptical galaxies in the sparse Fornax cluster have a mean S value of 3, while

for ellipticals in the rich Virgo cluster it is about 6. The interpretation of this tendency is far from being unambiguous, but the dependence on the environment suggests that interaction between galaxies may play a role.

Other morphological properties, for example the relation between the spatial distribution of clusters and the light profile of the host galaxy, or the luminosity function of globular clusters, also bear potential information which may finally lead us to an understanding of the formation history of GCSs and thus to gain deeper insight in the formation and structure of the host galaxies themselves. This field is still in the phase where the investigation of individual galaxies provides interesting and useful contributions to the general knowledge. The elliptical galaxy NGC 4636 appears to violate these general properties. NGC 4636 is supposed to be a member of the Virgo cluster of galaxies though it is lying well outside the main body of the cluster, in a region where the density of galaxies is quite low. Using photographic plates, Hanes (1977) determined a specific frequency of 9.9 ± 3 for the GCS of this galaxy, which is a surprisingly high value considering location and environment of NGC 4636. We reobserved NGC 4636 using CCD imaging to investigate the properties of its GCS with higher accuracy.

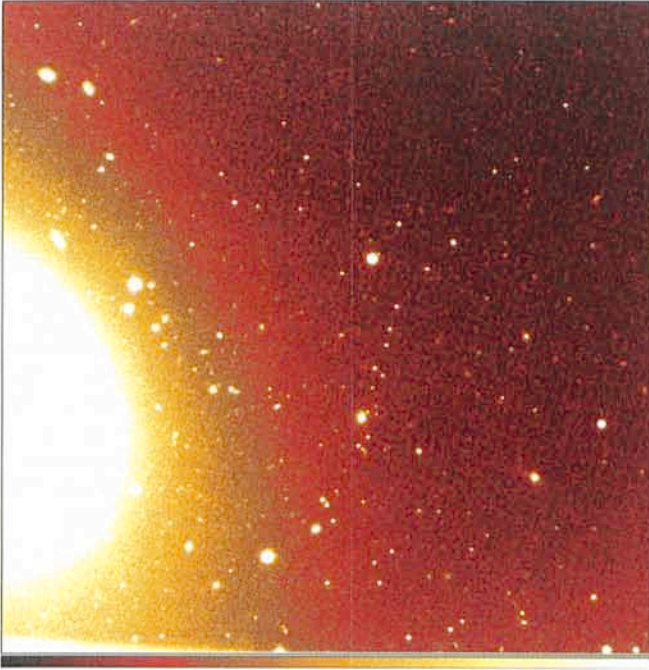


Figure 1: Six NTT frames combined to a single image of one hour effective exposure time. The frame shows a $7.5' \times 7.5'$ field north-east of NGC 4636.



Figure 2: The image shown above results from subtracting a model of the galaxy light, which has been obtained by a median filtering technique. This is the frame on which we performed our search and photometry of globular cluster candidates. The crowding of stellar-like images near the galaxy centre is striking.

2. Our NTT Observations of NGC 4636

NGC 4636 was observed at the NTT using EMMI and a 1k Thomson chip in July 1992, in the context of a collaboration between German and Italian groups interested in the GCS problem. The seeing during our run was only moderate ($1.5''$) and this prevented an investigation of the luminosity function beyond its turnover (see section 4), but the data quality turned out to suffice for a study of the main properties of the GCS of NGC 4636. We combined six frames in the V filter of 10 minutes each to a frame of an effective exposure time of one hour (Figure 1). We modelled the galaxy light by a median filtering technique and subtracted it from the original frame to obtain a homogeneous background. We then ran DAOPHOT on the resulting image (Figure 2). About 1500 point sources down to a magnitude of 24.5 were identified. At the faint magnitude limit we reached a completeness in finding point sources of 60%.

We calibrated our data by simulating aperture photometry on a frame centred on NGC 4636. The zeropoint has been obtained from the photometry published by Poulain (1988), and we estimate a zeropoint error of 0.05 mag.

To account for contamination with background objects we statistically subtracted the objects found on a frame $7'$ away from the galaxy centre, and considered the remaining objects as globular clusters belonging to NGC 4636.

3. The Specific Frequency of NGC 4636

To calculate the total number of globular clusters, we had to correct for the incomplete spatial coverage of the galaxy and for the fact that we only see the brightest part of the luminosity function (see below). After all corrections, we obtained a total number of 3500 ± 200 globular clusters around NGC 4636, which corresponds to a specific frequency of $S = 7.3 \pm 2.0$, if $(m - M) = 31.2$ and $M_v = -21.7 \pm 0.3$ are adopted. As can be noticed, the error in S is quite substantial. This is the consequence of the fact that S is very sensitive to the absolute brightness of the galaxy, and an error of 0.1 in $(m - M)$ implies an error of 10% in S .

This S value of 7.3 ± 2.0 for NGC 4636 is marginally below the one found by Hanes (1977), and slightly higher than the mean value for elliptical galaxies in the Virgo cluster. It is thus at the upper limit of what can be considered a "normal" specific frequency. However, the question remains what distinguishes NGC 4636 for example from NGC 4697, another Virgo elliptical with $S = 3.5$, but almost twice as bright. There is much room for speculation. NGC 4636 has an X-ray luminosity ten times as high as NGC 4697 (Roberts et al. 1991) and presumably a high dark matter content (Saglia et al. 1992). While the X-ray flux is not generally correlated with S , as the pair NGC 1399 and NGC 1404 in the Fornax cluster shows (Richtler et al.

1992), it may indicate a large total mass which in combination with a rich environment causes effective accretion of matter. This matter could be for example in the form of dwarf galaxies. We recall in this respect that the dwarf spheroidal in the constellation Fornax possesses 5 globular clusters. Adding 500 dwarf spheroidals of the Fornax type to NGC 4636 could account for 2500 clusters, but would increase its total luminosity by only 0.1 mag.

4. The Luminosity Function of the GCS: Gaussian or Power Law?

Apparently, globular cluster luminosity functions (GCLFs) exhibit a nearly universal shape, which in the past has been represented by Gaussians with dispersions of 1.3 mag and a peak or "turnover" of $M_v = -7.1 \pm 0.3$ mag, as derived for several ellipticals in the Virgo cluster (Secker & Harris 1993). For NGC 4636, we find the turnover to be at $M_v = 24.1$. This corresponds to a distance modulus of $(m - M) = 31.2 \pm 0.3$, which is in good agreement with previously determined distances of NGC 4636 (31.1 ± 0.4 using the supernova 1993a, Capaccioli et al. 1990; 30.96 ± 0.08 by surface brightness fluctuation, Tonry et al. 1990).

We believe that the choice of a Gaussian for a GCLF does not bear any physical significance. In particular, the possible existence of a universal turnover magnitude does not mean that there is a

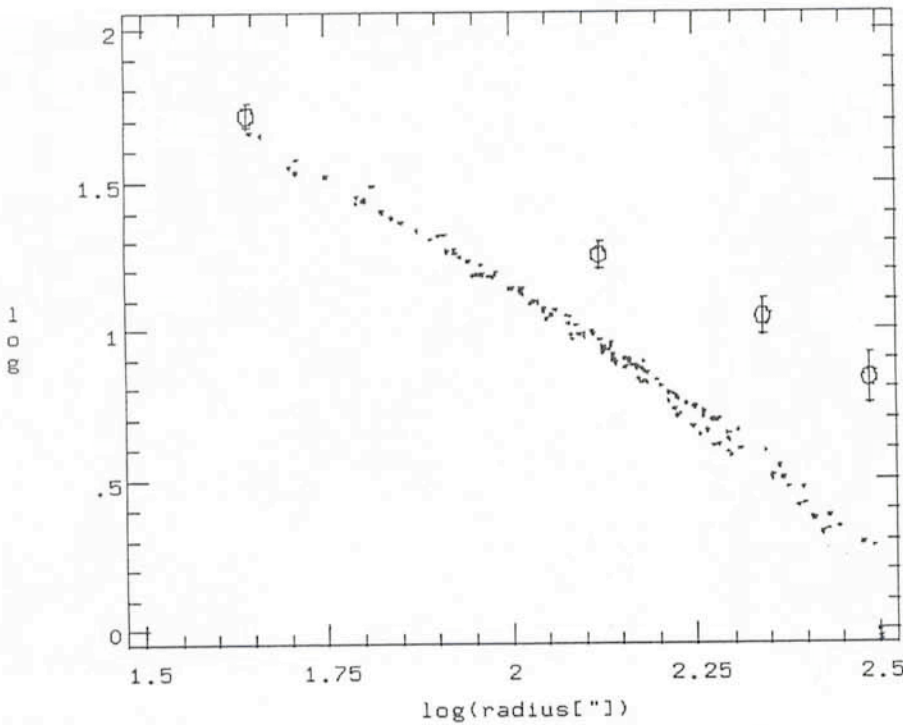


Figure 3: This plot compares the profile of the surface density of globular clusters with the light of NGC 4636. The abscissa is the logarithm of the galactocentric radius (arcsec) along the major axis. The ordinate is the logarithm of the number of globular clusters per square arcmin. Open circles represent the globular cluster profile. The small dots are measurements of the galaxy light. The density profile of globular clusters is flatter than the galaxy light. This suggests that the globular clusters do not share the dynamical history of the field population.

characteristic mass among globular clusters connected with this characteristic magnitude. Richtler (1993) and Harris & Pudritz (1993) show that the mass distribution of globular clusters in the Milky Way, M31, and some Virgo galaxies is well described by a power law $\frac{dN}{dm} \sim m^{-\alpha}$ where α is about -1.7 . In the Milky Way and M31, i.e. in those galaxies where the luminosity function can be followed well beyond the turnover magnitude, this power law continues beyond the turnover magnitude and has a cut-off at very low masses, probably due to the dissolution of less massive clusters. Concerning NGC 4636, we transformed the luminosities of globular cluster candidates to masses using the relation given by Mandushev et al. (1991), and calculated the mass distribution of the globular cluster in NGC 4636. We found $\delta = -1.9$ which fits well to the Milky Way system. The existence of a power-law (which is equivalent to the absence of a characteristic mass scale) and its apparently universal shape are remarkable features. A satisfactory explanation has yet to be found.

5. The Density Profile

A further interesting question is whether the surface density of globular

clusters decreases with increasing galactocentric distance in the same way as the galaxy light itself. If it does, this would indicate that globular clusters and field population behave dynamically in the same way and probably date from the same epoch of formation. For many galaxies this is not easy to investigate due to the large scatter in the globular cluster counts in small number statistics. In case of rich systems like the one discussed, the statistics are more trustworthy. We find the density profile of the GCS of NGC 4636 to be flatter than the galaxy halo light itself. If we represent both profiles by a power law $\varrho \sim r^{-\alpha}$, where ϱ is the surface density of globular clusters and r the projected galactocentric distance, we get $\alpha = -1.0 \pm 0.1$ for the GCS and $\alpha = -1.5 \pm 0.1$ for the galaxy light. The density profile is plotted in Figure 3, where the ordinate is the logarithm of the number of globular clusters per square arcminute. The abscissa is the logarithm of the galactocentric radius in arcseconds along the major axis. The small dots are measurements of the galaxy light with an arbitrary offset. The four open circles represent the globular cluster density profile. Interestingly, this has also been found in other rich globular cluster systems (NGC 1399, Wagner et al. 1991; NGC 4472, Cohen 1988;

NGC 4365 and 4649, Harris et al. 1991), while in poorer systems the GCSs seem to follow the light of the host galaxy (NGC 3379, Pritchet & van den Bergh, 1985; NGC 1404, Richtler et al. 1992). Again, this can be understood as an indication that rich cluster systems might be partially formed through merger or accretion processes.

6. Concluding Remarks

This investigation of GCS of NGC 4636 demonstrates that more questions are open than answered. The fundamental problem of what determines the total number of globular clusters in a galaxy is still open, but the first steps to an answer point in directions that are closely connected with general problems of galaxy structure and evolution. Moreover, the use of globular cluster luminosity functions as distance indicators will perhaps play an important role in the forthcoming VLT era. A huge potential of information about the physics of galaxies and their stellar populations awaits its exploitation.

References

- Baum, W.A., 1955, *PASP*, **67**, 328.
- Capaccioli, M., Cappellaro, E., Della Valle, M., D'Onofrio, M., Rosino, L. and Turatto, M., 1990, *ApJ* **350**, 110.
- Cohen, J., 1988, *AJ* **95**, 682.
- Fischer, P., Hesser, J.E., Harris, H.C., Bothun, G.D., 1990, *PASP* **102**, 5.
- Hanes, D.A., 1977, *MemRAS* **84**, 45.
- Harris, W.E., van den Bergh, S., 1981, *AJ* **86**, 1627.
- Harris, W.E., Smith, M.G., Myra, E.S., 1983, *ApJ* **272**, 456.
- Harris, W.E., 1986, *AJ* **91**, 822.
- Harris, W.E., 1987, *ApJ Lett.* **315**, L29.
- Harris, W.E., 1991, *ARAA* **29**, 543.
- Harris, W.E., Allwright, J.W.B., Pritchet, C.J., van den Bergh, S., 1991, *ApJS* **76**, 115.
- Harris, W.E., Pudritz, A.E., 1993, *AJ*, in press.
- Mandushev, G., Spassova, N., Staneva, A., 1991, *A & A* **252**, 94.
- Poulain, P., 1988, *A & AS* **72**, 215.
- Pritchet, C.J., van den Bergh, S., 1985, *AJ* **90**, 2027.
- Richtler, T., Grebel, E.K., Domgörgen, H., Hilker, M., Kissler, M., 1992, *A & A* **264**, 25.
- Richtler, T., 1993, 11th Santa Cruz Sommer Workshop proceedings, The globular cluster-galaxy connection, in press.
- Sandage, A., 1961 *The Hubble Atlas of Galaxies*, Carnegie Inst. Washington Publ. N.618.
- Saglia, R.P., Bertini, G., Stiavelli, M. 1992, *ApJ*, **384**, 433.
- Shapley, H., 1918, *ApJ* **48**, 89.
- Secker, J., Harris, W.E., 1993, *AJ* **105**, 1358.
- Tonry, J.L., Ajhar, E.A., Luppino, G.A., 1990, *AJ* **100**, 1416.
- Tully, R.B., Shaya, E.J., 1984, *ApJ* **281**, 31.
- Wagner, S., Richtler, T., Hoop, U., 1991, *A & A* **241**, 399.

Imaging the Globules in the Core of the Helix Nebula (NGC 7293)

J.R. WALSH, ST-ECF, ESO

J. MEABURN, Dept. of Astronomy, University of Manchester, England

Introduction

NGC 7293 is one of the closest planetary nebulae and the only one in which small scale structures can be easily resolved on ground-based images. The distance is about 130 pc [1] and the central star has an effective temperature of $\sim 120,000$ K [2] making it a typical high ionization planetary nebula with emission lines of HeII and higher ionization species. On account of its proximity the projected size of the nebula is very large – the bright inner rings are $13'$ in diameter but there is a prominent ring structure of radius $10'$ and faint extensions, clearly belonging to the nebula, out to at least $15'$; the projected size is thus at least half a degree (eg. [3]). On the large scale, the nebula shows some resemblances to a helix (hence its name) in the low ionization emission (eg [NII]) but in high ionization emission a central, nearly spherical, volume [4] is seen. Some attempts have been made to understand the velocity structure in terms of a radially expanding helix but the real 3-D structure is probably more barrel-shaped with an expansion velocity of ~ 25 km/s, al-

though higher velocity structures have been found ([5], [3]).

Knots and Tails

Around the periphery of the inner low ionization shell there are numerous small ($\sim 1''$) emission knots, some with tails pointing radially away from the star [6]. With the NTT and EFOSC2 in 1990 (before the commissioning of EMMI) we obtained CCD images in low ($H\alpha + [NII]$) and high ([OIII]) ionization emission in good seeing of some of these knots. The result was unexpected: whilst in low ionization emission the knots show up as bow-shaped structures with a bright tip on the side of the globule nearer to the central star and a tail extending radially outwards, at [OIII] no emission was seen, only a depression in the local smooth [OIII]; the knots were thus seen *in absorption*. On consideration, this is not so surprising if the knots are dusty and are seen against background [OIII] emission [7]. If a dense dusty knot lies on the near side of the central emitting [OIII] volume then it will absorb the background [OIII] radiation and appear

dark. Of the knots observed by Meaburn et al. [7] the one with the highest absorption had a central extinction of 0.5 mag. and a projected diameter of $1.4''$ (3×10^{15} cm). If such a globule were spherical and had a dust content typical of interstellar gas and with interstellar gas-to-dust mass ratio then the density is $\sim 5 \times 10^5$ cm $^{-3}$ and its total mass $\geq 10^{-5} M_{\odot}$.

New Observations

With the new large CCD chips and the big field available for imaging at the Cassegrain focus of the NTT with EMMI we can obtain in one image the whole of the central region of the Helix nebula and examine in detail all the knots and tails. This was done in August 1992 and some of the spectacular images are shown here. Figure 1 shows the whole of an $H\alpha + [NII]$ Thomson 1024 2 CCD image covering the central $7.5'$ of NGC7293. The star at the centre is the ionizing star of the nebula. In Figure 2 is shown the corresponding [OIII] image. Comparison of Figure 1 and 2 shows that not all the globules seen in emission

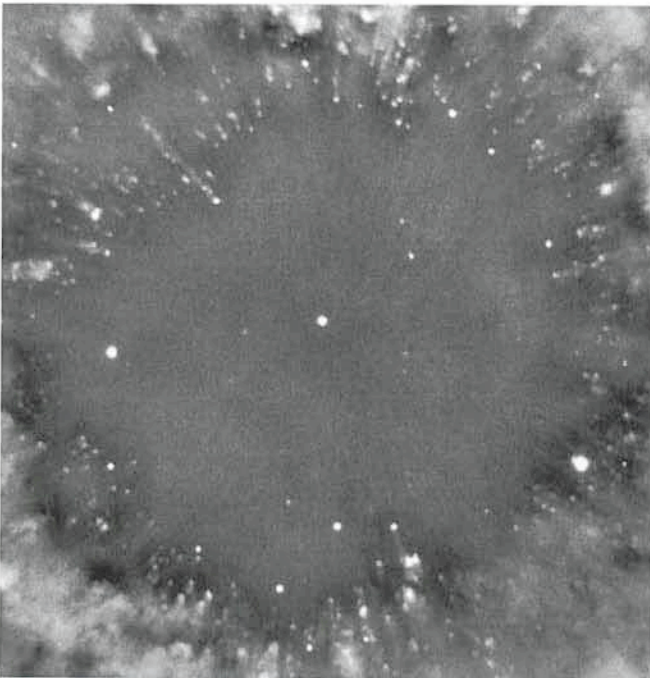


Figure 1: A photographic representation of the NTT + EMMI CCD image of the core of NGC7293 taken with an $H\alpha + [NII]$ filter. A logarithmic intensity scale was used and the size of the field is $450 \times 450''$ ($10'' = 1.9 \times 10^{16}$ cm); north is at the top and east to the left.

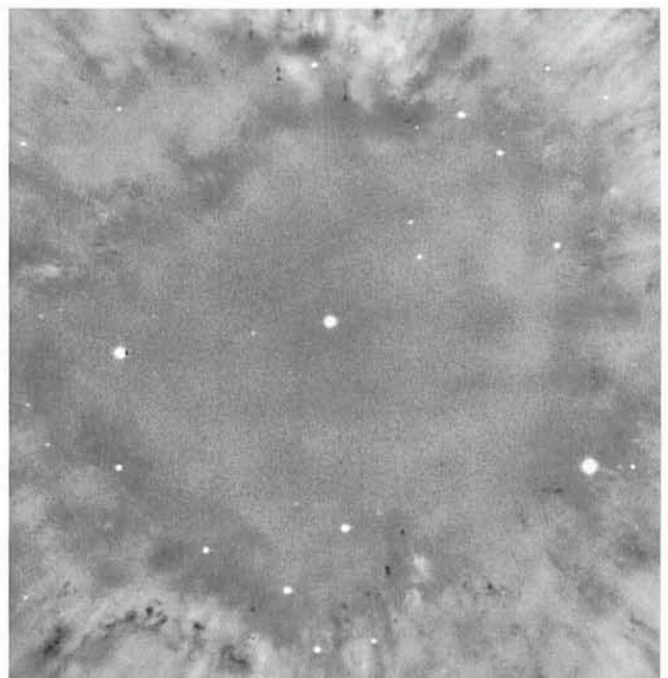


Figure 2: A photographic print of the NTT + EMMI CCD image of the Helix nebula taken with an [OIII] 5007Å filter is shown at the same scale and orientation as Figure 1.

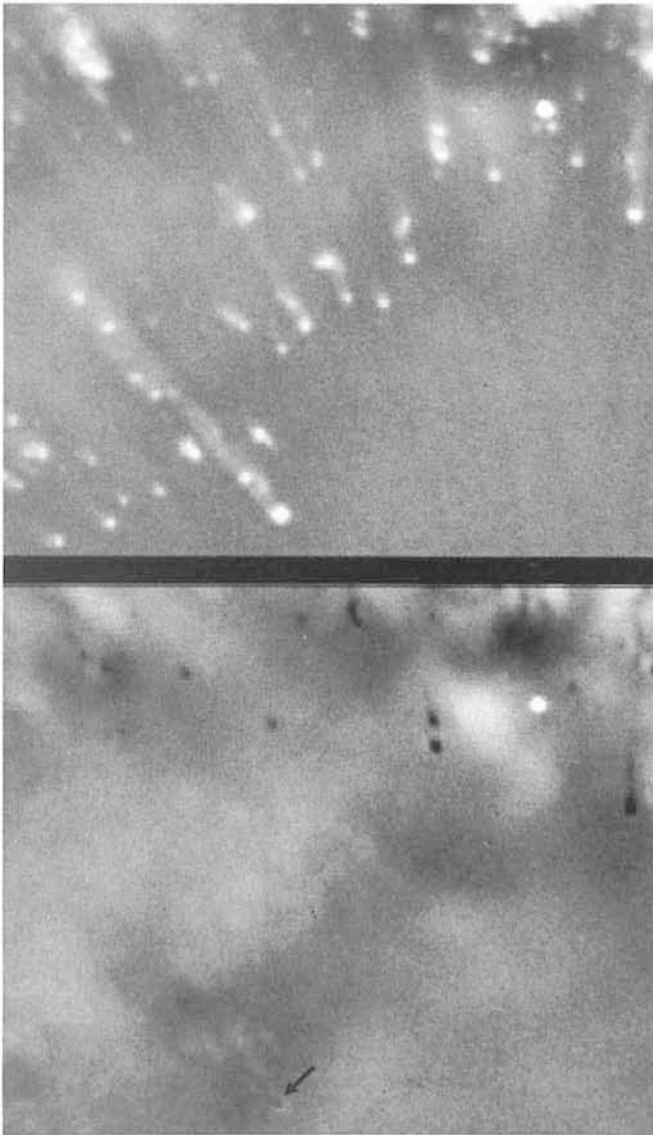


Figure 3: An enlarged view of both the $H\alpha + [NII]$ (upper) and $[OIII]$ (lower) images of the globules and tails in the north-east corner of Figure 1 is shown. The bright globule which shows both $H\alpha + [NII]$ and $[OIII]$ emission is arrowed.



Figure 4: An enlarged view of both the $H\alpha + [NII]$ (upper) and $[OIII]$ (lower) images of the region of extended dust absorption to the south-east of the core of the Helix nebula. The largest globule with the deepest absorption is indicated.

on Figure 1 are found on Figure 2. This can be simply understood in terms of the globules being distributed along the line of sight through the nebula, some being on the near side of the $[OIII]$ zone, some on the far side; only those on the near side give rise to observed absorbing globules. Of the ~ 600 globules counted in emission on Figure 1, some 40% are found in absorption in Figure 2, consistent with this hypothesis. Only three globules were seen with $[OIII]$ emission from the bow-shaped heads, and one of these is seen in the lower left of Figure 3 (arrowed), which is an enlargement of a region to the north-east of the central star. The three globules with $[OIII]$ emission are also those closest in projected distance to the central star; presumably they must be embedded in the $[OIII]$ zone whilst the other globules are in lower ionization

surroundings. Figure 4 shows an enlargement of the large scale dust feature to the south-east. The globule in the centre of this field (arrowed), which appears to have no low ionization emission, is the largest found with a maximum diameter of $4''$ and also has the deepest absorption.

Nature of the Globules

The low ionization crescent-shaped heads to the globules are presumably attributable to radiative ionization by the photons from the central star, with most globules being beyond the O^{++} ionizing zone where the photons have lower energy. However, central stars of planetary nebulae are known to have high velocity winds (typically 2000 km/s and mass loss rates $\sim 10^{-8} M_{\odot} \text{ yr}^{-1}$) so that there may be wind impacting the

neutral globules and producing a bow shock around the globule. In addition, if the globules are stationary then there will be ionized gas streaming past at ~ 20 km/s from the expanding nebula. All these effects may contrive to drag material off the globule and entrain it in a radial tail as observed. Meaburn et al. [7] showed that the size and density of the globules are such that they could survive long enough for such ablation processes to be important.

One of the abiding puzzles is the ionization mechanisms for the tails. Early work ([8], [9]) suggested they could be ionized by the diffuse radiation field since they are shadowed by the optically thick globule from the direct ionizing radiation of the central star. Hartquist & Dyson [10] and Dyson, Hartquist & Biro [11] suggest that the material in the tail could be a low Mach number shock

ionized flow caused by interaction with a low velocity wind, perhaps arising in the expanding ionized gas rather than in the stellar wind itself. Clearly the ionization mechanism in the vicinity of these globules and their tails need to be explored more closely and NGC7293 provides an excellent site.

Where do the globules come from? Perhaps they represent clumpy ejecta from the progenitor asymptotic giant branch (AGB) star ejecta during a phase of mass loss or are formed through instabilities when the hot fast wind from the central star collides with the slow higher density red giant wind. Dyson et al. [12] have suggested that the knots could be remnants of SiO maser spots which were formed in the atmosphere of the AGB star and have survived ejection and photoionization. CO emission has been detected from some of the globules even though the beam is larger than

the globules themselves [13]. The CO linewidths are small suggesting molecular gas at ~ 25 K. Further observations at high spatial resolution in the optical and millimetre will enable the parameters of the globules, such as the gas and dust content, to be determined and their formation and evolution to be more thoroughly investigated. So far no other planetary nebulae with similar small-scale structures have been observed but there is no reason to think that the Helix is atypical and such structures probably exist in all planetary nebulae. Until more are found the Helix will continue to be an ideal laboratory for the study of these ionized-neutral/dusty interfaces.

References

- 1 Daub, C.T., 1982, *ApJ*, **260**, 612.
- 2 Bohlin, R., Harrington, J.P. & Stecher, T.P., 1982, *ApJ*, **255**, 87.

- 3 Walsh, J.R. & Meaburn, J., 1987, *MNRAS*, **224**, 885.
- 4 Meaburn, J. & White, N.J., 1986, *ASS*, **82**, 423.
- 5 Meaburn, J. & Walsh, J.R., 1980, *Astrophys. Lett.*, **21**, 53.
- 6 Vorontsov-Velyaminov, B.A., 1968. In *Planetary Nebulae*. IAU Symp. No. 34 eds. Osterbrock, D.E. & O'Dell, C.R., Reidel, p.256.
- 7 Meaburn, J., Walsh, J.R., Clegg, R.E.S., Walton, N.A., Taylor, D. & Berry, D.S., 1992, *MNRAS*, **255**, 177.
- 8 Kirkpatrick, J.P., 1972, *MNRAS*, **176**, 381.
- 9 Van Blerkom, D. & Arny, T., 1972, *MNRAS*, **156**, 91.
- 10 Hartquist, T.W. & Dyson, J.E., 1993, *QJRAS*, **34**, 57.
- 11 Dyson, J.E., Hartquist, T.W. & Biro, S., 1993, *MNRAS*, **261**, 430.
- 12 Dyson, J.E., Hartquist, T.W., Pettini, M. & Smith, L.J., 1989, *MNRAS*, **241**, 625.
- 13 Huggins, P.J., Bachiller, R., Cox, P. & Forveille, T., 1992, *ApJ*, **300**, L17.

OTHER ASTRONOMICAL NEWS

Detection of Faint Extended Structures by Multiresolution Wavelet Analysis

F. MURTAGH¹, W.W. ZEILINGER¹, J.-L. STARCK² and H. BÖHNHARDT³

¹ST-ECF; ²ESO, OCA Nice, Cisi-Ingénierie Valbonne; ³University of Munich

1. Introduction

The wavelet transform, in common with other image transforms such as the Fourier or the Haar transforms, can be used to produce insightful perspectives on image data. Some particular attributes of the wavelet transform will be discussed in the next section, which seem to make it very appropriate for astronomical image data. Two illustrative examples will be used, where the original images do not provide much indication of underlying faint extended structure. The wavelet transform can effectively uncover such faint structure. It is a new mathematical tool which ought to be kept in mind when exploring and analysing image data.

2. Multiresolution Analysis with the Wavelet Transform

We will briefly motivate the use of wavelets by making reference to (i) the property of multiresolution usually associated with the wavelet transform; and (ii) the perspective of the wavelet transform as a discrete convolution filter.

It has been known for a long time that multiresolution approaches to images allow an image to be interpreted as a sum of details which appear at different resolutions. Furthermore, each scale of resolution may pick up different types of structure in the image. For example, a coarse resolution may pick up gross structure, and finer resolutions allow progressive insights into faint and textured structures.

Consider the convolution of an image with a Gaussian. The effect is to smooth the image. Now consider that Gaussian to have a scale parameter, a function of the standard deviation (e.g. 1s, 2s, 3s, ..., where s is the standard deviation). By varying the scale parameter, a sequence of Gaussian-filtered images is arrived at. These provide a sequence of resolution scales. The Gaussian function is not a wavelet; for the latter certain properties are required, such as translation invariance, and a "scaling property" – a dilation invariance property – which relates the filtered images at two successive scales. The wavelet used in this article is isotropic, which is unlike some other wavelets used to enhance

alignments or to develop useful strategies for image compression. An isotropic wavelet appears to be a good choice for the investigation of astronomical objects.

The natural incorporation of a suite of resolution scales in the wavelet transform has been beneficially used in different application fields. Such multiresolution analysis is particularly appropriate for astronomical data since the structures we want to recognize have very different scales. A priori we cannot know the size of a local neighbourhood where contrast should be enhanced, i.e. we cannot define in advance an optimal resolution level for analysing an image. The wavelet transform implicitly caters for a more sophisticated astronomical image model than the simple "background plus objects" image model. The latter, implicitly, is very widely used: object detection packages estimate the local background, and then define protrusions from this as objects; or in image restoration, a two-channel algorithm regularizes the background differently from non-background objects. In practice, astronomical images

often encapsulate more complex, superimposed objects and/or structures than is allowed for by the traditional image model.

Let us take image restoration as an example. There are different ways of enforcing, e.g., the smoothness of the background, or of planetary objects, by adapting the widely-used Richardson-Lucy (RL) method. A good alternative is de-noising through shrinking noisy wavelet coefficients. The latter define the wavelet-transformed image. Furthermore wavelet coefficients are obtained which define the transformed image at varying levels of resolution. The original image may be reconstructed from the series of wavelet-transformed images. A noise-removal strategy is based on the wavelet coefficients being clipped in value if they are considered to be associated with noise. Such an approach has been pursued by various authors. This strategy was investigated by Starck and Murtagh (1993) with the conclusion that such de-noising, in the framework of RL restoration, leads to significantly improved detection of faint objects. This de-noised RL image restoration method, used in the preparation of some of the images discussed below, is available in the MIDAS image processing system (version N093).

In this article we wish to see what insights the wavelet transform, at some appropriate resolution level, can offer in terms of uncovering faint extended structures and physical processes. Differing structures, which are not at all apparent in the given image, may become salient at other resolution scales. We select a range of *differences* of reso-

lution levels of the image, – which are sensitive to faint structures, and which are produced and output in the new MIDAS wavelet package. Thus, what may be referred to as a “level 1” image is the difference between the original image and the first wavelet-transformed image; the “level 2” image is the difference between the first and the second wavelet-transformed images; etc. Similar objectives have also been pursued using another wavelet-based approach, the H-transform. The latter is available in MIDAS as a command FILTER/ADAPTIV.

3. Cometary Coma Analysis

The abilities of the wavelet transform to provide insight on cometary comas was tested with images of the periodic comet P/Swift-Tuttle. The data were collected with the 1.2-m telescope at the Calar Alto Observatory in Spain in October and November 1992 and were kindly provided by Dr. K. Birkle of the Max-Planck-Institut für Astronomie, Heidelberg.

Figure 1 shows the cometary coma of P/Swift-Tuttle observed through the CN molecule filter of the IHW filter set. The isophote pattern is asymmetric with respect to the nucleus (= central brightness peak) and highly irregular which usually indicates the presence of jets in the coma. Figure 2 gives the level 4 wavelet transform result for the CN image. It is also easily possible to determine the geometry, the curvature and the approximate position angles of the jets at the nucleus from the wavelet image.

Compared to other methods for the coma structure enhancement (see Larson and Sekanina, 1984; A’Hearn et al., 1986; Schulz, 1990; Boehnhardt and Kohoutek, 1992) the wavelet analysis can be applied in a very convenient and straightforward way to cometary coma images. Most importantly, it does not depend on the accurate determination of the nucleus position as a reference point for angular or radial shifts (method of Larson and Sekanina, and of Schulz) or for the alignment of the images analysed (all other methods). Therefore, the interpretation of the wavelet analysed coma structures should not suffer from the presence of image processing artifacts or “diseases” (artificial structures, modified geometry, “blindness” as regards ring structures) as do each of the previous methods.

In summary, the wavelet analysis of cometary images promises to become a very useful tool for the enhancement of faint coma and tail structures. The identification of jets, fans, shells and brightness excess areas, and the derivation of their characteristics from such images can be used for the determination of important properties of cometary nuclei (rotation motion and axis, nucleography of activity centres) from ground-based observations.

4. Physical Processes around Elliptical Galaxies

The HST PC (Planetary Camera) image of elliptical galaxy NGC 4261, and the NTT SUSI image of the same object, as described in Zeilinger et al. (1993), were used. The objective was to uncov-

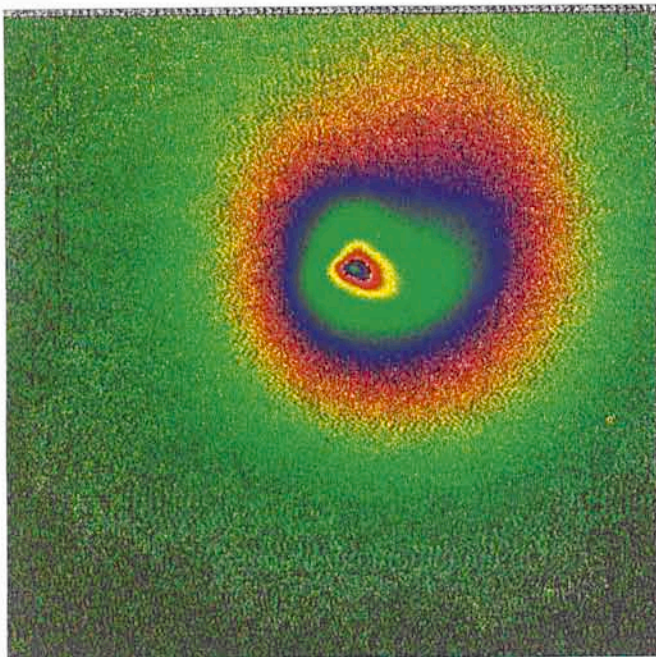


Figure 1: Comet P/Swift-Tuttle, October-November 1992.

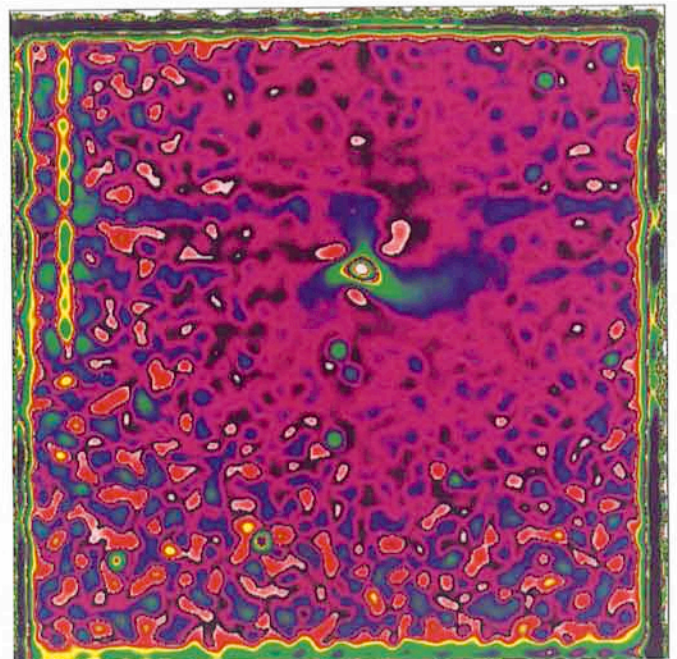


Figure 2: Wavelet transform of Figure 1 image, enhancing coma.

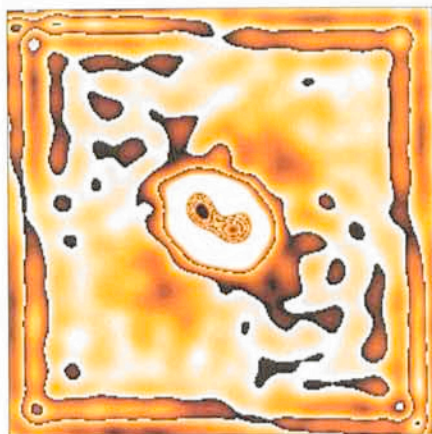


Figure 3: Wavelet transform of the SUSI image of NGC 4261.



Figure 4: Wavelet transform of the PC image of NGC 4261 (level 4).

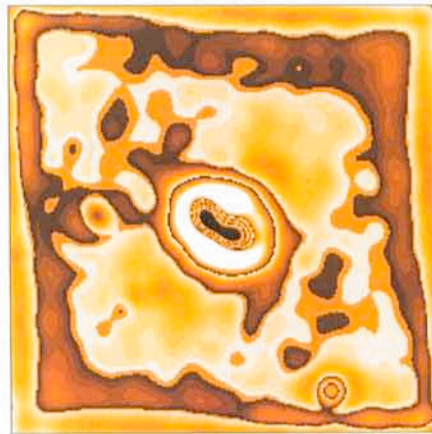


Figure 5: Wavelet transform of the PC image of NGC 4261 (level 3).

er the morphological characteristics of infalling matter in the central region of the galaxy. The original images provided no direct clues. Availability of a pair of images from different instruments with very different resolutions and signal levels affords a very good framework for validating the faint structures uncovered by the wavelet transform, as will be seen. (See also p. 28 of this issue.)

To lessen the impact of different effects due to image borders and image resolution, the SUSI image was re-binned to the scale of, and rotated to be aligned with, the PC image. Both images are shown in Zeilinger et al. (1993). The SUSI image was sharpened, and the PC image was restored, using 40 iterations of the de-noising RL method referenced in Section 1 above.

Figure 3 shows a wavelet transform image (level 4) of the de-noised and sharpened SUSI image. Figures 4 and 5 show two wavelet transform images (levels 3 and 4) of the de-noised and

restored PC image. A rather severe intensity transfer function has been used to emphasize the faint features external to, and closely adjacent to, the central dust lane of the galaxy. In the ground-based and level 3 space-born images one notices a clear protrusion to the right-hand side (which is far less pronounced in the level 4 PC image). Similarly, much of the detail in the upper left-hand side is common to these images. These features may be interpreted in terms of a warp related to the central disk. Emphasized features in the background, and towards the image borders, are artifacts which are of course uninteresting.

5. Conclusion

The wavelet transform provides a powerful exploratory tool for the analysis of faint features associated with processes which are superimposed and/or not easily distinguished. It is undemand-

ing in terms of image pre-preparation or modelling. If faint and complex features are present, then it offers an excellent way of heuristically demarcating them.

References

- A'Hearn, M.F.S., Hoban, S., Birch, P.V., Bowers, C., Martin, R. and Klinglesmith III, D.A., 1990, *Nature*, **324**, 649.
- Boehnhardt, H. and Kohoutek, L., 1992, *Icarus*, **99**, 106.
- Larson, S.M. and Sekanina, Z., 1984 *Astron. J.*, **89**, 571.
- Schulz, R., 1990, PhD thesis, University of Bochum.
- Starck, J.-L., 1993, "The wavelet transform", MIDAS Manual, Version N093.
- Starck, J.-L. and Murtagh, F., 1993, "Image restoration or sharpening with noise suppression using the wavelet transform", submitted.
- Zeilinger, W.W., Moller, P. and Stiavelli, M., 1993, *The Messenger*, this issue.

StarGates and StarWords

AN ON-LINE YELLOW PAGES DIRECTORY FOR ASTRONOMY

M. A. ALBRECHT, ESO, and A. HECK, Observatoire Astronomique, Strasbourg, France

1. General

Two new databases have been made available at ESO under Starcat (Pirenne et al., 1993). They are products of the Star's Family encompassing databases, data sets, dictionaries, directories, mailing labels, and so on, compiled by the second author (see Heck, 1991c). They offer a comprehensive *yellow pages* service of astronomical institutions world-wide as well as a lookup data-

base of acronyms and abbreviations used in astronomy and related sciences.

2. StarGates

StarGates is an on-line database of astronomy, space sciences, and related organizations in the world. It offers essentially the information listed in directories on paper published previously under the acronyms IDAAS (Heck,

1989a), IDPAI (Heck, 1989b) and ASpScROW (Heck, 1991 a&b), and currently available under the homogenized name of *StarGuides* (Heck, 1993 a&b). *StarGates* has however the advantage of being permanently updated. To date, more than 6,000 entries from about 100 countries are accessible.

Besides astronomy and space sciences, related fields, such as aeronautics, aeronomy, astronautics, atmo-

ANNOUNCEMENTS

Programmes Approved for Period 52

KEY PROGRAMMES

ESO No.	Principal Investigator	Title of submitted programme	Telescope
1-003-43K	de Lapparent et al.	A redshift survey of galaxies with $z \leq 0.6$ using multi-slit spectroscopy	NTT
1-005-43K	Rhee/Katgert et al.	Peculiar motions of rich clusters of galaxies	3.6m
1-012-43K	Bergeron et al.	Identification of high redshift galaxies with very large gaseous halos	NTT
1-014-43K	Mazure et al.	Structure and dynamical state of nearby clusters of galaxies	3.6m
1-019-47K	Vettolani et al.	A galaxy redshift survey over a fair sample of the Universe	3.6m
1-022-47K	Tammann et al.	The distance of the Centaurus Group: A test for various distance indicators	NTT
1-023-49K	Böhringer et al.	Redshift survey of ROSAT clusters of galaxies	3.6m, 2.2m, 1.5m
2-001-43K	Miley et al.	A study of the most distant radio galaxies	3.6m, NTT
2-007-43K	Cristiani et al.	A homogeneous bright quasar survey	2.2m, 1.5m, 1m
2-009-45K	Reimers et al.	A wide angle objective prism survey for bright QSOs	3.6m, 1.5m, 0.9mDu
2-013-49K	D'Odorico et al.	A statistical study of the intergalactic medium at high redshifts	NTT
3-001-43K	Israel et al.	CO as a tracer for the molecular content of the Magellanic Clouds	SEST
4-004-45/51K	Turatto et al.	A photometric and spectroscopic study of supernovae of all types	3.6m, NTT, 2.2m, 0.9Du
5-001-43K	Mayor et al.	Radial velocity survey of southern late-type Hipparcos stars	1.5m Danish
5-004-43K	Gerbaldi et al.	Astrophysical fundamental parameters of early-type stars of the Hipparcos Survey	1.5m
5-005-45K	Hensberge et al.	High-precision radial velocity determinations for the study of the internal kinematical and dynamical structure and evolution of young stellar groups	3.6m
6-003-45K	Danziger et al.	Optical identification content in selected regions of ROSAT All Sky X-Ray Survey	3.6m, 2.2m, 1.5m
7-008-51K	Habing et al.	Infrared standards for ISO	NTT, 2.2m, 1m
7-009-49K	Oblak et al.	CCD and conventional photometry of components of visual binaries	1m, 50cm, 0.9mDu
9-002-49K	Epchtein et al.	Deep near infrared survey of the southern sky (DENIS)	1m
9-004-51K	Ferlet et al.	Is our halo dark matter made of compact objects?	GPO, 1.5m Danish

Name(s)	ESO No.	Title of submitted programme and telescope(s)
Abbott/Pasquini/Fleming	07127	Time-series CCD photometry of cataclysmic variables discovered by ROSAT (0.9m Dutch).
Abbott/Shafter	07125	Time series CCD photometry of old novae (0.9m Dutch).
Acker/Cuisinier/Gesicki/Gorny/Tylenda	04035	WR nuclei of planetary nebulae: physical and chemical properties (1.5m).
Acker/Cuisinier/Gesicki/Gorny/Tylenda	04034	Wolf-Rayet nuclei of planetary nebulae: distances and expansion (1.4m CAT).
Alcalá/Covino/Krautter/Terranegra/Wichmann	07121	Spectroscopic and photometric monitoring of strongly variable weak-line T Tauri stars (0.5m, 3.6m).
Alloin/Blietz/Cameron/Rouan	01002	Diffraction limited broad-band studies of the Seyfert galaxies NGC 7469 and NGC 1068 (3.6m).
Andreani/La Franca/Miller/Cristiani/Goldschmidt/Read	02026	The cosmological evolution of the clustering of quasars (3.6m).
Antonello/Mantegazza/Poretti	03012	First overtone mode Cepheids in Magellanic Clouds (0.9m Dutch).
Appenzeller/Beckmann/Nussbaum/Schoeller/Van Elst/Wagner/Weigelt	02036	Speckle imaging and speckle spectroscopy of nearby Seyfert galaxies (2.2m).
Azzopardi/Breysacher/Lequeux/Muratorio	01078	Final search and spectroscopic study of Wolf-Rayet stars in NGC 300 (3.5m NTT).
Baessgen/Bremer/Diesch/Grewing	04043	Detailed studies of old, extended planetary nebulae (1.5m).
Barthel/Hes	02050	The high-redshift nature of GPS radio sources: searching for the most distant quasars (2.2m)
Bergeron/Le Brun	01082	Identification of the gaseous systems detected by their CIV and Ly α in the quasar spectra of the HST KP (3.5m NTT).
Bertaux/Lallement/Beust	07115	Search for cometary water vapour towards β Pictoris (1.4m CAT).
Bertola/Persic/Pizzella/Salucci	01020	Modelling the dark matter component in Sa galaxies (1.5m).
Beuermann/Grupe/Thomas H./Reinsch/Fink	02006	Spectroscopic indicators for the soft X-ray excess in AGN (2.2m).
Beuzit/Lagrange/Tessier/Vidal-Madjar/Ferlet	07098	IR Observations of the β -Pictoris disk with adaptive optics (3.6m).
Blaauw/Srinivasan-Sahu	04052	The Distance of the Vela molecular ridge (1.4m CAT).
Bockelee-Morvan/Gautier/Owen	07131	Search for cometary gas around β Pic and Fomalhaut (SEST).
Bouvier/Beuzit/Perrier/Sams	07114	High angular resolution imaging of close pre-main sequence binaries (3.6m)
Bower/Böhringer/Ellis/Castander/Couch	01074	The dynamical structure of galaxy clusters at $z = 0.5$ (3.6m).
Brandner/Zinnecker	07058	Component colours and spectroscopy of low-main-sequence (PMS) binaries (0.9m Dutch, 1.5m, 3.5m NTT).

Name(s)	ESO No.	Title of submitted programme and telescope(s)
Broadhurst/Moeller/Szalay	01031	Cluster mass profiles via amplification of background galaxy fluxes (3.5m NTT).
Bues/Karl	07081	Spectral variability of single magnetic white dwarfs (1.5m).
Buonanno/Vietri/Marconi	05008	Young globular clusters in the Milky Way (2.2m).
Cabrit/Cesarsky/Lagage/Olofsson/Pantin	07096	10 micron spectro-imaging of young outflow sources (3.6m).
Cacciari/Bragaglia/Fusi Pecci/Carretta	05010	Spectroscopic study of blue horizontal branch stars in globular clusters (1.5m).
Calvani/Sulentic/Marziani	02052	Orientation effects in radio loud AGN (1.5).
Capaccioli/Freeman/Ford/Hui/Arnaboldi	01086	Dynamics of the outer halos of elliptical galaxies (3.5m NTT)
Caraveo/Bignami/Meregheggi/Mignani/Goldoni/Pacini/Salvati	06018	Optical studies of isolated neutron stars detected as X/gamma-ray sources (3.5m NTT).
Carollo/Danziger/De Zeeuw	01116	Linking stellar population and orbital structure in elliptical galaxies (2.2m).
Carrasco G./Loyola	07060	UBVRI photometry of FK5 faint stars (0.5m).
Casoli/Boselli/Braine/Combes/Fouqué/Gavazzi/Karachetseva/Kazes/Lequeux	01003	The CO emission of isolated spirals (SEST).
Castellani/Brocato/Piotto	05027	White dwarfs in old open clusters (3.5m NTT).
Caulet/Hasinger/Pietsch/Smith	03033	Probing the IS gas of the superbubble LMC2 (3.6m).
Cayrel/Nissen/Beers/Spite F./Spite M./Andersen J./Nordstroem/Barbuy	07029	Survey of very metal-poor stars and nucleosynthesis in the galaxy (1.5m).
Char/Labra/Berrios/Maldini/Jankov/Foing/Neff/Di-Sheng	07132	Survey de la variabilité chromosphérique d'étoiles à rotation rapide (0.5m, 1.4m CAT).
Chiosi/Ortolani/Bertelli/Vallenari	03037	Star formation history of the Magellanic Clouds (2.2m).
Cimatti/Freudling	02016	A millimetric view of distant radio galaxies ($z > 1$) (SEST).
Clausen/Storm/Tobin/Hilditch/Hill/Gimenez	03025	Eclipsing binaries in the Magellanic Clouds – distances and absolute dimensions (3.5m NTT).
Collins/Nichol/Guzzo	01045	Multiobject spectroscopy of distant clusters of galaxies (3.6m).
Combes/Saint-Pé/Tomasko/Demailly/Faucherre/Encrenaz	08014	Very high spatial resolution study of Titan in the near IR (3.6m).
Corradi/Schwarz H.	04046	Do bipolar nebulae have the hottest central stars of PNe? (1.5m).
Costa/Grebel/Macconnell/Roberts/Wing	07052	Red supergiants as tracers of Galactic spiral arms (1.5m).
Courvoisier/Bouchet/Blecha/Paltani	02046	Coordinated observations of 3C 273 (1.5m, SEST).
Cox/Bronfman/Roelfsema	04047	A study of the photon dominated region facing Trumpler 14 (SEST).
Cunow/Naumann/Ungruhe/Sommer	01040	Magnitude calibration for homogeneity studies of the Universe (0.9m Dutch).
Danks/Sembach/Caulet	04048	Gas kinematics and physical conditions in the Vela supernova remnant (1.4m CAT).
Danziger/Baade/Della Valle	07023	Optical spectroscopy of the visible counterpart of the bright radio millisecond pulsar J0437-4715 (3.6m).
Danziger/Baade/Gouiffes/Della Valle	07022	Fast photometry of the millisecond pulsar candidate (3.6m).
Danziger/Bouchet/Gouiffes/Lucy/Fransson/Mazzali/Della Valle	03005	SN 1987A (SEST, 1.5m Danish 2.2m, 3.6m).
Danziger/Carollo	01117	Optical and infrared colour gradients in early-type galaxies (2.2m, 1.5m Danish).
Danziger/Liu	04049	Observations of molecular hydrogen emission from planetary nebulae (3.5m NTT, 1.5m).
Danziger/Mendez/Kudritzki/Mazzali/Lucy/Ciarullo/Jacoby/Roth/Soffner	01053	Determining distances to galaxies with well-studied SN Ia's using the PNLF method (3.5m NTT).
De Angelis	08023	Asteroid photometry for pole and shape determination (0.9m Dutch).
De Boer/Will/Bomans/Seggewiss	03006	Spectroscopic improvement of the age determination of NGC 1948 (1.5m).
De Medeiros/Lèbre/Charbonnel	07107	Lithium and rotation in subgiant stars (1.4m CAT).
De Ruiter/Lub	02075	Variations of emission line and continuum intensities in Seyfert nuclei (0.9m Dutch, 1.5m).
De Winter/Thé	07137	Detection of mass-outflow indicators of newly discovered young stellar objects of intermediate mass (0.9m Dutch).
De Winter/Van den Ancker	07135	Astrophysical properties of newly found early-type young stars associated with strong IRAS-sources (0.5m Danish, 1.5m, 0.5m).
Della Valle/Bianchini/Duerbeck/Oegelman/Orio	07025	Novae as standard candles: calibrations of nova shells (3.6m).
Dennefeld/Bertin/Boulanger/Moshir	01050	The nature of the faintest IRAS galaxies and galaxy evolution (3.6m).
Dieters/Van der Klis	07138	Spectrophotometry of CP Pub: Weighing the white dwarf (1.5m).
Doyle/Houdebine/Gunn	07033	Eclipse imaging of active binaries: coronal mass ejections & related phenomena (1.4m CAT).
Drossart/Forni/Benit/Bibring/Lellouch/Rosenqvist	08013	Observations of the Jovian system at 4 microns with COME-ON PLUS (3.6 m).
Dürbeck/Seitter	07046	Accretion disk properties and masses of bright exnovae (1.5 m).
Duquenois/Mariotti/Mayor/Perrier	07104	Infrared imaging of very low mass companions to nearby stars (3.6 m).
Duquenois/Mayor	07103	Stellar duplicity of very low mass stars (1.5 m Danish).
Elst	08010	L5 Trojan search (Schmidt).
Falomo/Pesce/Treves	02005	The environment of BL Lacertae objects (3.5 m NTT).
Favata/Barbera/Micela/Sciortino	07042	Lithium abundance determination in a sample of volume-limited main-sequence K stars (1.4 m CAT).
Favata/Barbera/Micela/Sciortino/Schachter	06004	Identification and classification of candidate stellar Einstein Slew Survey sources (1.4m CAT, 1.5 m).
Favata/Micela/Sciortino	07041	Lithium abundance in a sample of active binaries with known levels of X-ray emission (1.4 m CAT).
Felenbok/Jablonka/Alloin/Arimoto/Bica/Balkowski/Cayatte/Kraan-Korteweg	01062	1. Spectrophotometric properties of spiral galaxies; 2. Search in the Galactic plane toward the Great Attractor (3.6 m).

Name(s)	ESO No.	Title of submitted programme and telescope(s)
Ferlet/Hobbs/Wallerstein	04023	Variable interstellar absorption within the Vela supernova remnant (1.4 m CAT).
Ferrari/Bucciarelli/Massone/Pizzuti/Koornneef/ Lattanzi/Lasker/Postman/Siciliano/Le Poole Forni/Bibring/Benit	05030	Photometric calibrations for the southern sky surveys (0.9 m Dutch).
Freudling/Alonso/Da Costa/Wegner	08012	Observations of the Jovian system at 2 microns with COME-ON-PLUS (3.6 m).
Fusi Pecci/Cacciari/Bragaglia/Ferraro/Carretta	01090	The peculiar motion of galaxies and the density of the Universe (1.5m Danish, 1.5m).
Gahm/Carlqvist/Mattila/Kaas	05009	UV survey of Galactic globular clusters (1.5 m Danish).
Galletta/Piccoli/Tomadini	04025	Serpentine structures in the Chamaeleon Dark Clouds (Schmidt).
Gehren/Baumüller/Fuhrmann/Reetz	09001	A search for Sun companions (1.4 m CAT).
Gemmo	07026	CNO abundances in metal-poor stars (3.6 m).
Genzel/Beckers/Léna/Sams/Brandl	07039	An infrared search for companions to white dwarfs (2.2 m).
	01066	Diffraction limited K-band studies of high-z galaxy evolution and morphology (3.6 m).
Gochermann/Tappert	03018	Physical and chemical parameters of LMC supergiants from medium-resolution spectroscopy (1.5 m).
Gochermann/Tappert	03017	Physical parameters of LMC supergiants from UBVR-I-JHKL photometry (1 m).
Gochermann/Zaum/Tappert	03019	UBV photometry of LMC galactic foreground and member stars (0.5 m).
Gosset/Manfroid/Vreux/Smette	07013	Study of eclipses of the SB1 system WR22 (0.5 m Danish).
Gosset/Moreau	02031	A multi-technique quasar survey: the variability criterion (Schmidt).
Gosset/Moreau	02030	An objective-prism survey for high redshift quasars: a feasibility test (Schmidt).
Gouiffes/Oegelman/Augusteyn/Bouchet	03030	Optical search for the pulsar in SN1987A. (3.6 m).
GredeI	04017	Narrow band imaging of Herbig-Haro objects and jets in H and K (2.2 m).
GredeI	04016	Near-infrared spectroscopy of Herbig-Haro objects and jets (3.5 m NTT).
GredeI/Kopp	04018	Interstellar molecular absorption lines towards southern OB associations (1.4 m CAT).
Grenier/Gouiffes/Oegelman	07139	Fast photometry of the Vela gamma-ray pulsar (3.6 m).
Griffin R.E./Griffin R.E.M./Mayor/Clube	05017	Radial velocities of stars in the Clube selected areas (1.5 m Danish).
Gustafsson/Andersen J./Edvardsson/Nissen	05031	The transition from the thick to the thin galactic disk (1.4 m CAT).
Henning/Launhardt	05001	A 1.3mm continuum and CO outflow search for extreme class I sources (SEST).
Hensberge/David/Verschueren	05032	Study of the double-lined eclipsing binary NGC 2244-200 = V578 Mon (0.5 m Danish)
HES/Barthel/Peletier	02028	Infrared imaging of hotspots in radio sources (2.2 m).
Heydari-Malayeri/Rigaut	03008	High resolution investigation of the most massive stars in the Magellanic Clouds (3.6 m).
Hillier/Kudritzki/Lennon/Butler/Hamann/ Wesołowski	07141	Constraints on massive star evolution from abundances in LMC WC stars (3.5 m NTT).
Hoffmann	08001	Structure of suspected composite asteroids (1.5 m Danish).
Hutsemékers/Van Drom/Remy	02021	Polarization properties of BAL QSOs (3.6 m).
Ivanste/Fouqué/Richtler/Quintana	01017	The distribution of dwarf galaxies in the Fornax Cluster (3.6 m).
Iovino/Chincarini/Garilli/Maccagni/Saracco	01093	K-band galaxy counts: the way to Q0? (2.2 m).
Israel/De Graauw/Van der Hulst/Lacy/Kelly	01095	Low resolution spectroscopy of galactic nuclei in the near-IR (3.5 m NTT)
Ivison/Seaquist/Hughes/Schwarz H.	07001	A simultaneous multi-frequency study of symbiotic stars: The cm-mm continuum (SEST).
Jerjen/Binggeli	01096	Exploring the spatial structure of the Centaurus Cluster by surface photometry of its dwarf galaxies (1.5 m Danish).
Jorissen/Mayor/North	07050	The evolutionary status of S stars and dwarf Barium stars (1.5 m Danish).
Jüttner/Baschek/Stahl/Wolf	03011	Abundances from early B-type giants in selected regions of the Magellanic Clouds (3.6 m).
Kaper/Hammerschlag/Blondin	06010	Simultaneous optical, UV, and X-ray observations of HMXRB Vela X-1 (1.4 m CAT).
Kneer/Bender/Krautter	01015	Spectroscopy of distant, faint clusters of galaxies (3.6 m).
Knude/Bowyer	04053	Distances of local EUV shadowing clouds (0.5 m Danish).
Kopp/Smette	02048	Search for CO in quasar absorption lines (SEST).
Kostiuk/Käuffl/Livengood	08021	Morphology of Jupiter's thermal infrared aurorae (3.6 m).
Krautter/Alcalá/Schmitt/Mundt/Wichmann/ Zinnecker	07071	Search for weak-line T Tauri stars in Chamaeleon and Lupus (1.5 m).
Kudritzki/Mendez/Gabler/Puls/Roth	07090	Mass loss rates of central stars of planetary nebulae (3.5 m NTT).
Kürster/Hatzes/Cochran/Dennerl/Döbereiner	07002	High precision stellar radial velocities, part III (1.4 m CAT).
Kürster/Schmitt	07143	Towards a butterfly diagram for AB Dor (1.4 m CAT).
Lagage/Pantin	07095	Profile and composition of the inner dust disk of the β -Pictoris star (3.6 m).
Lagerkvist/Magnusson/Erikson	08005	Pole orientations and shapes of asteroids (1 m).
Lagrange/Vidal-Madjar/Ferlet/Corporon/De- leuil/Gry/Tobin	07116	High resolution survey of β Pictoris with the CES (1.4 m CAT).
Lamers/De Graauw/Waters/Loup/Van Hoof	07144	Infrared spectroscopy and imaging of LBV's (3.5 m NTT).
Lennon/Kudritzki/Dufton	03041	An intermediate dispersion spectroscopic survey of B-supergiants in the SMC (3.5 m NTT).
Lennon/Kudritzki/Husfeld/Herrero/Gabler	07016	Spectroscopy of luminous blue stars in the Local Group galaxies NGC 6822, IC 1613 and WLM (3.5 m NTT).
Liller/Alcaino/Alvarado/Wenderoth	03002	UBVR-I photometry of Magellanic Clouds cluster standards (1m).
Lin Yun	07091	Near-infrared imaging of young stellar objects in Bok globules (2.2m).
Lin Yun	07019	Narrow-Band imaging of T Tauri stars associated with Bok globules (0.9m Dutch).
Lin Yun/Clemens	07047	Spectral energy distributions of young stellar objects in Bok globules: millimeter fluxes (SEST).

Name(s)	ESO No.	Title of submitted programme and telescope(s)
Lin Yun/Clemens	07028	HCN survey of physical conditions in cores of star-forming Bok globules (SEST).
Lindblad P.A.B./Lindblad/Joersaeter	01036	Photometry of nearby barred spiral galaxies (1.5m Danish).
Lindblad/Joersaeter/Vaesterberg/Lindblad P.A.B.	02029	Active nuclei of NGC 613 and NGC 1365 (1.5m).
Loiseau/Combes	01097	CO observations of active interacting galaxies – III (SEST).
Lorenzetti/Moneti/Spinoglio/Liseau	07066	The initial luminosity function in the Vela star forming region (2.2m).
Loup/Hron/Kerschbaum/Zijlstra/Waters	07145	Oxygen-rich AGB-stars with 60 micron excess (1m, 1.5m).
Macchetto/Giavalisco/Steidel/Sparks	01098	Optical and near-infrared spectroscopy of radio-quiet galaxy candidates at $z > 3$ (3.5m NTT).
Magnan/De Laverny/Menessier	07021	UBVRI photometry of Mira variables during a whole cycle and study of the light curve in different cycles (0.5m).
Mandolesi/Crane/Attolini/Palazzi	04054	Small scale structure of diffuse interstellar clouds (1.4m CAT).
Marano/Zamorani/Zitelli/Cimatti/Giacconi/Hasinger	02038	Deep multi-colour imaging for faint X-ray sources and a search for faint quasar candidates ($22.0 < MB < 24.5$) (3.5m NTT).
Mariotti/Beuzit/Duquennoy/Eckart/Perrier	07049	Diffraction-limited imaging of the brown dwarf candidate G29-38B (3.6m).
Mathys/Landstreet/Lanz/Manfroid/Hubrig	07063	Ap stars with resolved magnetically split lines (1.4m CAT).
Megeath/Wilson	04003	A survey for dense gas in a young GMC (SEST).
Menard/Léna/Malbet/Català/Monin/Schuster	07100	Deep high angular resolution imaging of selected young stellar objects with COME-ON PLUS (3.6m).
Mermilliod/Mayor	05003	Constraints on stellar formation from orbital elements of cluster binaries (1.5m Danish).
Mermilliod/Turon/Gomez/Sellier/Guibert/Robichon	05014	Photometric calibration for open clusters observed with Hipparcos (1.5m Danish).
Meylan/Azzopardi/Dubath/Lequeux	01118	Search for dark matter in the Fornax dwarf spheroidal galaxy (3.5m NTT).
Meylan/Djorgovski/Thompson	02060	A search for quasar protoclusters at high redshifts (3.5m NTT).
Moeller/Warren	01033	The size and morphology of normal galaxies at $z=3$ (3.5m NTT).
Molaro/Rebolo/Martin E./Charles/Casares	06007	Search for lithium in black-hole systems (3.5m NTT).
Moneti/Zinnecker/Wilking	07118	Infrared imaging and photometry of southern T Tauri binary systems (2.2m).
Montmerle/André/Casanova/Cesarsky/Lagage	07097	Protostars and star formation activity in the Chamaeleon I cloud (3.6m).
Moorwood/Kotilainen/Van der Werf/Oliva	02008	Near-infrared spectroscopy of starburst and Seyfert galaxies (3.5m NTT, 2.2m).
Motch/Hasinger/Pietsch	06021	Spectroscopic study of a new luminous supersoft X-ray binary in the Galaxy (1.5m).
Mottola/Lagerkvist/Di Martino/Neukum	08024	Physical studies of Trojans and Outer Belt asteroids (1m).
Nußbaumer/Mürset/Schild/Schmid/Schmutz	07068	Wind structure of red giants in symbiotic systems (1.4m CAT).
Oliva/Moorwood/Origlia	05005	Near infrared spectroscopy of Magellanic Cloud clusters (3.5m NTT).
Oliva/Reconditi/Origlia/Moorwood	04007	Infrared line imaging of SMC/LMC supernova remnants (2.2m).
Omont/Walmsley/Chini/Lèbre/Menessier/Nyman/Forveille	07087	Bolometer monitoring of Mira variables (SEST).
Orio/Bianchini/Della Valle/Massone/Oegelman	07150	Optical identification of supersoft X-ray sources (1.5m Danish).
Pagani/Castets/Langer	04027	Search for ^{16}O ^{18}O towards cold dark clouds at 234 GHz (SEST).
Palazzi/Penprase/Casey	04024	High resolution spectroscopy of central stars in reflection nebulae (1.4m CAT).
Pallavicini/Gratton/Randich	07056	Lithium abundance and post-main sequence evolution (1.4m CAT).
Pallavicini/Haisch/Schmitt/Pasquini	06008	Chromospheres, coronae and winds of cool giants (1.4m CAT).
Panagi/Andrews/Bouchet	07055	Transient and short period phenomena in late-type stars (0.5m, 1m).
Paquet/Arimoto/Moellenhoff	01046	Line-strength gradients in disks of S0 galaxies (1.5m).
Paquet/Davies/Bender	01038	Low mass E/S0's: the building blocks of giant ellipticals? (3.5m NTT).
Paresce/Clampin/Roberto/Ferrari/Abbott	07151	Deep imaging of circumstellar disks with the NTT coronagraph (3.5m NTT).
Pasquini/Belloni	06003	X-ray sources and binaries in M67 (3.6m).
Pasquini/Randich/Andersen J.	07059	Hunting young, nearby G stars (1.4m CAT).
Patat/Barbon/Benetti/Cappellaro/Turatto	07152	The intrinsic colours of supernovae of type 1a (0.9m Dutch).
Peterson/D'Odorico/Moorwood/Tarengi/Yoshii/Silk	01073	Galaxy counts to faint K-prime magnitudes (2.2m).
Pettersson	07155	Young stellar objects in the direction of the Gum Nebula (0.9m Dutch, Schmidt).
Piotto/Aparicio/Djorgovski	05036	Stellar luminosity functions of the outer halo globular clusters (3.5m NTT).
Pogodin	07005	Circumstellar envelopes of AE Herbig stars of the PCyg-subgroup with inhomogeneous structure (1.4m CAT).
Pottasch/Manchado/Garcia-Lario/Sahu K.C.	04058	Direct imaging and photometry of proto-planetary nebulae candidates (0.9m Dutch).
Pottasch/Manchado/Garcia-Lario/Sahu K.C.	04057	Infrared spectroscopy of newly discovered IRAS proto-planetary nebulae (3.5m NTT).
Pottasch/Manchado/Garcia-Lario	04056	Optical spectroscopy of BQ[] stars and related objects (1.5m).
Prusti/Abraham/Palla	07151	Luminosity function of pre-main-sequence stars in Lupus (2.2m).
Ramella/Falco/Fabricant/Dressler/Tucker	01025	Spectroscopy of the giant gravitational arc in C10657-56 (3.5m NTT).
Rasmussen/Joergensen	01034	The fundamental plane for E and S0 galaxies in the Fornax (1.5m Danish).
Reimers/Köster	07080	An empirical test of the mass-radius relation for white dwarfs (3.6m).
Reinsch/Beuermann/Thomas H./Becker/Trümper/Motch/Pakull	06016	Optical counterparts of binary millisecond pulsars and supersoft X-ray sources (2.2m).
Reinsch/Beuermann/Thomas H.	06011	The nature of the peculiar cataclysmic variable KO Velorum (0.9m Dutch).
Reipurth	04020	Herbig-Haro jets from newborn stars (3.5m NTT).
Reipurth/Lago/Pedrosa	07061	H α emission lines in T Tauri stars: profiles and variability (1.4m CAT).
Richtler/Hilker/Gieren	03009	CCD Strömgren photometry of LMC cluster and field stars (1.5m Danish).
Rigaut/Léna/Gehring/Cuby	07099	High angular resolution imaging of η Car (3.6m).

Name(s)	ESO No.	Title of submitted programme and telescope(s)
Röttgering/Bremer	02065	Compact radio galaxies and the continuum alignment effect (2.2m).
Roueff/Kopp/Le Bourlot/Gerin	04059	Search for CS and CN in the diffuse clouds close to ζ Oph (SEST).
Rutten/Harlaftis/Dhillon/Van Paradijs	06002	Spatially-resolved spectra of accretion disks in cataclysmic variables (2.2m)
Saglia/Davies/Baggley/Colless/Burstein/ Bertschinger/McMahan/Wegner	01007	Peculiar velocities of galaxy clusters in the Pisces-Cetus supercluster (3.6m)
Schild/Tennyson/Miller	04006	Search for the molecular ion H^3+ in Orion (2.2m).
Schild/Vogel/Nußbaumer/Mürset/Schmid	07040	Symbiotic stars in the Magellanic Clouds (2.2m, 3.6m).
Schober	08019	Variable lightcurves of asteroids 258, 369 and 582 (0.5m).
Schutte/Van Dishoeck/Helmich/Tielens/Gredel	04004	Interstellar ice composition toward southern infrared sources (3.5m NTT).
Seaquist/Ivison/Evans/Schwarz H.	07034	A maser survey of symbiotic Miras (SEST).
Shaver/Wall/Kellermann	02001	A search for radio-loud quasars at $z > 5$ (3.6m).
Siebenmorgen/Zijlstra/Gredel	04032	The dust composition in Herbig-Haro objects (3.5m NTT).
Simon/Saleck/Stutzki/Winnewisser	04038	Abundance and excitation of CN, ^{13}CN and $C^{15}N$ in OMC1 (SEST).
Sivan/Perrin	04002	Spectrophotometry of reflection nebulae illuminated by late type stars (1.5m).
Sommer-Larsen/Christensen/Beers/Flynn	05007	Bright blue horizontal branch field stars in the inner galactic halo (1.5m).
Soucall/Kneib/Fort/Mellier	01027	Spectroscopic survey of the galaxies in S295, and redshift determination of the arcs in MS2137-23 (3.5m NTT).
Spite F./Spite M./François/Hill	05026	Abundances of Lithium and heavy elements in NGC 2004 (3.5m NTT).
Stark/Gredel	04011	Molecular absorption lines toward cometary interstellar cirrus clouds (1.4m CAT).
Stecklum/Eckart/Henning/Fischer	07102	High angular resolution observations of Herbig Ae/Be and Vega-like stars (3.6m)
Stecklum/Henning/Pfau	07086	NIR photometry of candidate pre-main sequence stars (1m).
Sterken	07015	Long-term photometry of variables (0.5m Danish)
Sterken	07014	Pulsating B stars in NGC 3293 (0.5m Danish).
Stirpe/Gianuzzo	02037	Are narrow line Seyfert 1 nuclei variable? (1.5m)
Surdej et al.	02047	Spectroscopic identification of gravitational lens candidates (3.5m NTT).
Telles/Kotilainen/Terlevich	01075	High resolution near-infrared imaging of HII galaxies (2.2m).
Thé/Grady/Perez	07051	High resolution and S/N spectroscopy of edge-on proto-planetary disk systems (1.4m CAT).
Thé/Molster	07010	Planet formation in proto-planetary dust clouds of Herbig Ae/Be stellar systems (0.5m).
Theuns/Warren	01056	Search and identification of intergalactic planetary nebulae in galaxy clusters (3.5m NTT).
Thomas H./Trümper/Beuermann/Reinsch/ Simon	06013	Spectroscopic identification of ROSAT X-ray sources near the South Ecliptic Pole (SEP) (1.5m)
Tinney	07070	A spectral atlas for the latest M-dwarfs (3.5m NTT).
Tinney	07069	Parallaxes of VLM stars (2.2m).
Tinney/Mould/Reid	05016	The kinematics of stars at the bottom of the main sequence (3.6m).
Toussaint/Reimers/Hünsch	07106	A high resolution study of short-lived absorption in three M giants (1.4m CAT).
Turon/Mermilliod/Gomez/Sellier/Guibert/ Robichon	05006	The core-halo structure of open clusters observed with Hipparcos (Schmidt).
Van de Steene/Sahai/Pottasch	07111	A search for molecular envelopes in newly discovered planetary nebulae (SEST).
Van der Blik/Gustafsson	07053	Chemical abundances analysis of the royal standard stars for ISO (1.4m CAT).
Van der Hülst/Van der Werf/De Graauw/Israel/ Joubert/Baluteau	03026	Excitation of HII regions in the Magellanic Clouds (3.6m).
Van der Kruit/De Grijs/Peletier	01021	Optical surface photometry of edge-on spiral galaxies (1.5m Danish).
Van der Werf/Van der Hülst	03027	Excitation of molecular and ionized gas in the Magellanic Clouds (2.2m).
Van Dishoeck/Helmich/Hogerheijde	04005	The chemical state of southern star-forming regions (SEST).
Van Dishoeck/Langevelde/Hogerheijde	04009	The nature and dust content of young stellar objects in Chamaeleon (SEST).
Van Winckel/Balm/Waelkens	07048	CH^+ of the Red Rectangle Nebula (1.4m CAT).
Vidal-Madjar et al.	09002	Is our halo dark matter made of compact objects? (Schmidt).
Waelkens	07030	η Orionis (1.4m CAT).
Waelkens/Mayor	07031	Radial-Velocity variations in post-AGB stars (1.5m Danish).
Wagner	02035	High resolution spectroscopy of the NLRS of NGC 1068 and NGC 1386 (3.6m).
Walsh/Walton/Pottasch	04015	Spectral classification and distances for binary star planetary nebulae (2.2m).
Wampler/Hazard/Turnshek	02044	An absorption-line study of chemical abundances in quasar nuclei (3.5m NTT, 3.6m).
Wampler/Wang	03035	The SN 1987A environment (3.5m NTT).
Wanders/Bergvall/Oestlin/Van Groningen/ Roennback/Olofsson/Oerndahl	02071	Host galaxies of intermediate-redshift quasars (3.5m NTT).
Warren/Iovino/Shaver	01055	The evolution of the galaxy correlation function (3.6m).
Warren/Pownall/Hewett	01113	$H\alpha$ emission from galaxies at $z > 2$ (2.2m).
Waters/Zijlstra/Käufli/Van Winckel/Meixner	07093	10 micron direct imaging of detached envelopes around post-AGB stars (3.6m).
Way/Quintana/Infante	02073	A spectrophotometric survey of AGN in rich clusters of galaxies (2.2m).
Weigelt/Beckmann/Davidson/Kohl/Nußbaum/ Schöller/Seggewiss/Van Elst	07101	Speckle masking and speckle spectroscopy observations of stellar objects (2.2m).
West M.J./Bothum	01057	Globular cluster populations in Hickson compact groups (3.5m NTT).
West R./Hainaut/Marsden/Meech/Smette	08017	Activity in very distant comets (3.5m NTT).
Westerlund/Azzopardi/Breysacher	03004	Low-luminosity carbon stars in the Large Magellanic Cloud (2.2m).
Wild/Cameron/Eckart/Rothermel	02025	$^{12}CO/C^{18}O$ ratio in the nucleus of Centaurus A (SEST).
Wild/Eckart	01028	The molecular ISM of the starburst galaxy NGC 5188 (SEST).
Wolf/Kaufer/Mandel/Stahl/Gaeng/Gummers- bach/Sterken	07017	Structure and variability of the winds of A-type supergiants (0.5m).

Name(s)	ESO No.	Title of submitted programme and telescope(s)
Wolter/Maccacaro/Cillegi	06014	Search for distant clusters of unusual objects among unidentified EMSS sources (2.2m).
Zamorani/Giacconi/Hasinger/Marano/Mignoli/Zitelli	06015	Spectroscopic follow-up of ROSAT discovered X-ray sources in the "Marano Field" (3.6m).
Zijlstra/Loup/Waters/Tinney/Groenewegen	03028	TIMM observations and infrared photometry of obscured AGB stars in the LMC (3.6m).
Zinnecker/McCaughrean/Meylan	03031	Testing the starburst paradigm in 30 Doradus (2.2m).

ANNOUNCEMENT

ESO/EIPC Workshop on The Light Element Abundances

Marciana Marina, Isola d'Elba
22–28 May 1994

A joint ESO/EIPC workshop on the Light Element Abundances will be held from 22 to 28 May 1994, at the Elba International Physics Center, Marciana Marina, Isola d'Elba, Italy.

The workshop is intended to discuss the theory and observations of the light elements ($z < 5$) in relation to the following topics:

- Primordial Abundances
- Elements at High Redshift
- Stellar Processes
- Interstellar Processes
- Galactic Evolution
- Isotopic effects

Organizing Committee:

P. Crane (ESO), R. Ferlet (Paris), F. Ferrini (Pisa), D.L. Lambert (Austin), P. Molaro (Trieste), P. Nissen (Aarhus), B. Pagel (NORDITA), L. Pasquini (La Silla), G. Steigman (Columbus).

Contact Address:

Phil Crane, European Southern Observatory
Karl-Schwarzschild-Str. 2, D-85748 Garching bei München,
Germany
e-mail: crane@eso.org fax: +4989320-06-480/320-23-62

ANNOUNCEMENT

ESO Workshop on QSO Absorption Lines

ESO, Garching
21–24 November 1994

An ESO workshop on QSO absorption lines will be held from 21 to 24 November 1994, at the Headquarters of the European Southern Observatory, Garching bei München, Germany.

The workshop is intended to discuss the theory and observations of QSO absorption lines in relation to the following topics:

- Galactic halo and interstellar medium
- Low-redshift systems
- Intrinsic absorption lines and BAL systems
- Ly-alpha clouds
- Damped systems
- Metal systems
- Probing the large scale structure
- Probing the Universe at high redshifts

Organizing Committee:

S. D'Odorico, G. Meylan, P. Petitjean, P. Shaver, J. Wampler, ESO.

Contact Address:

Georges Meylan, European Southern Observatory
Karl-Schwarzschild-Str. 2, D-85748 Garching bei München,
Germany
e-mail: gmeylan@eso.org fax: +4989320-06-480/320-23-62

The European Southern Observatory (ESO) is an intergovernmental organization responsible for astronomical research in the southern hemisphere. The eight member States of ESO are Belgium, Denmark, France, Germany, Italy, the Netherlands, Sweden and Switzerland. As the prime European astronomical centre, ESO occupies a leading position in the world's scientific community. Its research work is of great value to many areas of science and industry.

Applications are invited for the position of (m/f):

Associate Director for Science (ref. ESD205)

within the Science Division at the ESO Headquarters, in Garching near Munich, Germany.

Assignment: a strong research-orientated scientific staff with diverse expertise is essential if ESO is to fulfil its mandate of providing and maintaining an international competitive multi-telescope observatory for its community of users. Within this framework, the Associate Director for Science will be responsible to the Director General for the overall quality of scientific research at ESO, for guiding the rebuilding and expansion of the scientific staff in anticipation of the Very Large Telescope era, for coordinating the participation of the scientific staff in the VLT project and for revitalizing the ESO Fellowship and Studentship programmes. A further responsibility will be to ensure the broad participation of the European astronomical community in all ESO activities and in particular in the VLT/VLT Interferometer programme.

Experience: the chosen candidate will have an outstanding record of achievement in one or more areas of modern astrophysics and will be widely experienced in the use of large ground-based optical telescopes. This will be combined with excellent management and leadership skills.

Contractual conditions: the Associate Directorship is intended as a tenured staff appointment. Nevertheless, serious consideration will be given to outstanding candidates willing to be seconded to ESO on extended leaves from their home institutions.

ESO remuneration and conditions: remuneration will be commensurate with background, experience and family status of the incumbent. The basic tax-free monthly salary will not be less than DM 12,402.-. To this may be added an expatriation allowance and other allowances depending on family status.

ESO staff enjoy highly-favourable working conditions and have every opportunity to demonstrate their skills in an international and creative environment equipped with advanced technologies.

Applications should specify the job reference and be submitted before October 31, 1993 to: The Director General, Prof. R. Giacconi, European Southern Observatory, Karl-Schwarzschild-Straße 2, D-85748 Garching near Munich, Germany. Tel. (089) 32006250.

ESO Studentship Programme

The European Southern Observatory has positions available for 12 research students. Six of these positions are at the ESO HQ in Garching, the other six at the Observatory, La Silla, Chile. Since students normally stay approximately 2 years, this means that each year a total of 6 students (3 at each location) may be accepted. These are applicable to any student enrolled in a Ph.D. (or equivalent) programme in institutions in the member states.

Potential candidates or their supervisors may obtain detailed information about the programme by requesting the updated brochure and application forms from the Personnel Administration and General Services at ESO HQ, Karl-Schwarzschild-Str. 2, D-85748 Garching bei München, Germany.

There is now an annual closing date of 15 October for applications.

ESO Users Manual 1993

The new (1993) edition of the ESO Users Manual has just become available and been distributed to Institutes in the ESO member States. Institutes which have not received a copy may obtain one on request addressed to the

ESO Visiting Astronomers Service
Karl-Schwarzschild-Str. 2
D-85748 Garching b. München, Germany

Tentative Time-Table of Council Sessions and Committee Meetings

November 4–5	Scientific Technical Committee
November 8–9	Finance Committee
November 25–26	Observing Programmes Committee
December 1–2	Council

All meetings will take place in Garching.

The Proceedings of the Second ESO/CTIO Workshop on

Mass Loss on the AGB and Beyond

(ESO Conference and Workshop Proceedings No. 46)

have now been published. The 479-p. volume, edited by H.E. Schwarz, is available at a price of DM 70,- (prepayment required).

Payments have to be made to the ESO bank account 2102002 with Commerzbank München or by cheque, addressed to the attention of

ESO, Financial Services
Karl-Schwarzschild-Str. 2
D-85748 Garching b. München, Germany

Please do not forget to indicate your complete address and the title of the Proceedings.

New ESO Preprints

June–August 1993

Scientific Preprints

920. T.R. Bedding: The Orbit of the Binary Star Delta Scorpii. *Astronomical Journal*.
921. F. Matteucci: Iron and Magnesium Evolution in Giant Elliptical Galaxies. A Cimatti and S. di Serego Alighieri: Stellar and Scattered Light in a Radio Galaxy at $z=2.63$.
G. Marconi et al.: Chemical Evolution of Blue Compact Galaxies. Papers presented at the Kiel Conference "Panchromatic View of Galaxies: their evolutionary puzzle".
922. C.M. Carollo et al.: Metallicity Gradients in Early-Type Galaxies. *Monthly Notices of the Royal Astronomical Society*.
923. P. Crane et al.: High Resolution Imaging of Galaxy Cores. *Astronomical Journal*.
924. N. Meyssonier and M. Azzopardi: A New Catalogue of $H\alpha$ Emission-Line Stars and Small Nebulae in the Small Magellanic Cloud. *Astronomy and Astrophysics Suppl.*
925. H. van Winckel et al.: An Atlas of High Resolution Line Profiles of Symbiotic Stars. Part I: Coudé Echelle Spectrometry of Southern Objects and a Classification System of $H\alpha$ Line Profiles. *Astronomy and Astrophysics*.
926. Bo Reipurth and H. Zinnecker: Visual Binaries Among Pre-Main Sequence Stars. *Astronomy and Astrophysics*.
927. M. Heydari-Malayeri et al.: HDE 269828: A Reddened Massive Star Cluster. *Astronomy and Astrophysics*.
928. M. Stiavelli et al.: Core Sub-Structure of Elliptical Galaxies: the Core Resolution Technique Applied to NGC 1399. *Astronomy and Astrophysics*.
929. J.K. Kotilainen and M.J. Ward: The Host Galaxies of Seyfert Type 1 Nuclei. *Monthly Notices of the Royal Astronomical Society*.
930. A.F.M. Moorwood and E. Oliva: Infrared Spectroscopy of Starburst and Seyfert Galaxies. Invited paper to appear in CIRP5: Topical Conference on Infrared Astrophysics. Infrared Physics (ed. F.K. Kneubühl).
931. M.A. Prieto and W. Freudling: New Evidence for an Anisotropic Radiation Field in NGC 5252. *The Astrophysical Journal*.
932. S.G. Djorgovski and G. Meylan: Appendices and Tables to appear in *Structure and Dynamics of Globular Clusters – Proceedings of a Workshop held in Berkeley, California, July 15th to 17th, 1992*, to honour the 65th birthday of Ivan King.

STAFF MOVEMENTS

Arrivals

Europe

SIML, Erich (D), Clerk (General Services)
TEUPKE, Svea (D), Secretary
ZELLER, Kurt (CH), Head of Personnel
HUBERT, Georgette (D), Secretary
CUMANI, Claudio (I), Associate
HUIZINGA, Edwin (NL), Fellow
AUSSEM, Alexandre (F), Coopérant
PETERSON, Bruce (Aus), Guest Professor
PETITJEAN, Patrick (F), Associate

Chile

KNEE, Lewis B.G. (Can.), Fellow (SEST)
MANFROID, Jean (B), Associate (Senior Visitor Progr.)
CLAESKENS, Jean-François (B), Coopérant
BRANDNER, Wolfgang (D), Student

Departures

Europe

BEELEN, Marion (NL), Secretary
PLÖTZ, Franz (D), Electro-Mechanical Engineer
BECKERS, Jacques (USA), VLT Programme Scientist
ZAGO, Lorenzo (I), Engineer/Physicist
SIEBENMORGEN, Ralf (D), Fellow

Chile

WILD, Wolfgang (D), Fellow
SMETTE, Alain (B), Coopérant/Associate

933. M.H.D. Ulrich: The Energy Budget on the Irradiation Model of Quasars. 2nd Workshop on Theory of Accretion Disks, MPI Garching, March 1993.

934. F. Murtagh and M. Sarazin: Nowcasting Astronomical Seeing: a Study of ESO La Silla and Paranal. *Publications of the Astronomical Society of the Pacific*.

ESO, the European Southern Observatory, was created in 1962 to . . . establish and operate an astronomical observatory in the southern hemisphere, equipped with powerful instruments, with the aim of furthering and organizing collaboration in astronomy . . . It is supported by eight countries: Belgium, Denmark, France, Germany, Italy, the Netherlands, Sweden and Switzerland. It operates the La Silla observatory in the Atacama desert, 600 km north of Santiago de Chile, at 2,400 m altitude, where fourteen optical telescopes with diameters up to 3.6 m and a 15-m sub-millimetre radio telescope (SEST) are now in operation. The 3.5-m New Technology Telescope (NTT) became operational in 1990, and a giant telescope (VLT=Very Large Telescope), consisting of four 8-m telescopes (equivalent aperture = 16 m) is under construction. It will be erected on Paranal, a 2,600 m high mountain in northern Chile, approximately 130 km south of the city of Antofagasta. Eight hundred scientists make proposals each year for the use of the telescopes at La Silla. The ESO Headquarters are located in Garching, near Munich, Germany. It is the scientific-technical and administrative centre of ESO where technical development programmes are carried out to provide the La Silla observatory with the most advanced instruments. There are also extensive facilities which enable the scientists to analyze their data. In Europe ESO employs about 200 international Staff members, Fellows and Associates; at La Silla about 50 and, in addition, 150 local Staff members.

The ESO MESSENGER is published four times a year: normally in March, June, September and December. ESO also publishes Conference Proceedings, Preprints, Technical Notes and other material connected to its activities. Press Releases inform the media about particular events. For further information, contact the ESO Information Service at the following address:

EUROPEAN
SOUTHERN OBSERVATORY
Karl-Schwarzschild-Str. 2
D-85748 Garching bei München
Germany
Tel. (089) 32006-0
Telex 5-28282-0 eo d
Telefax: (089) 3202362
ips@eso.org (internet)
ESOMC0::IPS (decnet)

The ESO Messenger:
Editor: Marie-Hélène Ulrich
Technical editor: Kurt Kjær
Printed by Universitäts-Druckerei
Dr. C. Wolf & Sohn
Heidemannstraße 166
80939 München 45
Germany
ISSN 0722-6691

935. C. Aspin et al.: Near-IR Spectroscopy and Imaging Photometry of M1-16: Bipolar H₂ Jets in a Post-AGB Transition Object. *Astronomy and Astrophysics*.
936. G. Meylan: Some Clues About the Dynamics of Globular Clusters from High-Resolution Observations. Invited review in *Ergodic Concepts in Stellar Dynamics*, eds. D. Pfenniger and V.G. Gurzadyan (Berlin: Springer), in press.
937. L. Origlia et al.: The 1.5-1.7 Microns spectrum of Cool Stars: Line Identifications, Indices for Spectral Classification and the Stellar Content of the Seyfert Galaxy NGC 1068. *Astronomy and Astrophysics*.
938. L.F. Rodríguez and Bo Reipurth: the Exciting Source of the Herbig-Haro 111 Jet Complex: VLA Detection of a One-Sided Radio Jet. *Astronomy and Astrophysics*.

Technical Preprints

52. A.F.M. Moorwood: IR Instrumentation for the VLT. To appear in Proceedings of SPIE Conference No. 1946 on Infrared Detectors and Instrumentation (ed. A. Fowler), Orlando, April 1993.
53. G. Finger et al.: Image Sharpening by On-Chip Tracking in IRAC2. To appear in Proc. of SPIE Conference No. 1946 in Infrared Detectors and Instrumentation (ed. A. Fowler), Orlando, April 1993.
54. J.M. Beckers: Progress in High Resolution Astronomical Imaging Including Active and Adaptive Optics. Invited lecture at the 16th meeting of the International Commission for Optics, August 9-13, 1993, Budapest.
55. N. Hubin et al.: Results of a System Study for the ESO Very Large Telescope Adaptive Optics. To be published in the Proc. ICO-16 Satellite Conf. on "Active and Adaptive Optics", Garching, August 2-5, 1993.

Contents

M.-H. Ulrich: A Message from the New Editor	1
TELESCOPES AND INSTRUMENTATION	
R. Mueller, H. Hoeness, J. Espiard, J. Paseri, P. Dierickx: The 8.2-m Primary Mirrors of the VLT	1
H.U. Käuffl: Ground-Based Astronomy in the 10 and 20 μm Atmospheric Windows at ESO - Scientific Potential at Present and in the Future	8
E. Gosset, P. Magain: On the Linearity of ESO CCD # 9 at CAT + CES	13
T.M.C. Abbott, P. Sinclair: CCD Linearity at La Silla - a Status Report	17
SCIENCE WITH THE VLT	
J. Lequeux: The Magellanic Clouds and the VLT	19
M. Stiavelli: Nuclei of Non-Active Galaxies with the VLT	21
R. Ferlet: From Planets to the Big Bang with High-Resolution Spectroscopy at the VLT	25
REPORTS FROM OBSERVERS	
W.W. Zeilinger, P. Møller, M. Stiavelli: Probing the Properties of Elliptical Galaxy Cores: Analysis of High Angular Resolution Observational Data	28
C. Alard, A. Terzan, J. Guibert: Light Curves of Miras Towards the Galactic Centre	31
M. Kissler, T. Richtler: E.V. Held, E.K. Grebel, S. Wagner, M. Capaccioli: NGC 4636 - a Rich Globular Cluster System in a Normal Elliptical Galaxy	32
J.R. Walsh, J. Meaburn: Imaging the Globules in the Core of the Helix Nebula (NGC 7293)	35
OTHER ASTRONOMICAL NEWS	
F. Murtagh, W.W. Zeilinger, J.-L. Starck, H. Bönnhardt: Detection of Faint Extended Structures by Multiresolution Wavelet Analysis	37
M.A. Albrecht, A. Heck: StarGates and StarWords - an On-Line Yellow Pages Directory for Astronomy	39
ANNOUNCEMENTS	
Programmes Approved for Period 52	41
Announcement of ESO/EIPC Workshop on "The Light Element Abundances"	46
Announcement of ESO Workshop on "QSO Absorption Lines"	46
Associate Director for Science	46
ESO Studentship Programme	46
ESO Users Manual 1993	46
Tentative Time-Table of Council Sessions and Committee Meetings	46
Proceedings of Second ESO/CTIO Workshop on "Mass Loss on the AGB and Beyond"	46
New ESO Preprints (June-August 1993)	47
Staff Movements	47